Intelligent Extruder for Polymer Compounding

Final Technical Report
Prepared by

Alper Eker
Mark Giammattia
Paul Houpt (P-I)
Aditya Kumar
Oscar Montero
Minesh Shah
Norberto Silvi
Timothy Cribbs (GEIS)

GE Global Research
Automation and Controls Laboratory
Room KWD215, 1 Research Circle
Schenectady, NY 12309

Period of Performance
1/8/99-12/31/02

Prepared for
U.S. Department of Energy, Office of Industrial Technology
Contract DE-FC02-99-CH10972

Table of Contents

Index of Figures

Acknowledgements

This material is based upon work supported by the U.S. Department of Energy under Award No. DE-FC02-99-CH10972. The authors wish to acknowledge the guidance and generous use of facilities of the Coperian Werner & Pfleiderer Corporation and GE Plastics. At W&P in Ramsey, N.J., we are particularly indebted to John Curry and Rich Taylor of their engineering team for their sustained in-kind support, ideas and guidance throughout the program, and to Eberhard Dietrich in sales for perspective on markets and applications. Many valuable contributions were provided by technology and manufacturing staff at GE Plastics, Selkirk, NY and Mt. Vernon IN, including: Robert Hossan, Ashish Kulkarni, Bo Liu, Eric Mortensen, Eric Gohr, Horst Oberst (retired), and Dennilu Sosa. Prof. David Bigio, Dept. ME, U. Md, College Park, provided valuable expertise in process modeling.

Disclaimer

1 Abstract

"Intelligent Extruder" described in this report is a software system and associated support services for monitoring and control of compounding extruders to improve material quality, reduce waste and energy use, with minimal addition of new sensors or changes to the factory floor system components. Emphasis is on process improvements to the mixing, melting and de-volitization of base resins, fillers, pigments, fire retardants and other additives in the "finishing" stage of high value added engineering polymer materials. While GE Plastics materials were used for experimental studies throughout the program, the concepts and principles are broadly applicable to other manufacturers materials. The project involved a joint collaboration among GE Global Research, GE Industrial Systems and Coperion Werner & Pleiderer, USA, a major manufacturer of compounding equipment. Scope of the program included development of algorithms for monitoring process material viscosity without rheological sensors or generating waste streams, a novel detection scheme for rapid detection of process upsets and an adaptive feedback control system to compensate for process upsets where at line adjustments are feasible. Software algorithms were implemented and tested on a laboratory scale extruder (50 lb/hr) at GE Global Research and data from a production scale system (2000 lb/hr) at GE Plastics was used to validate the monitoring and detection software. Although not evaluated experimentally, a new concept for extruder process monitoring through estimation of high frequency drive torque without strain gauges is developed and demonstrated in simulation. A plan to commercialize the software system is outlined, but commercialization has not been completed.

2 Introduction

2.1 Background

U.S. polymer resins and their compounds are produced at the rate of 90 billion lb/ yr, one-third of which are engineering thermoplastics valued at more than $1/lb and used in applications from small electrical connectors to medical products, optics to computer cases, kitchen countertops, and automotive fenders and bumpers. Before reaching the injection molder manufacturer, nearly every pound of resin passes through a final "finishing" stage in a compounding line (**Figure 1**), in which component materials are blended in a 1000 to 15,000 hp extruder to achieve critical properties such as melt flow behavior, color, mechanical strength, and fire resistance. Injection molders depend on the values of these properties for their equipment to produce quality parts. Variations in resin properties increase the initial setup time for injection molding and readjustments during a run, resulting in more scrapped parts due to incomplete or excessive mold flow or substandard properties such as color. The outcome, for both molders and resin makers, is productivity loss, missed deliveries, additional landfill scrap, higher production costs, and

dissatisfied customers. *By improving the quality of material produced to meet molders' expectations, the compounding industry and its customers benefit while energy and waste generated in recycle is reduced.*

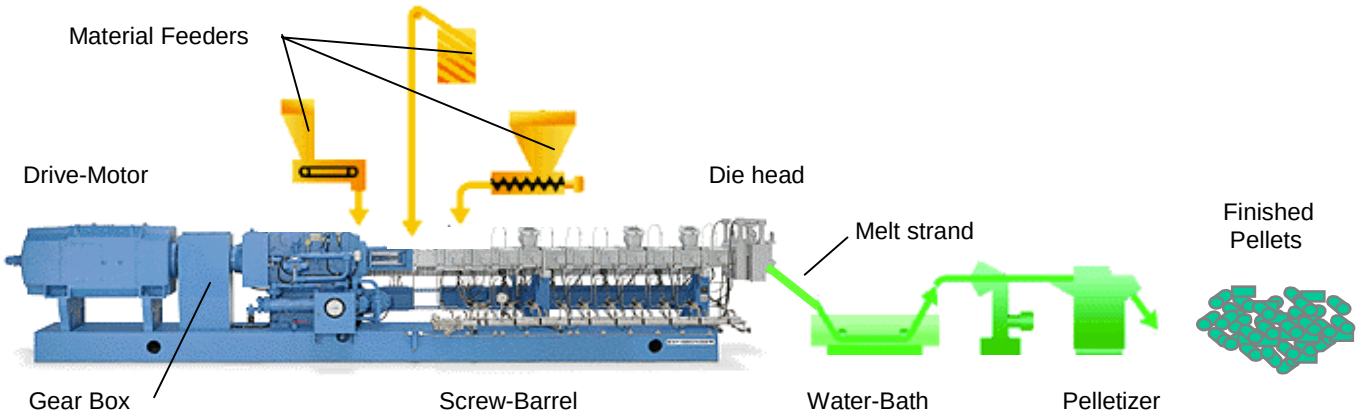

Figure 1 Extruder for Polymer Compounding

2.2 Compounding basics

Extruders are widely used, not only in polymer preparation, but throughout the petro-chemical and food industries for mixing, blending, reacting, cooking, devolatilizing and numerous other tasks, often at the end of the manufacturing chain where material quality attributes are established and value has been added. **Figure 1** shows the principle components. Dry materials are conveyed from storage hoppers with loss-of-weight feeders into various ports in the barrel. The screw conveys, recirculates, mixes and kneads the materials toward the die head, imparting sufficient work to achieve the required degree of mixing and temperature and pressure rise by the time it reaches the die head that melted material emerges in continuous multiple strands. After cooling in a water bath, the solid polymer strands are chopped into pellets and packed in boxes or railcars for shipment to injection molding customers.

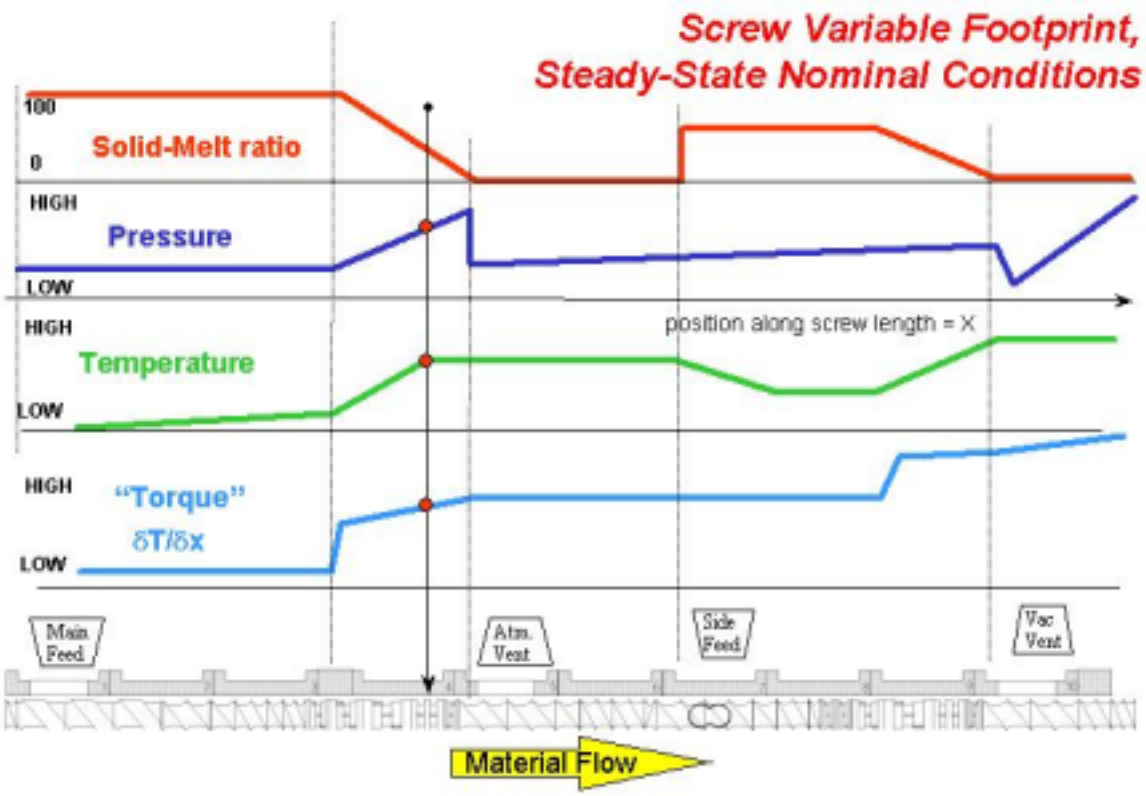

Figure 2 Profile of Material State in Extruder

Figure 2 shows what the internal material state transitions might look like, moving from the input to the output of the extruder barrel at the die head, recognizing that at any position the material flow and melt state is highly complex and 3-dimensional. The design of the screw is a complex science and art is not part of our investigation. For a given screw, base resin and complementary components to create a desired alloy, there is a desired profile the process engineer seeks. This cartoon example illustrates typical complexities encountered, with dry ingredients added at two locations, an open de-volatization vent, and changes in the solid melt ratio along the barrel, but ultimately producing 100% melt at the die head with an appropriate melt temperature and pressure to assure well mixed strand formation. Heaters and/or cooling jackets are located along the barrel length to help maintain temperature conditions in the melt, but the bulk of the energy that melts and blends the material comes from the screw drive.

2.3 Problem and program objectives

The objective of the intelligent extruder program is to develop and demonstrate a prototype software-based monitoring, diagnostic, and control package that will reduce production variability, energy use, and offgrade or waste stream generation.

Both large manufacturers and small independent operations, have used extruders and associated feeders, mixers, and pelletizers for polymer compounding for many years without exotic automation equipment. But market forces are driving change in the industry:

- Smaller lots of material, especially those made to order with short lead times (72 hr), put a premium on efficiency of setup and changeover, which today can consume an entire shift.
- To improve the productivity of their equipment, injection molders are narrowing acceptable quality limits on material properties (melt viscosity and color) from their resin suppliers.
- Price deflation and cost pressures mandate increased productivity (dollars per pound produced), while reducing energy used and landfill waste generation.
- For products in demand, every pound of recycle processed is a pound loss in virgin material capacity that will lead to missed orders or expensive capital equipment to raise plant capacity to compensate for low first-pass yield.

Some of the principle sources of variability in compounding are illustrated in . Variability can be attributed to: (1) operator errors; (2) incoming material variations; (3) equipment faults of various types; (4) process faults/upsets. Each listed fault types in the figure can have an impact quality metrics of importance.

Developing a coherent and *systems-based* approach to these challenges is the objective of this program, leading to products and services that the GE-Coperian Werner-Pfleiderer Corp. team can sell, and that resin manufacturers can exploit for increased profitability.

A cross-functional team was formed to identify the most important needs in compounding as identified in. Prioritized goals by the team included:

- *Reduce operator errors.* Continuous online monitoring could reduce or eliminate human errors by detecting them quickly and allowing corrective intervention

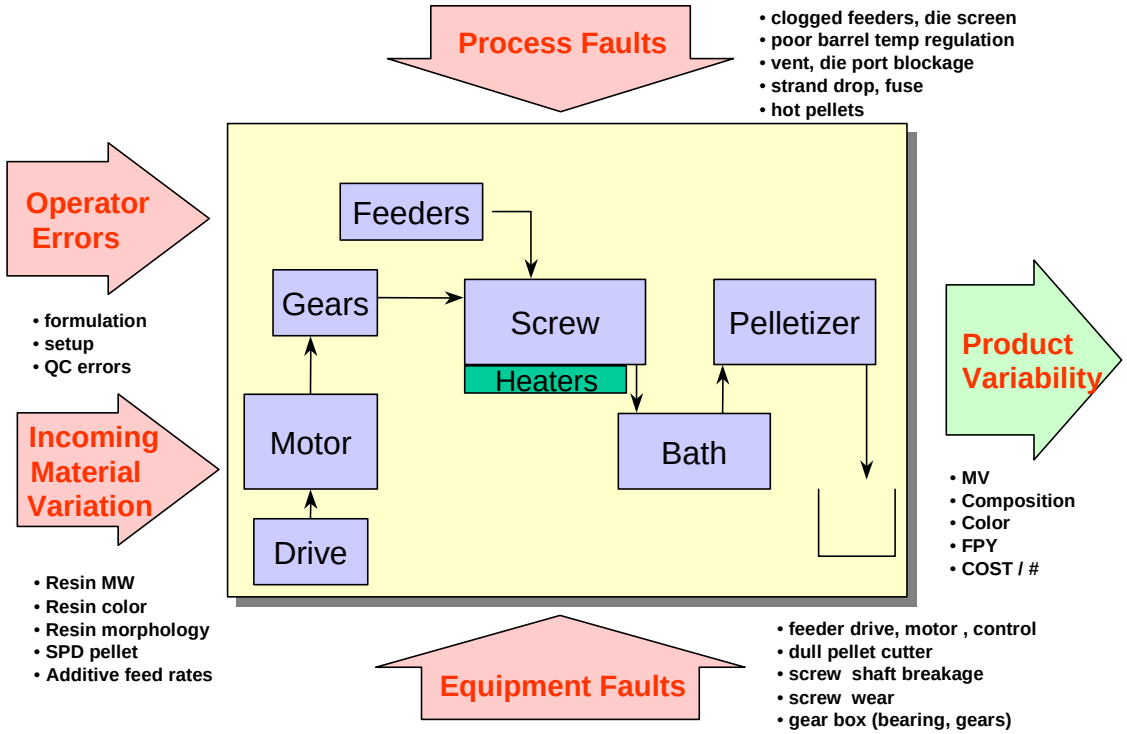

Figure 3 Sources of Finishing Variability

- *Reduce the effects of incoming material variation*. New inferential sensing technology could be used to provide a continuous on line estimate of property shifts, which can be used in closed loop or manually to initiate trim corrections with secondary feeds or other machine adjustment.
- *Detect and correct process faults.* Algorithms to detect and diagnose process faults could be used to quickly divert product and/or initiate operator intervention to make corrective action before upsets produce a degraded product.
- *Anticipate and detect equipment faults.* New diagnostic methods could look for online data trends characteristic of impending faults (e.g., screw wear).

The objective of the intelligent extruder program is to develop advanced diagnostics and controls, responsive to the challenges described above, which show technical feasibility to reduce product variability, increase first-pass yield, while reducing energy use and waste generation in the compounding of polymer resin. The primary deliverables include: demonstration of software and algorithms to provide process and equipment diagnostics for a defined scope of fault coverage; provide an “inferential” predictor of output material properties (melt viscosity) from available temperature, pressure, power, speed, and torque

and internal extruder data derived from torque; provide closed-loop control based on estimates from the inferential predictor; prove that the methods scale from laboratory to full-scale production for at least one GE polymer material; and implement, test, and integrate all software/controls for demonstration purposes on commercially available industrial hardware.

2.4 Prior and related work

A vast literature exists on modeling, diagnostics and adaptive control in general, and we make no attempt at a comprehensive survey here. What follows are some of the past and ongoing work of others that motivated this work. In the following, citation numbers in bracket [] refer to references in Section 14 of this report.

In an effort to develop more comprehensive closed loop controls for composition and MFI, the use of melt flow rheometers has been popular and is used widely, for example as described by Gottfert [6] and Dealy [7], the latter providing a useful survey of known techniques, but the cost, maintenance and generation of a waste stream of these sensors is a major drawback. Moreover, to minimize the waste produced, low flow rates are employed with the result that latency in obtaining a suitable measurement can be several minutes. Sensors working in the near IR have been developed for extruder rheological measurements, exemplified by the work of Hansen et al [10], but these costly devices are at least today expensive and complex to use at the production level. A promising, non-contact transient IR spectroscopy being developed by McClelland et al is described in [16]. This technique uses laser induced transient ultrasound spectroscopy to extract information about composition and viscosity (among other properties). Following correspondence and discussions by Prof. McClelland with the GE team, this method looked very promising as an at-line system since it could work with hot strands as they emerged from a die head, and we will continue to follow his developments. Like all optical systems, it may be a challenge to use in a production environment due to contamination, steam, suspended dust and other grime. Many other at-line sensors have been studied for use in compounding, particularly for color. On-line colorimetry using video based systems for pellet color, for example, are available for sale by Macbeth instruments and others. But these systems suffer accuracy from the end “stress whitening” that results from cutting strand into pellets. The GE team has developed and demonstrated, but not commercialized, a video colorimetry system (see Campo et al[2]) that works directly on strand and uses off the shelf RGB video cameras and can measure color to within 1.5 delta E (in the CIE L-a-b color coordinate system). While all of these systems have shown promise for production operations, they all have limitations, and will still require a QA lab for calibration and maintenance.

Prior work by the GE team on process control for extruders was focused on color control by Houpt [2] which was enabled by a real-time video based colorimeter above. Process control in extruders can go beyond the alloying or non-reactive blending addressed in this

program, e.g. Pabedinskas [5] and Curry [13, 14]. In fact, the team believes reaction control is a promising future direction for the *Intelligent Extruder* system development. In this program, our goal has been to overcome deficiencies of controls that arise from transient dynamics that confound the simplest steady-state relationships or transfer-functions between system inputs and responses. And while there is no shortage of solid fundamental work in understanding process dynamics for purposes of process optimization and screw design (see e.g. Curry [13-15], McKay [8]), such models are typically unsuitable for control design owing to their complexity. Rather, the philosophy is to extract the simplest possible model to capture the "important" dynamics (where what constitutes importance is the outputs in response to inputs are correct), and further to link these models that relate measurable process variables (speed, torque, feed rates, temperature etc.) to un-measurable ones (viscosity etc). Purely heuristic models such as derived from neural networks (e.g. Eerikainen et al [9] who have applied such methods to food extrusion) have been extremely popular in many other fields, or taking a fuzzy modeling and control approach (see Isermann [4] for an overview), and may yet provide value for this effort. But "neuro-fuzzy" approaches almost always over-parameterize data that models input/output behavior to match and require lots of (scarce) data. There is usually little physical insight to what is going on that can be explained by the model fits. Models that formed the basis of our work were first used by Gao and Bigio [11,12]. These models were originally aimed at studying residence time distributions for extruders (how we have adapted and extended the models is described in Section 5.1 of this report). Diagnostics and controls based on these models are described in detail in this report. The underlying philosophy of model based detection and some of the potential techniques considered for use in this effort are described in a survey by Gertler in [3]; the reader interested in a comprehensive treatment of the subject can consult his excellent book [17] which also provides numerous examples in the "art" of the methodology as applied here.

3 Overview of Tasks and Key Results

In this section we provide a summary of the major task objectives, actual accomplishments and provide a road map to the relevant sections of the report where the details are discussed.

Work was broken down into eight major tasks plus program management. The eight major tasks are summarized below, with details provided in Sections 4-13 of the report. The approach to and estimates of projected benefits is described in Section 11.

3.1 Task 1: System Requirements

Objective

Four major sub-systems were identified for development, including

- Extruder process diagnostics
- Extruder inferential estimation
- Extruder inferential control system
- Control implementation platform

The goal for this task was to identify requirements for each of these systems applied to polymer compounding applications, recognizing that our vision for *Intelligent Extruder* included other products (see Commercialization Plan details in Section 12.1). Table 1 provides a brief summary of the purpose of each system to be developed, key functional requirements, and where applicable, specific targets to be achieved. These requirements, identified by a cross-functional team, address many of the upsets known to occur in typical polymer processing operations. A more comprehensive list of "critical to quality" (CTQ) parameters which is the source of Table 1, is provided in Table 2. The team examined more than 60 potential needs, grouped by sub-system. After prioritizing based on impact and likelihood, the proposed functionality was proposed.

System	Key Requirements	Specific targets
Inferential Process Sensing / Estimation: Obtain estimates of process model constants and dynamic variables from measurable machine sensors (drive torque, die pressure, speed, etc) with minimum material use and lab checks	*Identify key system model parameters (see 5.1.2) and provide means to track changes from process shifts and grade changes* *Estimate process viscosity (or corresponding melt flow index (MFI) from model and machine variables*	Model parameters to match input/output dynamic response Viscosity(MFI) +/- 10% or better (vs. 5% 1-σ for typical lab rheometry)
Process diagnostics- Use process understanding and models to detect and classify process upsets of interest	Detect and correctly classify process upsets from raw material variations, feeder anomalies (blockage, drift, sensor bias etc)	95% Detection of feeder/resin shift faults as defined in Section 8.2, with 10% false alarm rates
Inferential control – Building on above systems, develop control strategy to make feeder or drive adjustments on-line to keep process viscosity within specs	Regulate viscosity to no worse the twice the measurement error variance steady state; provide adaptive framework to simplify the modeling efforts over material grade changes	For correctable upsets, maintain viscosity +/- 10% of target value Achieve continuous adaptation for "neighboring" grades to minimize transition waste material
Control implementation platform	Design all software to be capable of running on typical industrial DCS process control equipment and/or PC-class industrial controllers	Target PC class control computer interfaced to drive PLC within scope of demonstration program

Table 1: System Requirements for Intelligent Extruder

The main conclusion from examining Table 2, is that most upsets of importance derive from problems external to the extruder (feeders and material variation). The drive, gearbox and controls are comparatively reliable and have extensive diagnostics of their own, or are already provided by 3rd parties, e.g. vibration based gear-box monitors. Clearly, there are other important process defects that lead to rejected material, e.g. color, surface defects and mechanical strength. But other means must be provided for tracking

color shifts/upsets since these are rarely, except in extreme cases, detectable from machine variables. But viscosity, important in its own right, is often leading indicator of problems in composition which in turn is linked to material properties. Thus it was the opinion of the team that considerable benefits derive from detecting and managing viscosity related upsets, which became the primary focus of this effort.

System	Fault	Likelihood	CTQ Impacted (0=none; 1= weak; 3=moderate; 9=strong)										Total
	(1=LOW;2=MED;3=HI)	1<LIK<4	Capacity	Melt V	Composition	FP Yield	Ult Yield	Pellet Size	Pellet App.	Matl Cost	Proc EHS	Other	Weighted
	blocked main feed port	3	9	9	9	9	9	9	9	9			**216**
	blocked chute	3	8	8	9	9	9	8	8	9			**204**
	blocked sec feed port	3	8	7	8	8	8	3	5	9			**168**
FEEDERS	resin l.o.w. feed controller	2	8	8	8	8	8	8	8	8			**128**
	pigment line block	2	8	6	9	6	6	2	6	9			**104**
	filler feeder drive	1	9	9	9	9	9	5	5	9			**64**
	filller conveyer	1	9	9	9	9	9	5	5	9			**64**
	transfer conveyer drive	1	9	9	9	9	9	0	0	9			**54**
	pigment l.o.w. drive	1	8	6	9	6	6	2	6	9			**52**
	drive computer	1	9	0	0	0	0	0	0	9			**18**
SCREW	drive power electronics	1	9	0	0	0	0	0	0	9			**18**
DRIVE	drive setup error	1	9	0	0	0	0	0	0	9			**18**
	drive / DCS comm error	1	9	0	0	0	0	0	0	9			**18**
	gearbox lube pump	2	9	0	0	0	0	0	0	9			**36**
	gearbox lube contamination	2	6	0	0	0	0	0	0	4			**20**
MOTOR	motor shaft	1	9	0	0	0	0	0	0	9			**18**
and	motor winding	1	9	0	0	0	0	0	0	9			**18**
GEARS	motor brushes	1	9	0	0	0	0	0	0	9			**18**
	gearbox shaft	1	9	0	0	0	0	0	0	9			**18**
	gearbox bearings	1	9	0	0	0	0	0	0	9			**18**
	gearbox gears	1	9	0	0	0	0	0	0	9			**18**
	motor bearing	1	6	0	0	0	0	0	0	6			**12**
	feedport(s) blockage	4	8	7	7	7	7	4	6	8			**216**
	feed hopper bridge	3	8	7	9	7	6	8	5	7			**171**
	unmelt particle passage	4	6	4	0	5	6	3	5	4			**132**
	feed hopper buildup & sloughing	3	4	6	6	5	4	6	3	4			**114**
	vent port blockage	4	6	5	2	2	3	0	2	4			**96**
	clogged die port(s)	4	3	2	0	1	1	6	6	5			**96**
SCREW	strand fuse=fused pellets	4	0	0	0	0	0	9	9	5			**92**
	feed cycling (bad tuning?)	2	5	6	7	6	5	5	3	6			**86**
	blend separation in feeder	2	3	7	8	7	5	4	2	5			**82**
	worn screw elements	3	4	6	0	5	5	1	1	4			**78**
	wrong screw makeup	3	5	5	0	5	5	0	2	4			**78**
	clogged die screen	4	5	3	0	2	2	1	2	4			**76**
	wrong KWH/# input	4	5	2	0	3	4	1	1	3			**76**
	broken screw elements	2	7	8	0	7	7	1	1	6			**74**
	feed flooding	2	6	5	5	4	5	4	4	4			**74**
	vent vacuum failure	3	6	5	2	2	3	0	2	4			**72**
	pigment aglom. via cold working	2	2	2	6	5	7	0	5	5			**64**
	barrel heater(s) failure	3	4	1	0	1	1	2	1	1			**33**
	barrel temp sens failure	3	4	1	0	1	1	2	1	1			**33**
	strand drop	4	3	0	0	0	0	0	0	5			**32**

Table 2 "Complete" List of CTQs for Upset Coverage in Intelligent Extruder

3.2 Task 2: Process Models for Diagnostics and Controls

***Objective*- Develop simplified extruder process dynamic models suitable for use in advanced diagnostics and controls.** Because of the complex, dynamic nature of extruder physics, it was the team's experience that many past efforts at monitoring and diagnostics, e.g. based on simple statistical models, failed or were not robust. On the other hand, detailed 3-D extruder flow models are too complex to exploit in a real-time setting. The goal was to find a simple enough, but physically "correct", model to use in various aspects of the controls and diagnostic development.

Accomplishments – Motivated by work by Bigio and Gao [11,12], a lumped model is derived and which despite its simplicity, is adequate to capture the nonlinear input-output dynamics of the extruder. In response to changes in feeds and drive speed (inputs), the model predicts die pressure/temperature and torques (outputs). Details on the model derivation and its validation on both research scale and production scale extruders are contained in Section 5 and 10 of this report respectively. The model contains certain unknown parameters, which depend on the machine type and screw configuration, and on the material being used and operating conditions (temperatures, pressures, production rate). Explicit means to identify and adaptively track these parameters in a highly efficient manner are developed as part of Task 4, and are described in Section 6 of the report. The machine parameters need to be identified only once (for a given screw configuration), whereas the material parameters vary for each grade or major change in operating regime. Having an efficient means to identify and track model parameters is key to making all the methods developed in this program practical with a minimum of calibration/test and wasted material.

3.3 Task 3: Extruder Diagnostics

***Objective*—Develop and demonstrate algorithms for detection and classification of key extruder compounding system faults, emphasizing material feed sub-systems**

Accomplishments
The models from Task 2 and the identification methods from Task 4 form the basis of our proposed algorithms for fault detection. As discussed above in the requirements task, our investigation of process related faults suggested that feeder anomalies and material variation were among the most important events to be able to detect rapidly and take corrective action. In Section 8 of the report, the main method is derived. The derivation shows that detection of fault events derives from comparing measured variables with those predicted by a system model, assuming no faults exist. Differences that exceed a threshold indicate a fault condition. A new approach is developed in which the pattern of identified parameters following the fault occurrence can be used to isolate among the possible causes. A demonstration case study illustrates the method using data from the three-feeder research extruder with Noryl materials, in the presence of various property shifts and feeder faults. Section 8 also outlines how the method can be extended to materials with multiple constituents. It is shown that typical upset events can be detected in time frames as short as a few seconds up to a few minutes of operation. The main

limitation of the methodology is that faults are assumed to occur one at time. Multiple concurrent faults can be handled, but the decision logic is more complex (see Gertler[17]). Although concurrent extruder system faults are detectable, it may be impossible to disambiguate the root cause in general, but at least manual intervention via an alarm can be flagged.

3.4 Task 4: Extruder Inferential Estimation and Parameter Identification

Objective – Develop and validate experimentally, algorithms to identify unknown parameters in the extruder system models from Task 2. Using these models, derive and demonstrate means to "infer" or estimate process states, emphasizing viscosity or MFI, from machine variables.

Accomplishments

Model Parameter Identification

Simplified dynamic process models form the foundation for all the results in this program, including estimation, diagnostics and controls. In Section 6 of the report, we show that a total of six parameters must identified, four dependent on machine geometry and two of which depend on the specific material (and process operating conditions). Even though the two material parameters must be found for each grade of material (of which there may be hundreds), the fact that only two material parameters suffice to parameterize models for the estimation and diagnostics results that follow was surprising and counter-intuitive. Moreover, it can be shown that material of similar grades can be identified during the grade transition and lineout. That is, starting from a calibrated grade for which the coefficients are known, the models can be continuously adapted to grades with different MFI's and material feeds that influence it. While we offer no definitive "proof", we believe this capability can reduce by an order of magnitude the complexity of the data-base requirements that would otherwise be needed. Section 6 also illustrates the recursive on-line method for parameter identification using classical techniques, and provides a brief summary of experimental results on various grades of GE's Noryl (PPO) material.

Inferential Sensing and Estimation

Using the models and adaptive identification above, the goal of inferential sensing of viscosity is shown in Section 7 to be a straightforward extension using a linearized viscosity relation from Section 5. Using data from both our 25 mm research extruder and a 120 mm production facility for Noryl, we showed that viscosity predictions within +/- 10% or better can be obtained. The significance of this approach in comparison to traditional discrete lab quality control checks typically good for 2% accuracy, is that a *continuous* audit of viscosity results. Task 3 on leverages this capability in developing diagnostic algorithms.

Fast Response Torque Estimation

The team had proposed using "high frequency" components of shaft reaction torque as a measurement for use in estimation / diagnostics of screw condition, proper fill conditions, surge behavior etc. High frequency in this context means torque variation at or faster than the per-revolution rate of the screw. That such data would be informative and valuable in monitoring and diagnostics was conjecture based on preliminary experimental studies by one of the team members. Torque signals provided in the control electronics of most of the installed base of extruders is heavily filtered due to the noise that would be present, and because it is not required for proper drive operation. It was therefore believed that this could not provide information of interest at or near the frequencies that result from torque fluctuations on a per-revolution basis. Direct torque measurement with high bandwidth was found to be technically possible using a variety of strain-gauge or in-line shaft-strain devices, but not practical or cost effective for use in retrofit in a production environment, so this sub-task was initially abandoned. Late in the program, a concept was proposed using an adaptation of ideas used in conventional AC drive controls. A small effort was devoted to show the potential of this technique, using an "observer" torque estimation algorithm, optimized to provide high frequency torques. The results of a design and detailed circuit simulation study (without the details of the screw load) are provided in Appendix B. Observer based torque estimation requires measurement of certain voltages and currents (or power) in the machine, but it is feasible and inexpensive to add such sensors, and a CPU to do the required signal processing, even to existing drives. Since AC drives are used in a large percentage of the installed base and most new systems (particularly large machines), we believe this approach has merit for investigation in future studies. Since we did not have time or resources to go beyond the basic simulations studies, we can make no claim to benefits that would derive from this estimation scheme, but believe it merits experimental validation in future studies.

3.5 Task 5: Inferential Control System

***Objective*: Develop and demonstrate a computer control system that integrates all the diagnostic and estimation algorithms with a control system that allows automatic on-line recovery to correctable faults**.

Accomplishments

Section 9.1 summarizes the philosophy and approach to control design for inferential adaptive control of viscosity. The methodology integrates all elements developed during the program, i.e. to monitor viscosity with an estimator, to detect when an upset occurs, to classify the root cause of the upset, and initiate corrective action, all in a timely manner to minimize out of spec material. In Section 9.2, the details of design are presented with consideration to key tradeoffs which must be selected by the designer. The resulting control requires either sufficient natural process disturbance presence or introduction of small set-point perturbations (well within spec limits) to be able to reliably isolate root cause of the disturbance and to then take the right corrective action. A key benefit of this approach is shown in Section 9.3 to be the ability to reliably change the operating set

point. The significance of this is allowing a production operator to change grade on the fly, with the adaptive control re-tuning the models so that both control performance (e.g. stability) and detection algorithms follow the new set point automatically. This is one of the key benefits of the integrated *Intelligent Extruder* approach when viewed from a production point of view. Although our closed-loop feedback controller was only demonstrated on the research extruder, our success in proving scalability with the modeling and diagnostics (see Task 7 and the results in Section 10) gives us confidence that adaptive control will scale similarly.

3.6 Task 6: Control Platform and Experimental Extruder System

***Objective*: Implement and demonstrate the diagnostic and control systems developed in Tasks 1-5 on a research scale extruder.**

Accomplishments
Section 4 of this report describes the 25-mm research extruder used throughout this program. Using a 30HP drive, the Werner & Pfleiderer ZSK-25 is capable of producing about 50-100 lb/hr compared to commercial production rates of 2000 lb/hr and up. Using identical but scaled screw geometry, however, it is possible to correctly compound most polymer materials in the same manner as they will produced on the big machines. (Scaling is addressed in Task 7). This section of the report also identifies the lab test procedures used for measuring the actual material properties in the intelligent extruder validation. To prototype the various diagnostic and control strategies developed in the program, all logic was first implemented in well known and widely Matlab and/or Simulink, a high level analysis package by The Mathworks Inc. Using the "Real-Time Workshop" capability, it was possible to compile the various algorithms into executable software that would run real-time on a special target hardware system called D-Space. The D-Space package offered extensive data acquisition and user interface prototyping capability making interfacing and control of the extruder particularly easy. While this platform offers far greater computer power than needed to implement these algorithms on a commercial product, the software modules make rapid prototyping easy and all the code is in a C-language format that can be readily ported to other platforms, e.g. high end PLCs or plant distributed control systems that support C. Further details on the control algorithms developed and how they were implemented on the extruder control platform are described in Section 9 of this report. The software developed in this program is for research purposes only and is not available as a commercial product. Researchers and other potential users wishing to replicate the software should contact the principal investigator or GE Industrial Systems for more information.

3.7 Task 7: Production Scale Demonstration and Validation

***Objective*: Demonstrate that Intelligent Extruder diagnostics and control concepts developed on the lab scale system are extensible to production scale operations.**

Since the majority of the experimental work in this program was carried out on a small laboratory research extruder, a major question addressed in this task is: do the concepts work on extruders at more typical production rates which are 20-100x the production rate of the ZSK-25 lab system? As described in Section 10 of the report, data was obtained from a 120 mm extruder system at GE Plastics making the same Noryl grade used throughout our lab testing. The system was operating at approximately 2000 lb/hr, a typical production rate in the Selkirk, N.Y. facility. This was special test in which perturbations in feed rates were allowed (still keeping product within spec). Results show that the simplified modeling and adaptive parameter identification framework scales to predict viscosity within +/- 4% on the production rate machine. While it was not permitted to perturb the machine out of spec to produce faults, simulation with the model suggests identical qualitative behavior and that therefore all the proposed diagnostics should perform similar to the research extruder. The extruder line where tests were conducted did not have a means to close the loop on extruder feeds so it was not possible to demonstrate the closed loop control capability as planned within the original scope of this task. However, given that the modeling and adaptive identification methodology appeared to scale well, we are confident that production scale closed loop correction should be feasible to accommodate feeder upsets and base resin property shifts.

3.8 Task 8: Commercialization Plan

***Objective*: Develop a commercialization plan to transition the research results of the Intelligent Extruder program to a product and/or service offering for the polymer compounding industry.**

Accomplishments

Section 12 of this report provides an overview of the commercialization plan developed by the team to market the *Intelligent Extruder* as a value add product/service offering to potential customers in the polymer industry. The size of the market for potential retrofits and new installations is segmented. Alternative sales channels are identified. Market forces driving the need for such offerings are identified, leading to a summary opportunity fishbone for both polymer and non-polymer applications where *Intelligent Extruder* ideas are applicable. Based on the expected benefit (see Section 11) of approximately 2% in first pass yield, it was anticipated that an attractive value proposition could be presented to customers through a services offering for new and retrofit markets. Over the course of the program, three potential customers were approached who possessed large numbers of production extruders, and two proposals were submitted which included various elements of the *Intelligent Extruder* system concept. While the nature and details of these commercial discussions are proprietary, as of the date of this report submission, no sales or implementations have been consummated.

3.9 Publications and Patents

This research has resulted in one accepted paper in a refereed conference, with two other papers planned for submission in 2003.

Alper Eker, Aditya Kumar and Paul K. Houpt, "A Model Based approach for an Intelligent Extruder," 2003 IEEE Conference on Control Applications, June 2003.

One patent disclosure has been filed as part of the program,
"Model based estimation diagnostics and control of an extruder," Docket filing RD-30498 (GE Internal reference), April 12, 2002

4 Experimental Extruder Setup for Demonstrations

4.1 WP 25mm Lab Extruder Description

In this section, we describe the extruder setup used at GE Global Research to perform the experiment runs during the various phases of inferential estimation, diagnostics and control. The setup used consisted of a WP ZSK-25mm twin-screw extruder, two K-Tron loss-of-weight feeders with K-Tron feeder controllers and a high-performance data acquisition system from IOtech. Figure 4 shows the ZSK-25mm extruder used which was capable of maximum screw speed of 1200rpm, maximum throughputs of 100 lb/hr with a maximum torque of 164 Nm. The extruder was powered by a 30HP GE Innovation drive, which provided a measurement of total screw torque (estimated from motor current and voltage) and screw speed (measured using a high-resolution optical encoder). The extruder had six thermocouples along the barrel length and heating elements to control the temperatures in the corresponding barrel zones. In addition to these, the extruder had a thermocouple and pressure probe in the die zone to measure the melt product temperature and the die pressure. Finally, the K-Tron feeder controllers had provision to remotely command a desired set-point for the feed-rates and provided the measurement of the actual feed-rates estimated internally by monitoring the loss of weight in the feeder hoppers.

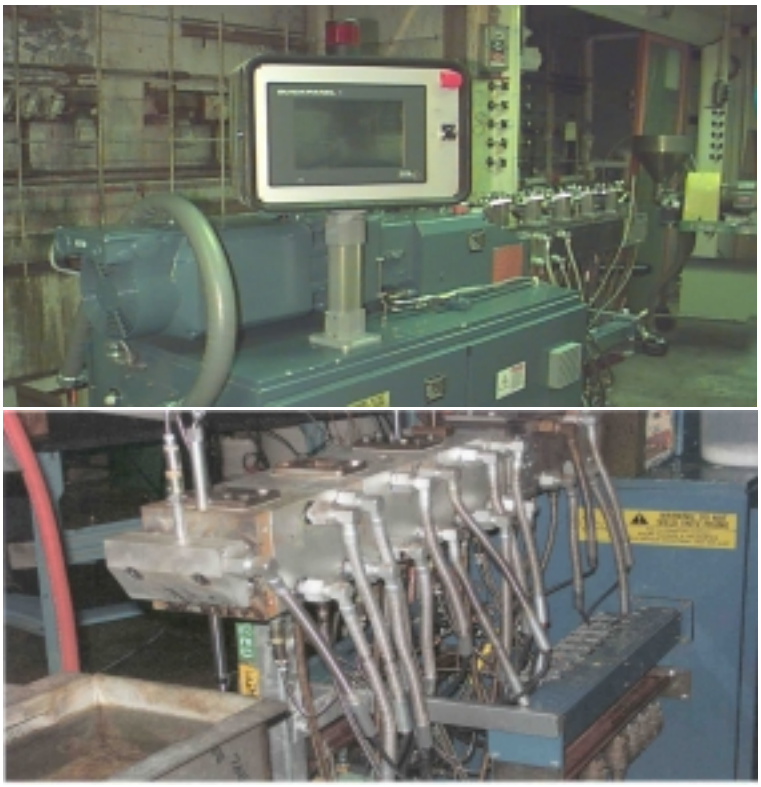

Figure 4: WP ZSK-25mm twin-screw extruder used at GE Global Research for experiment runs

4.2 Data Acquisition and Monitoring

The signals for the machine variables were recorded using an IOTech data acquisition system capable of recording up to 24 channels. The torque, screw speed and die pressure measurements were available as voltage signals, which could be directly interfaced with the IOTech equipment. Also, the IOTech equipment had extensions to directly hook up with thermocouple measurements. However, the feed-rate signals provided by the K-Tron feeder controllers were in frequency, which had to be converted to voltage signals using frequency to voltage converters before interfacing with the IOtech equipment. For our experiments we recorded the main signals, i.e. torque, die pressure, two feed-rates, screw speed and melt temperature, and for the most part they were recorded at a sampling rate of 10Hz-1kHz and later sub-sampled through software as required. The collected data was analyzed in Matlab and the algorithm development for modeling, inferential estimation, diagnostics and control was carried out using Matlab/Simulink. For analyzing the performance of the estimated viscosity using the measured extruder signals in comparison to lab measurements, we collected samples of the product pellets at several steady state operating conditions and measured their viscosity in the lab using two main techniques shown in Figure 5.

The capillary rheometer is commonly used to measure the static viscosity of the molten polymer at medium to high shear rates. On the other hand, the RDS rheometer measures the dynamic viscosity of the molten polymer subjected to oscillatory shear between two discs at low shear rates. The initial experiment runs with polycarbonate mixtures used both capillary and RDS rheometers, while in the later runs with Noryl (blend of polyphenylene oxide (PPO) and polystyrene (PS) obtained from GEP Selkirk), we exclusively used the capillary rheometer.

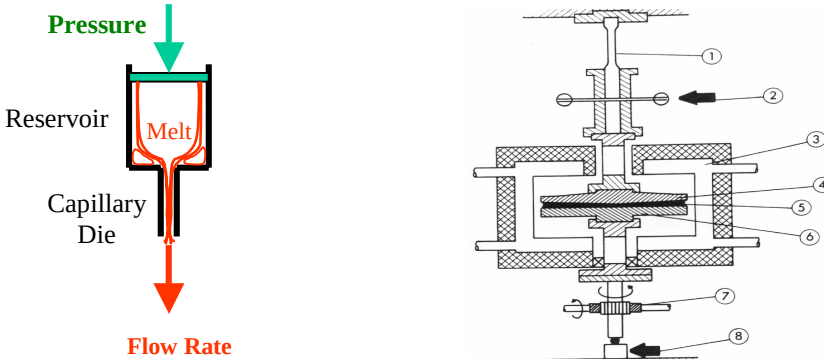

(a) Capillary rheometer (b) RDS rheometer

Figure 5: Schematic representation of capillary and RDS rheometers

4.3 D-Space Implementation for Closed-Loop Experiments

The final implementation of the developed algorithms for estimation and closed-loop control was done using D-Space, a high-end data acquisition and controls platform that readily allows implementing algorithms developed in Matlab/Simulink. In addition to

measuring the regular signals from the extruder, for the closed-loop control runs we also needed the capability to automatically adjust the feed-rates. This was achieved using two voltage to frequency converters that converted the voltage output signals from D-Space to corresponding frequency signals used by the K-Tron feeder controllers to adjust the feed-rate set-points. Figure 6 shows a screen shot of the GUI interface built in D-Space for on-line data acquisition, monitoring and closed-loop control. The interface allowed monitoring measured values of raw material feed-rates, measured and predicted (by model) values of die pressure and torque, estimated values of viscosity used in control and other parameters used in diagnostics, all in real time.

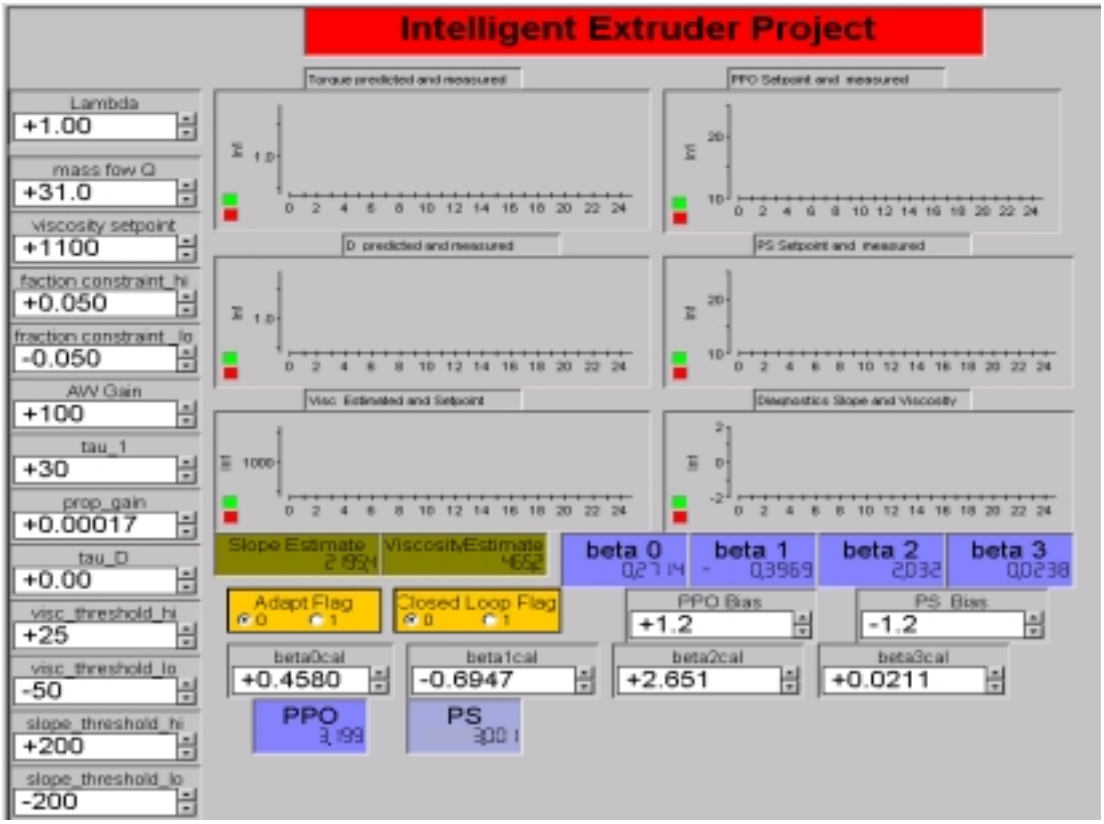

Figure 6: GUI interface for estimation and controls algorithms using D-Space.

In addition to experiments performed at GE Global Research on the ZSK-25mm extruder, we also obtained and analyzed data from production-scale extruders – 120mm, 2000lb/hr throughput – at GEP Selkirk.

5 Extruder Modeling for Estimation, Diagnostics and Control

We adopted a model-based approach to achieve the estimation, diagnostics and control objectives in a unified framework. There are several types of models that one can develop using measured input-output data, e.g. static correlations for steady state relationships or linear dynamic input/output dynamic models identified using standard identification techniques. However, models obtained by these methods are often sensitive to the particular data set and are not readily generalized. Moreover, they often lack any insight into the physical process itself. On the other hand, first principles physics for melt flows in extruders can be too complicated. A dynamic model which captures only enough of the behavior to enable proposed methods is the goal.

The developed model is a representation of the physical process of extrusion that captures the dynamic effect of common process inputs, e.g. raw material feed-rates and screw speed, on measured process outputs, e.g. total screw torque and die pressure, without getting into unnecessary details of the actual screw geometry and detailed material flow characteristics. In particular, we used the work of Gao et al [11,12] on steady state models for residence time distribution (RTD) in extruders as a starting point.

5.1 Process Description & Modeling

5.1.1 Process Description

Consider a typical extruder setup in Figure 7, which consists of the main drive, the extruder barrel with one or two (co- or counter-rotating) screws and feeders (screw or belt) for raw materials. Two or more raw materials (typically pre-blended with appropriate additives) are fed to the extruder at controlled feed-rates and mixed and melted in the extruder via the rotating screws with specifically designed conveying/ mixing/ kneading elements to produce the final molten product that is extruded at the end as strands through holes in a die plate. The molten strands are then typically cooled and solidified in a water bath and finally chopped into pellets for packaging and shipping as final product. While typically some heat for the melting of the solid raw materials is added to the extruder barrel externally through heating elements along the extruder barrel length, most of the heat required for melting the raw materials is provided by friction from the turning screws. This is especially true for the large industrial production-scale extruders. Moreover, the extruder geometry, specifically the individual screw elements and their sequence, varies from one application to another. In a typical plant, however, the extruder geometry is often optimized and fixed for a wide grade of products, and changed only occasionally for maintenance or when changing to very different product grades.

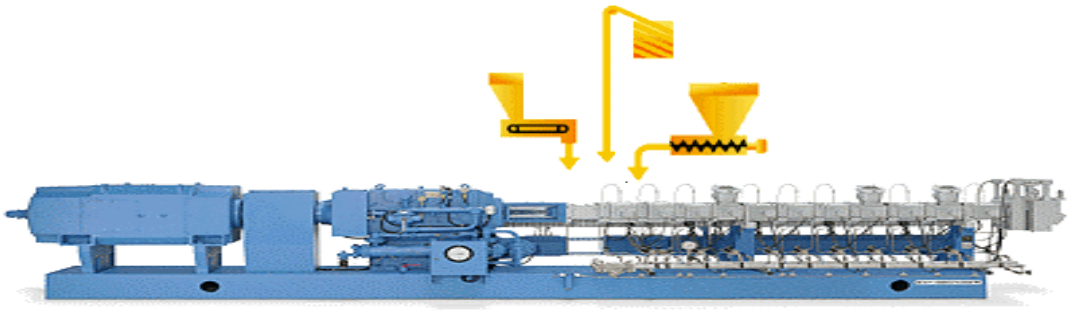

Figure 7: A typical extruder setup

5.1.2 Physics-Based Lumped Model

We start with a dynamic model that describes the dominant characteristics associated with the mixing of the raw materials. To this end we develop a lumped two-section dynamic mixing model that captures the effect of the inputs to the process (raw material feed-rates and screw speed) on the measured process outputs (total screw torque and die pressure: the pressure developed prior to the die plate as the molten product is stranded into the water bath).

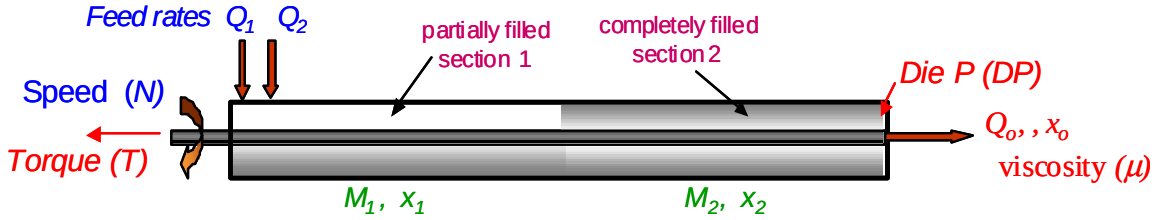

Figure 8: Schematic representation of extrusion process

Consider the schematic representation of a typical extrusion process shown in Figure 8. For simplicity here, consider extruders with two key raw materials fed at rates Q_1 and Q_2. In our experiments we worked with the NORYL resins from GE plastics which is produced from polyphenylene oxide (PPO) and polystyrene (PS), but the methodology can be generalized to multiple raw material feeds. The operating conditions of an extruder are typically characterized by the combination of total throughput $Q=Q_1+Q_2$ and screw speed N. Capacity of the machine depends on the screw design, material, and drive torque power capability. As process outputs we measure the total shaft torque T and the die pressure DP, which vary as a function of the operating conditions. Leveraging the work of Gao et al (1999, 2000) [1,2] for steady state RTD, we consider the extruder with two distinct sections during regular operation - a completely filled section (mixing, kneading) and a partially filled section (conveying). Note that in an actual extruder there are multiple conveying, mixing and kneading blocks and hence the partially/completely filled sections may be interspersed. It will be shown that for the purpose of capturing the overall dominant dynamics for use in estimation, diagnostics and control, it suffices to assume two "equivalent partially" filled and completely filled zones into the respective sections.

5.1.3 Dynamic Model for Internal Holdup and Compositions

Under steady state operating conditions with a specific total feed-rate (throughput) $Q=Q_1+Q_2$, and screw speed N, the total material holdup M_1 and M_2 in the partially and completely filled sections, respectively, are given by

$$M_1 = B\frac{Q}{N}, \qquad M_2 = A$$

Eq 1

where the ratio Q/N is referred to as the specific throughput and the parameters A, B are related to the maximum capacities of the completely filled and partially filled sections, respectively, depending on the specific screw design/geometry (see Gao et al (1999, 2000) [1,2] for more details). While the holdup M_2 in the completely filled section is constant, the holdup M_1 in the partially filled section varies with the operating conditions, specifically the ratio Q/N. In particular, the transient variation in the holdup M_1 due to changes in total feed-rate Q and screw speed N is described by the total material balance:

$$\frac{dM_1}{dt} = Q - Q_{1o}$$

Eq 2

In the above equation, the total inlet feed-rate to this section (from the feeders) is Q while the total outlet mass flow rate, denoted by Q_{1o}, varies with the operating conditions, in particular the fill fraction ϕ (i.e. the fraction of the total void volume filled with the material holdup) and the screw speed N. More specifically, the maximum flow capacity of this section Q_{1fc} corresponding to the maximum filled capacity M_{1fc} (based on the void volume from screw geometry) is proportional to the screw speed N, i.e., $Q_{1fc} = k\,N$ with the proportionality constant k depending on the screw design/geometry. During regular operation, when this section is only partially filled and the fill fraction is $\phi = M_1 / M_{1fc}$, $(0 < \phi < 1)$, the total outlet mass flow rate is given by

$$\begin{aligned} Q_{1o} &= k\phi N \\ &= k\left(\frac{M_1}{M_{1fc}}\right)N \\ &= \frac{M_1 N}{B} \end{aligned}$$

Eq 3

where $B=M_{1fc}/k$ is a parameter that depends only on the screw design/geometry. Combining equations Eq 2 and Eq 3 gives the dynamic mass balance relation for the holdup M_1:

$$\frac{dM_1}{dt} = Q - \frac{M_1 N}{B}$$

Eq 4

Note that at steady state, the inlet and outlet mass flow rates are equal, i.e. $Q=Q_{1o}$, and the dynamic material balance in Eq 4 reduces to the steady state version: $M_1 = BQ/N$. In contrast with the partially filled section, the total holdup M_2 in the filled section is constant (since the void volume is filled to maximum capacity). Furthermore, the outlet

flow rate from this filled section is always the same as the inlet flow rate, which in turn is the same as the outlet flow rate from the partially filled section, i.e. Q_{1o}.

Furthermore, in addition to the total material balance, we also need to capture variations in composition of this material holdup to be able to predict the final product composition as a function of the operating conditions (feed-rates & screw speed), which has a direct bearing on the product properties, e.g. viscosity. To this end, we denote the weight fraction of PPO in the material holdup in the partially and completely filled sections by x_1 and x_2, respectively. At steady state, these compositions are the same and are determined solely by the feed rates Q_1 and Q_2, i.e.

Eq 5

$$x_1 = x_2 = \frac{Q_1}{Q_1 + Q_2}$$

Similar to the dynamic total mass balance, we also need to model the transient variations in the compositions x_1 and x_2 in the partially and completely filled sections, respectively. The composition in these sections changes due to mixing of the two raw materials in the respective sections. More specifically, as the inlet feed-rates are changed thereby changing the raw material composition at the extruder inlet, this change in composition at the inlet propagates down the length of the extruder depending on the degree of mixing in various sections. The detailed mixing mechanisms are governed by the screw design for the various conveying, mixing, kneading sections and are too complex to model. For our purposes, we seek a simple parameterized mixing model where the parameters can be fit with measured input/output data to describe the overall effect of the mixing in the partially and completely filled sections. This is achieved by modeling the level of mixing in the individual sections through a combination of delay and recycle. Figure 9 shows schematically this representation in the two sections.

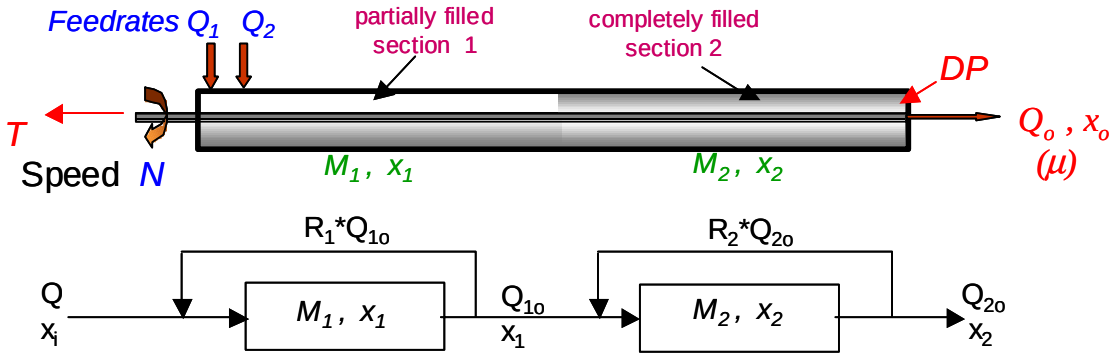

Figure 9: Schematic representation of mixing in partially and completely filled sections.

For instance, the mixing in the first section that governs relation between the composition x_1 and the inlet composition x_i, is governed by the delay depending on the ratio M_1/Q_{1o} and the recycle ratio R_1. The actual level of mixing can be captured by adjusting the recycle ratio R_1 between the extreme limits of 0 (no mixing) and infinite – in practice a

large value (perfect mixing). Similarly, the level of mixing in the second section is captured by the recycle ratio R_2. The overall model for the transient behavior of the compositions in the two sections is given in a compact form in the Laplace domain:

Eq 6

$$x_1(s) = \frac{Qe^{-t_{d1}s}}{Q + R_1 * Q_1(1 - e^{-t_{d1}s})}\ x_i(s), \quad \text{where} \qquad t_{d1} = \frac{M_1}{Q_{1o}}$$

$$x_2(s) = \frac{e^{-t_{d2}s}}{1 + R_2 * (1 - e^{-t_{d2}s})}\ x_1(s), \qquad \text{wher e} \quad t_{d2} = \frac{M_2}{Q_{2o}}$$

For a more detailed derivation of the above model, see APPENDIX-A Extruder Dynamic Models.

5.1.4 Torque, Die Pressure and Viscosity Relations

The above equations (Eq 4 and Eq 6) describe the dynamics for the material holdup M_1, M_2 (constant) and the compositions x_1, x_2. However, these internal state variables are not measured on-line and need to be related to the output variables that are measured, namely torque T and die pressure DP. The overall shaft torque arises from the combination of the resistive torque in the individual conveying, mixing, kneading sections and a detailed physics-based model involving the details of the screw design would be too complex. We seek to develop a simple overall relationship for the total shaft torque in the following general form:

Eq 7

$$T = \alpha_0 + \alpha_1 M_1(\alpha_2 + N)x_1 + \alpha_3 M_2 N x_2$$

The above expression for torque has three key terms, the offset and the two contributions from the partially and completely filled sections, respectively. The latter two terms depend on the respective holdups and compositions and the screw speed. We tested the validity of the above relationship for torque, using multiple measurements of torque at various steady state operating conditions. At steady state, using the corresponding steady state relations for the holdups, the above relation for torque reduces to the following relation:

Eq 8

$$T = \alpha_0 + \alpha_1\alpha_2 B\frac{Q}{N}x_i + \alpha_3 ANx_i + \alpha_1 BQx_i$$

$$= c_0 + c_1\frac{Q}{N}x_i + c_2 Nx_i + c_3 Qx_i$$

We tested the validity of this equivalent steady state relation using measured input-output data for feed-rates, screw speed and torque at various steady state conditions over multiple days.

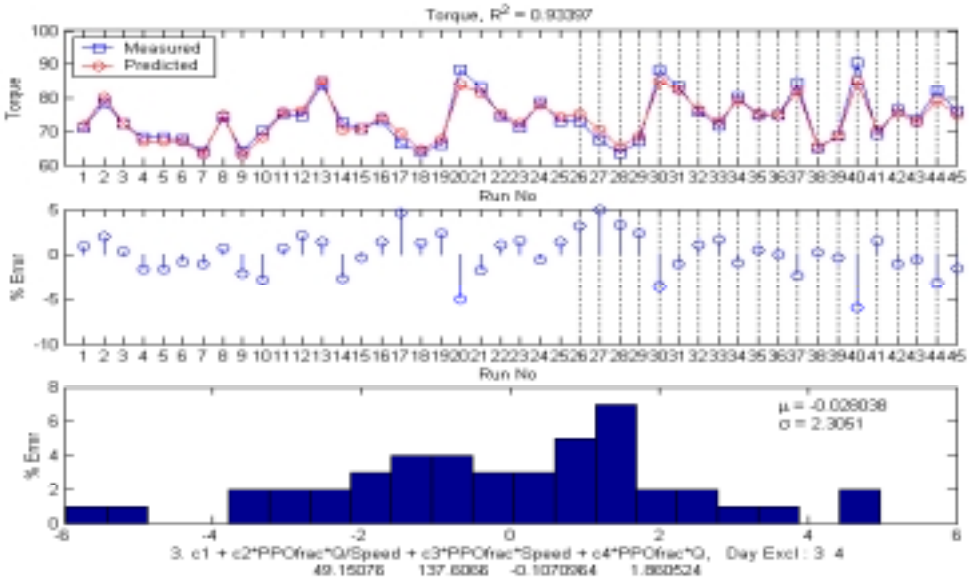

Figure 10: Input-output relation for torque at steady state

Figure 10 shows the comparison of the measured torque and the model fit using Eq 8 for 45 steady state points obtained on four separate days. In particular, we fit the model parameters c_i, or equivalently α_i, using the data from the first 25 points and tested its validity against the last 20 points. Clearly, the model validates very well against the measured torque data with an overall R^2 value of 93.4%.

Similarly, a relation for die pressure *DP* as a function of the process variables is obtained from physics using the laminar flow relation for pressure drop in a circular pipe (treating the die plate holes as an effective short pipe) for the molten product with a viscosity μ flowing through the die plate at a rate Q_o (for a detailed description of die pressure model see Appendix Section 2). It can be seen that the key parameters that affect the die pressure *DP* are the product throughput and viscosity.

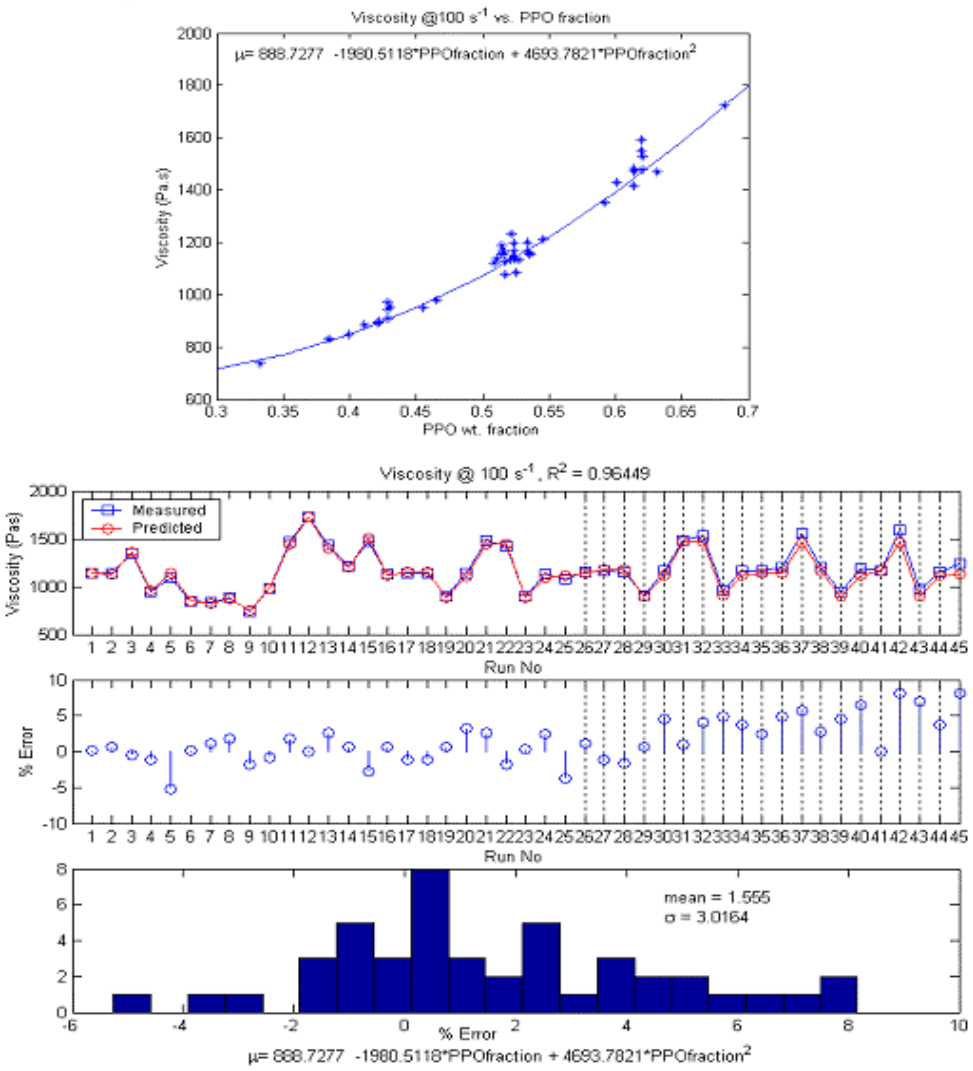

Figure 11: Comparison of measured viscosity variation with PPO fraction and model fit.

In general, the product viscosity at the die depends nonlinearly on the corresponding product composition, temperature and shear rate. For the NORYL product we tested, the viscosity of the product has a quadratic dependence on the weight fraction of PPO content. In general, the dependence of viscosity on composition may be described by a higher order polynomial. Figure 11 shows the plot of viscosity measured using a capillary rheometer for 45 samples collected at steady state conditions over 4 days with a wide composition range, and the fit obtained with a 2nd order equation using data from first two days and validating against data from the last two days. Clearly, the 2nd order equation for viscosity as a function of the product PPO weight fraction has a good fit with an R^2 value of 96.4% and maximum error between measured and fit values less than 8% (1σ – 3%). The dependence of viscosity on shear rate, is typically given by a power law, while its dependence on temperature is governed by an Arrhenius-type exponential function. For

our purposes, we approximate the nonlinear dependence of viscosity on composition, shear rate and temperature with a linearized relation:

Eq 9 $$\mu = \mu_o + \mu_1(x_o - \bar{x}_o) - \mu_2(Q_o - \overline{Q}_o) - \mu_3(T_o - \overline{T}_o)$$

The above relation describes the variation in the product viscosity around the nominal operating conditions $\bar{x}_o, \overline{Q}_o, \overline{T}_o$; here T_o denotes the melt temperature measured at the die. The above linearized relation for viscosity yields the following relationship for die pressure:

Eq 10
$$\begin{aligned} DP &= kQ_o[\mu_o + \mu_1(x_o - \bar{x}_o) - \mu_2(Q_o - \overline{Q}_o) - \mu_3(T_o - \overline{T}_o) \\ &= \beta_1 Q_o + \beta_2 Q_o \Delta x_o - \beta_3 Q_o \Delta Q_o - \beta_4 Q_o \Delta T \end{aligned}$$

The dynamic material holdup and composition relations and the relations for torque and die pressure comprise the overall dynamic model for the extrusion process, relating changes in the process inputs (feed-rates and screw speed) to the measured output variables (torque and die pressure)

Dynamic Process Model:

Eq 11
$$\frac{dM_1}{dt} = Q - Q_{1o} \qquad (Q = Q_1 + Q_2, \quad Q_{1o} = \frac{M_1 N}{B})$$
$$M_2 = A$$
$$x_1(s) = \frac{Qe^{-t_{d1}s}}{Q + R_1 * Q_{1o}(1 - e^{-t_{d1}s})}\, x_i(s), \qquad (x_i = \frac{Q_1}{Q_1 + Q_2}, \quad t_{d1} = \frac{M_1}{Q_{1o}(1 + R_1)})$$
$$x_2(s) = \frac{e^{-t_{d2}s}}{1 + R_2 * (1 - e^{-t_{d2}s})}\, x_1(s), \qquad (t_{d2} = \frac{M_2}{Q_{1o}})$$
$$T = \alpha_0 + \alpha_1 M_1(\alpha_2 + N)x_1 + \alpha_3 M_2 N x_2$$
$$DP = \beta_1 Q_o + \beta_2 Q_o \Delta x_o - \beta_3 Q_o \Delta Q_o - \beta_4 Q_o \Delta T$$

The above model is a simple low-order lumped model in the so-called state-space form with several input, state, output variables and parameters listed below.

Inputs

Q_1 : feed-rate of PPO
Q_2 : feed-rate of PS
N : screw speed

⇨

Q_i : total feed-rate = $Q_1 + Q_2$
x_i : weight fraction PPO at inlet = Q_1/Q_i

States

M_1 : mass holdup in partially filled section of screw
M_2 : mass holdup in completely filled section of screw
x_1 : wt. fraction PPO in partially filled section
x_2 : wt. fraction PPO in completely filled section

Outputs
Q_o : outlet mass flow rate
x_o : PPO fraction at outlet = x_2
T : total torque
DP : die pressure
Parameters
A,B : extruder geometry-dependent parameters for holdups
R_1, R_2 : recycle ratios to capture mixing in partially/completely filled sections
α_0-α_3 : parameters in torque relation
β_1-β_4 : parameters in die pressure relation

5.1.5 Dynamic Model Parameters

The parameters in the dynamic model in Eq 11 will depend on the specific extruder geometry and the product application and need to be identified from measured input/output data. However, the task of identifying these parameters is simplified by observing that the parameters can be categorized into two sets:

1. the first set consisting of the parameters A, B, R_1 and R_2 depend on the specific screw geometry and will be invariant once the extruder screw geometry is fixed.
2. the second set consisting of the parameters α_i and β_i depend on the particular process conditions and will change from one product grade (family) to another and these parameters need to be identified depending on the operating conditions.

An initial value of all the parameters can be obtained through an off-line least squares fit using the measured input-output data from an initial calibration experiment. Thereafter, we need to update only the process-dependent parameters α_i and β_i, while the machine-dependent parameters A, B, R_1 and R_2 are kept constant as long as the screw geometry remains unchanged. We will address the on-line identification of the process-dependent set of parameters α_i and β_i in a later on-line identification section. In this section, we present the results obtained by fitting the parameters to match the model input-output predictions with on-line measurements obtained during a calibration run.

Figure 12 and Figure 13 show the results of the initial off-line least squares fit comparing the model predictions for the torque and die pressure (shown in red) with the on-line measurements (shown in blue) obtained during an experiment run on 05/08/2001 on the 25mm extruder with NORYL polymer using nominal raw materials (PPO IV 0.46) and nominal composition (PPO fraction 0.52). Clearly, the model predictions match very well with the on-line measurements with R^2 values of 91% and 93% for die pressure and torque, respectively.

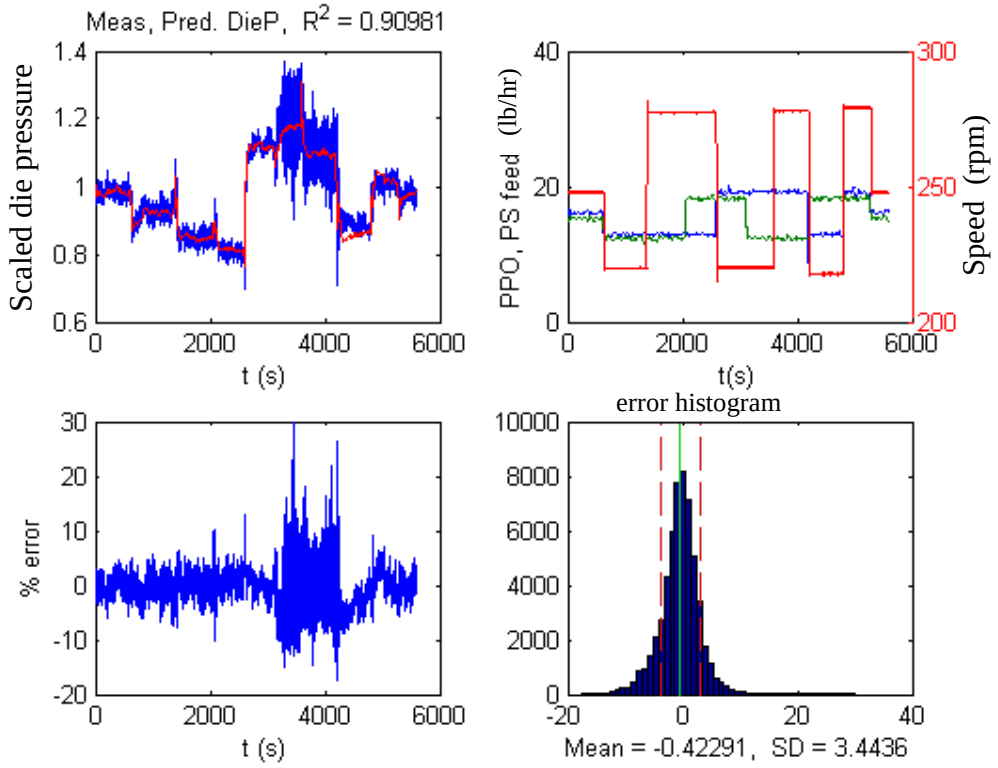

Figure 12: Comparison of Die Pressure measurement with model prediction

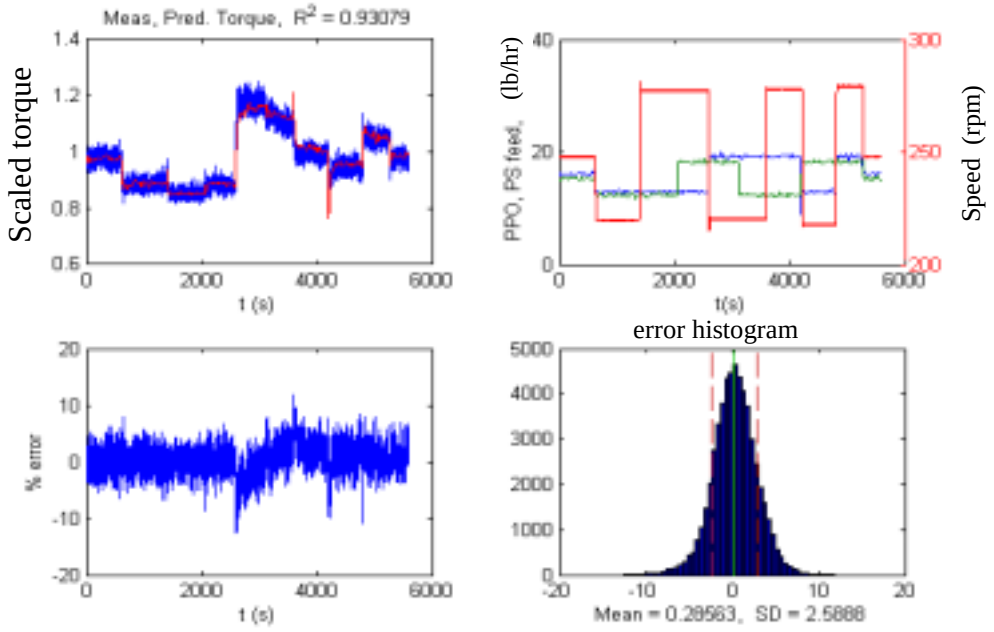

Figure 13: Comparison of torque measurement with model prediction

5.1.6 Comparison of Model Predictions

Despite the simplicity of the model it suffices for our purposes of predicting the responses in key measured outputs like total screw torque and die pressure as a function of the process inputs like feed-rates and screw speed and other process parameters. In particular, the model captures both the steady state and transient characteristics for the two measured outputs very well.

The transient response for total screw torque T shows an inverse response with respect to screw speed changes (see Figure 14). This occurs due to the fact that starting at some steady state as the screw speed is increased, the torque initially rises proportionally (see Eq-A 9). However, due to the increased speed more material is withdrawn from the partially filled section until the holdup M_1 in this section reaches a new lower steady state value – since total feed-rate Q is unchanged, the new steady state value has to be lower such that the outlet flow rate $Q_{1o} = M_1 N / B$ is the same as before the increase in screw speed N. Consequently, as a result of reduced holdup M_1, the total torque eventually reduces after the initial increase.

The die pressure DP shows an inverse response with respect to screw speed N (see Figure 15). This occurs due to the fact that starting from a steady state, as the screw speed N is increased, the outlet flow rate Q_{1o} from section 1 and hence from section 2 increases thereby leading to an initial increase in DP. But, again since the overall feed-rate has not been changed, the outlet flow rate will reach a final steady state value same as before the increase in the screw speed. However, the increased speed generates more heat due to viscous dissipation thereby increasing the melt temperature, which reduces the product viscosity and thus reducing the die pressure DP.

The die pressure DP shows an inverse response with respect to the PS feed-rate (see Figure 16). Initially, starting from a steady state, as the PS feed-rate is increased, the total throughput and hence the outlet product flow rate increases thereby increasing the die pressure. However, the increased PS feed-rate reduces the PPO weight fraction x_i, which eventually leads to a reduced PPO weight fraction x_{2o} at the outlet which leads to a reduced product viscosity and hence reduced die pressure DP. The die pressure doesn't exhibit such an inverse response with respect to PPO feed-rate since an increase in the PPO feed-rate leads to an increased throughput and an increase in x_{2o}, both of which contribute to an increased die pressure DP.

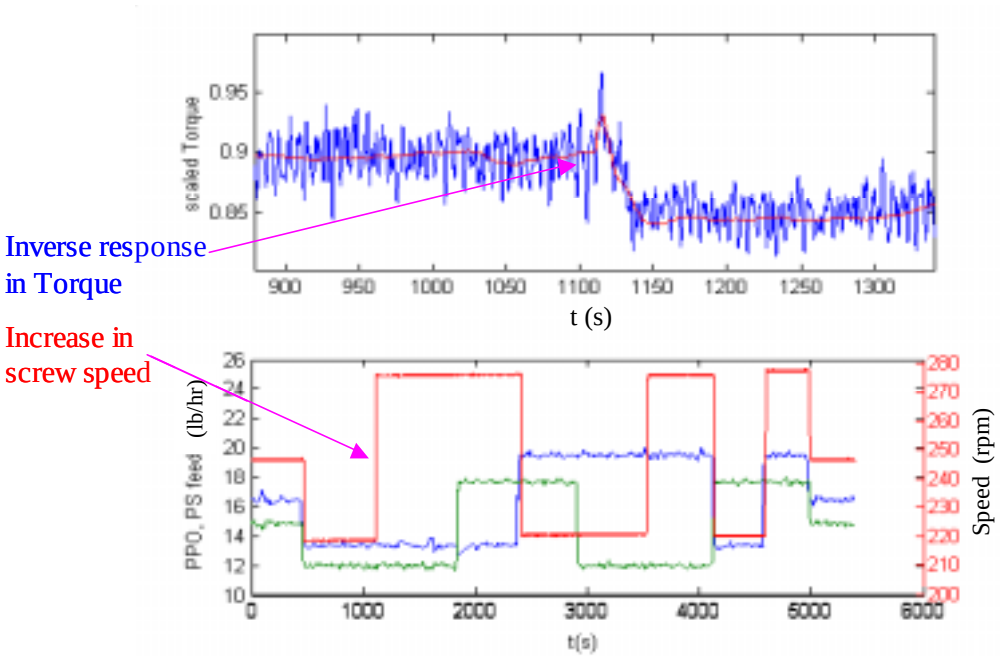

Figure 14: Inverse response in torque with respect to screw speed

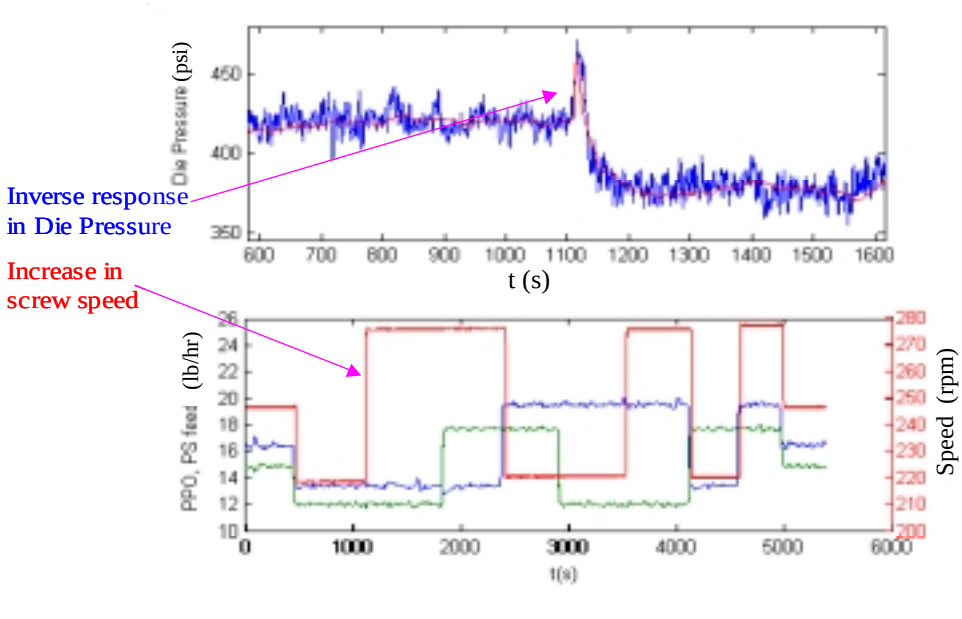

Figure 15: Inverse response in die pressure with respect to screw speed

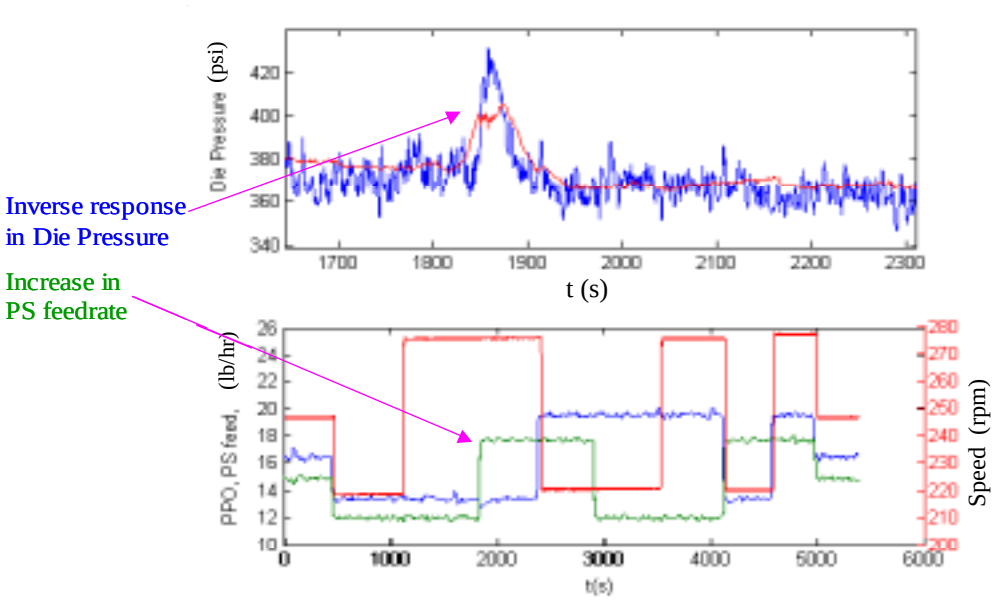

Figure 16: Inverse response in die pressure with respect to PS feed-rate

5.2 Extruder Modeling Summary

We have developed a simple, physics-based dynamic model for a typical extrusion process that can be applied to a wide variety of extrusion applications to describe their transient input-output behavior. We have demonstrated the application of the model on a lab-scale 25mm extruder to describe the dynamic input-output behavior, specifically the response in on-line measurements like torque and die pressure (readily measured in most extruder applications) as a function of variations in extruder operating conditions. Scale-up of the model to an industrial production-scale extruder is also demonstrated in Section 10.

The model has several unknown parameters, which need to be identified for specific applications based on on-line input-output measurements from experiments. However, the identification of these parameters is greatly simplified by grouping the parameters into machine-dependent and process condition-dependent sets. The former set of parameters need to be identified only once for a given extruder geometry, while the latter set of parameters will, in general, vary depending on the process conditions. This variation of the parameters will be addressed through on-line identification and used for the fault diagnostics and inferential estimation as described in later sections.

6 On-line Parameter Identification

The dynamic process model described in the previous section involves unknown model parameters that need to be identified from measured input-output data. These parameters will vary for different extruders and process applications. The physics-based nature of the model allows categorizing the parameters into two broad classes:

(i) parameters depending on the machine geometry (A, B, R_1, R_2), and
(ii) parameters depending on the material properties and process operating conditions (α_i, β_i).

The unknown model parameters can be identified for a given extruder setup once using experimental input-output data and a least-squares fit (see previous section). Thereafter, the machine parameters are fixed for the specific extruder and screw geometry. In contrast, the material parameters will in general vary from day to day, due to variations in process conditions, raw materials etc., and need to be identified on-line.

For the on-line identification, the machine-dependent parameters *(A, B, R_1, R_2)* are fixed at the values obtained by off-line identification, while the parameters α_i in the torque relation in Eq 7 and the parameters β_i in the die pressure relation in Eq 10 are to be identified on-line. In our experiment runs with NORYL PX5511 grade resin, we observed that the nominal set of parameters α_i (identified by off-line identification) captured the transient variation in torque with process condition changes quite well, in-spite of changes in raw material and composition. Moreover, the parameters α_i are difficult to interpret due to a lack of explicit relationship to physical parameters. On the other hand, the parameters β_i for die pressure have explicit relationship with physical parameters μ_i in the viscosity relation (see Eq 9 and Eq 10), given by:

Eq 12
$$\beta_1 = k\mu_o$$
$$\beta_2 = k\mu_1$$

where k is a machine/product grade (family) dependent calibration parameter. Furthermore, these parameters varied significantly under varying raw material and/or composition variations as expected from the physics. So, we focused exclusively on the on-line identification of β_i to meet the objectives of diagnostics and estimation.

Equation Eq 10 has two important features for our purposes.

1. It relates process inputs and process output, die pressure, where the parameters β_i have a physical significance owing to their explicit relationship to the parameters μ_i – we will exploit this to meet the objectives of estimation and diagnostics.
2. It is linear with respect to the parameters β_i.

Having a relation linear with respect to parameters allows use of on-line recursive adaptation techniques, with relatively low computational burden. To facilitate the online identification of the parameters β_i (or equivalently μ_i) we provided excitation to the system via a pseudo-random binary sequence (PRBS) variation in the inputs (feed-rates

and screw speed) and recorded the corresponding die pressure measurement. This excitation of the process (referred to as persistent excitation) is necessary for correct identification of the new parameters β_i under changing raw material/ process conditions.

For the online identification of the parameters β_i, we adopted the following well-known recursive least-squares formulation in our approach, given by (see e.g. Ljung[18] Chapter 11):

Eq 13
$$\hat{\theta}(t) = \hat{\theta}(t-1) + \frac{P(t-2)\phi(t-1)}{1+\phi(t-1)^T P(t-2)\phi(t-1)}[y(t) - \phi(t-1)^T \hat{\theta}(t-1)]$$

Eq 14
$$P(t-1) = P(t-2) + \frac{P(t-2)\phi(t-1)\phi(t-1)^T P(t-2)}{1+\phi(t-1)^T P(t-2)\phi(t-1)}$$

where $\theta = [\beta_0 \quad \cdots \quad \beta_3]^T$ denotes the parameters to be recursively identified, $\phi(t) = [1 \quad Q_o(t) \quad Q_o(t)x_o(t) \quad Q_o(t)\Delta T(t)]^T$ denotes the coefficients of these parameters in the die pressure relation in Eq 10 and *P(t)* is the parameter covariance matrix. The covariance matrix *P(t)* is initialized with a pre-selected positive definite covariance matrix P_o reflecting the confidence in the initial estimates of the parameters.

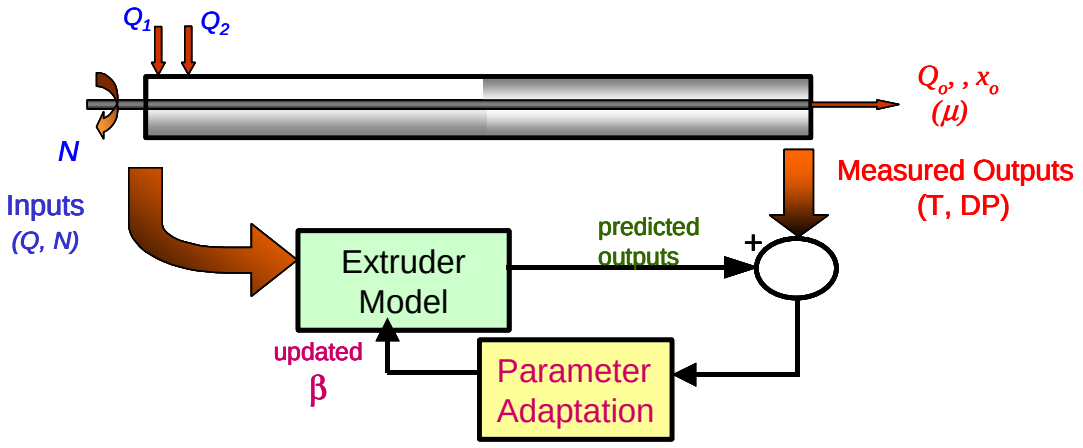

Figure 17: Schematic representation of on-line parameter identification approach.

Figure 17 shows the schematic approach for the on-line parameter identification for the extrusion process. In particular, the measured process inputs (feed-rates and screw speed) are fed to the model and its prediction for the outputs (die pressure) are compared with the on-line measurements to generate the residual error. Under nominal conditions, the residual error will be normally distributed (due to noise) with a zero mean. However, if the operating conditions change, e.g. change in raw material, feed composition, then the model predictions with the nominal parameters β_i will no longer match the measured values, i.e. the residual error will no longer be zero mean or normally distributed. Under

such a situation, the on-line identification of the unknown parameters β_i will be started with a pre-set sequence of persistently exciting variations in the inputs, PPO feed, PS feed and screw speed that yield a well-conditioned information matrix formed with vectors of $\phi(t) = [1 \quad Q_o(t) \quad Q_o(t)x_o(t) \quad Q_o(t)\Delta T(t)]^T$ in time (see [18] and Section 8 on fault diagnostics in this report for more detail).

6.1 On-Line Parameter Identification Results

We tested the on-line identification capability in multiple runs over several months for variations in raw material and composition from nominal conditions. We show the results of the model predictions compared with the on-line measurements for two representative runs after the recursive parameter adaptation, one with change in raw materials and another with a large change in composition (similar to a product grade change). In all cases, the parameter adaptation started with parameter values initialized for nominal conditions obtained by the least squares optimal fit obtained in Section 5.1.5.

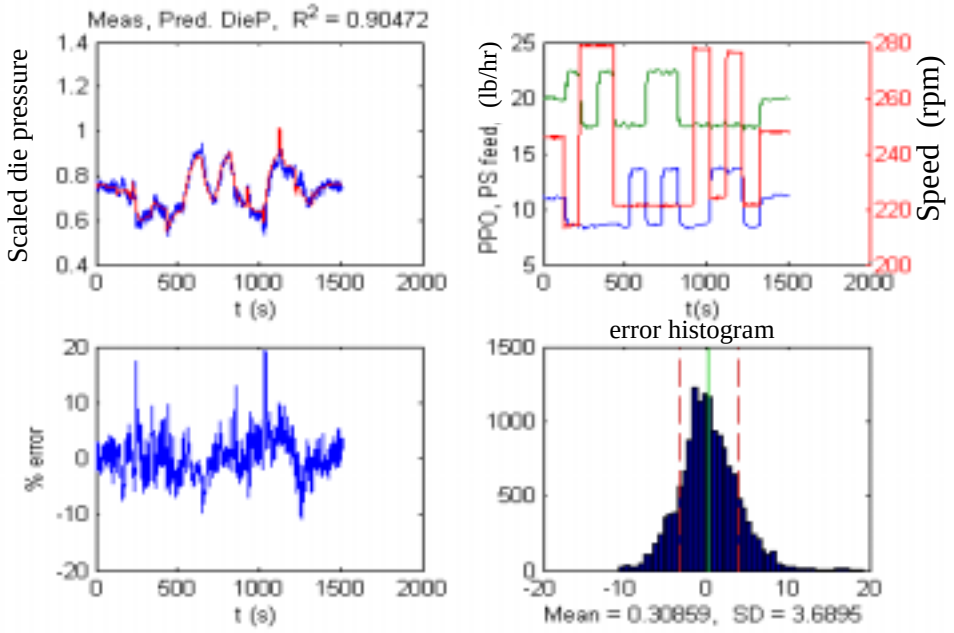

Figure 18: Comparison of model prediction after on-line adaptation vs measurement for die pressure under composition change from nominal conditions

Figure 18 demonstrates the match between die pressure predictions of the extruder model and measurements obtained in experiment run on 5/22/01 at GE GR for nominal raw materials (0.46 IV PPO) but a significantly different composition (PPO fraction 0.35) – this large change in composition corresponds to another product grade. During this run, a PRBS variation in the inputs (PPO, PS feed-rates and screw speed) was used and the parameters β_i were adapted following the above recursive least squares method starting from the nominal values obtained on 05/08/2001. Note that the die pressure during this run (Figure 18) is distinctly lower than that in the nominal run on 05/08/2001 (Figure 12)

- the die pressure is plotted after normalizing with respect to the nominal value of 450psi, i.e. the normalized die pressure is 1.0 at nominal conditions. This is as expected, since the lower PPO composition implies a lower product viscosity and hence lower die pressure. Clearly, the parameters β_i were adapted well to match the model predictions with the measurements and capture the effect of composition change, with a modified R^2 value of 90.5% and a normally distributed residual error between the measurement and the model prediction.

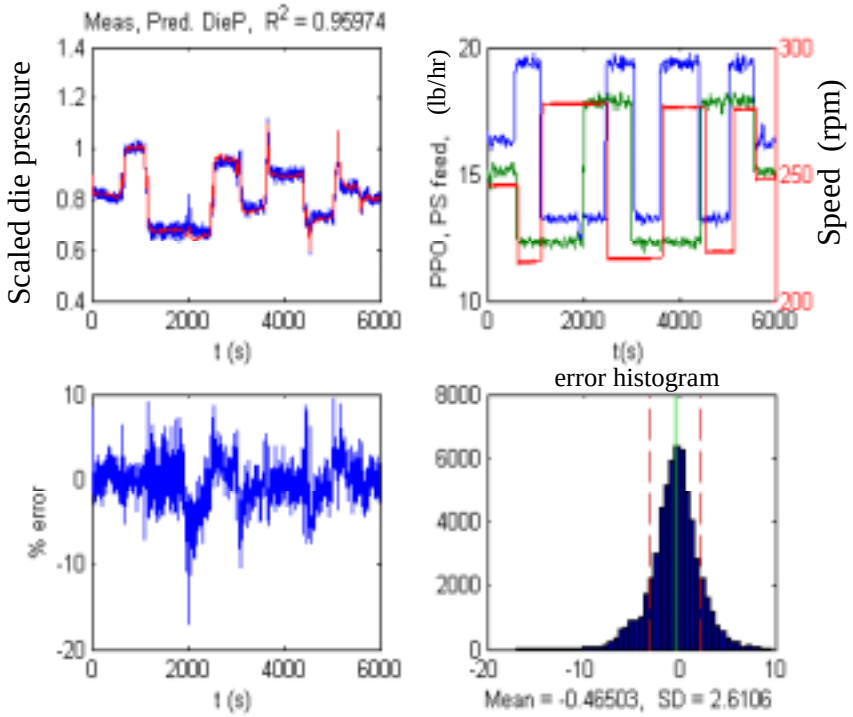

Figure 19: Comparison of model prediction after on-line adaptation and measurement of die pressure under raw material change from nominal conditions

Similarly, we conducted another experiment on 8/27/01 at GE GR with the nominal composition (PPO fraction 0.52) but with a different raw material. In particular, we used a low IV PPO (0.33 IV) and conducted a similar PRBS experiment to facilitate the on-line identification of the parameters β_i. Again, the lower IV PPO results in a product with lower viscosity and hence lower die pressure than in the nominal run.
Figure 19 demonstrates the fit obtained after the on-line identification between die pressure measurement and the model prediction with updated β_i. Clearly, the parameters were identified accurately to capture the effect of raw material change, with a modified R^2 value of 95.9% and a normally distributed residual error between the model prediction and measurement.

6.2 On-line Parameter Identification Summary

Process dependent parameters α_i and β_i in the torque and die pressure relations will, in general, change depending on changes in raw materials and feed composition. Under

nominal conditions, the initial set of parameters obtained for a family of product grades using the off-line least squares fit described in Section 5.1.5 will suffice for the model predictions for torque and die pressure to match with the on-line measurements. However, in the presence of deviations from nominal conditions, these parameters will need to be adapted on-line. We applied recursive on-line adaptation techniques to track changes in these parameters. For the NORYL grade polymers we studied, the nominal parameters α_i described the variations in torque despite changes in raw materials and composition. So we focused exclusively on the adaptation of the parameters β_i for die pressure. The on-line identification of the parameters β_i works very well in the presence of changing process conditions. The on-line identification of the parameters β_i to capture effects of changes in raw material and/or composition will be exploited in the subsequent sections for fault diagnostics and inferential sensing.

7 Inferential Sensing

In this section, methods are derived for the on-line inferential estimation of product viscosity from on-line measurements of the inputs (feed-rates and screw speed) and the outputs (die pressure). In a typical production environment, the product viscosity is measured only off-line using samples from the finished product in a QA lab. Very often, due to the limited resources and the large number of production lines and production batches each day, only one sample is collected per batch for the QA lab analysis. This leads to ineffective characterization of good/bad product batches: A batch of good material that was out of spec only at the end of the run may be rejected, and bad material that was good at the time of sampling may be passed with once per batch QA tests. Such inefficient characterization of production quality leads to avoidable losses of material and energy. The ability to monitor viscosity on-line is a significant leap that will enable quick classification of good or bad product and enable corrective action, e.g., on-line closed-loop control, to maintain products within specification limits and minimize waste production. We will address the on-line estimation of product viscosity using the physics-based modeling and adaptation framework of previous sections.

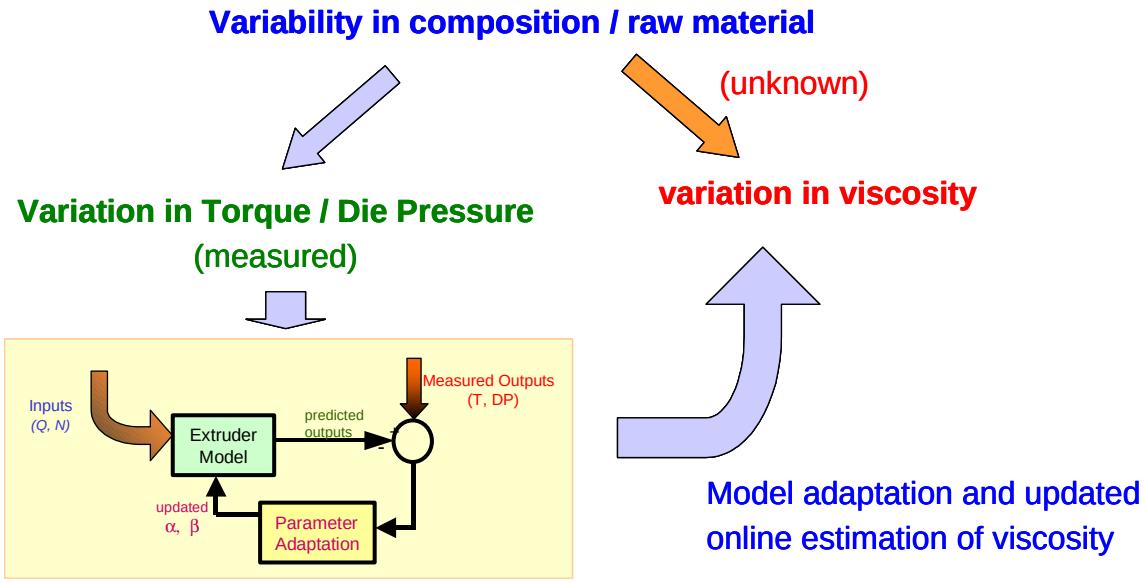

Figure 20: Approach for model-based estimation of viscosity

Figure 20 shows the approach for online viscosity estimation from the measurements of the process inputs and outputs. In particular, as the raw materials or feed compositions change, thereby changing the viscosity, we obtain a continuous estimate for the viscosity from on-line identification of the parameters β's. Once the extruder model parameters β's are identified, they are used to estimate nominal viscosity μ_0 and slope μ_1 using a value for k (see Eq 9, Eq 10 and Eq 12). The required value of k is obtained by comparing the parameters β's and the viscosity measured in the lab for samples collected during an initial calibration run, and then fixed thereafter for all other runs. The product viscosity is then estimated using the linearized viscosity relation (Eq 9) disregarding the shear rate and temperature effects since these are fixed for the lab measurements and the product quality specifications, i.e.

Eq 15 $$\mu = \mu_o + \mu_1 (x_o - \bar{x}_o)$$

and the product composition at the extruder outlet $x_o = x_2$ obtained from the dynamic model. The following figures depict the comparison of on-line viscosity estimates with the off-line lab viscosity measurements of samples collected at multiple steady state conditions with different compositions during each run. In all these comparison figures, the magenta line represents the estimated value of viscosity and blue line represents the off-line viscosity measurement in the lab.

7.1 Viscosity Estimation Results

Figure 21-Figure 26 that follow, show the viscosity estimation results for the multiple runs with nominal raw materials and lower IV PPO over a large composition range

spanning nominal compositions for several NORYL product grades at GEP Selkirk. The estimation results shown by magenta lines are compared with the corresponding off-line lab measurements of samples collected during steady state operating conditions in each run.

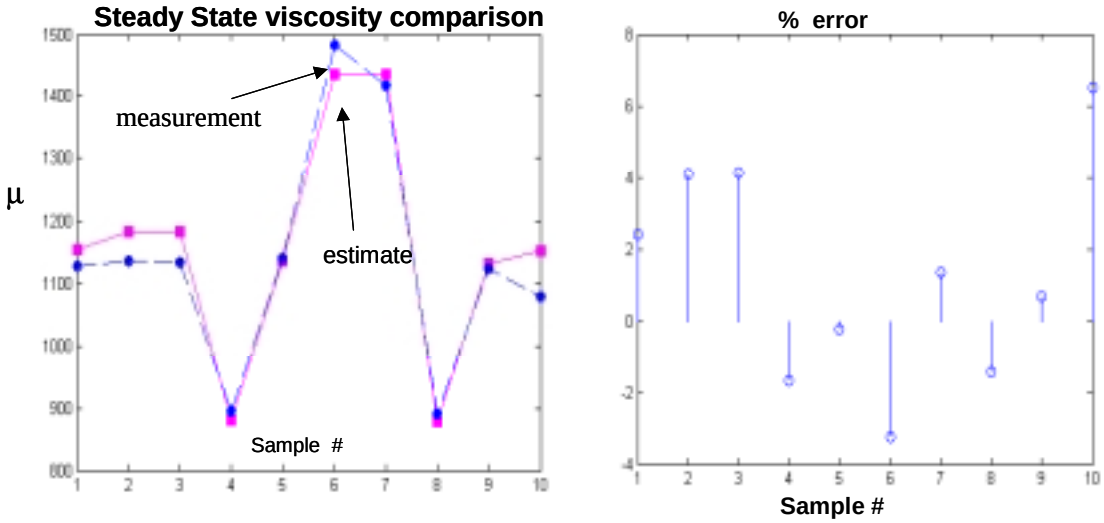

Figure 21: Comparison of on-line viscosity estimation and off-line lab viscosity measurements for experiment on 5/8/2001 with nominal (.46 IV) PPO blend

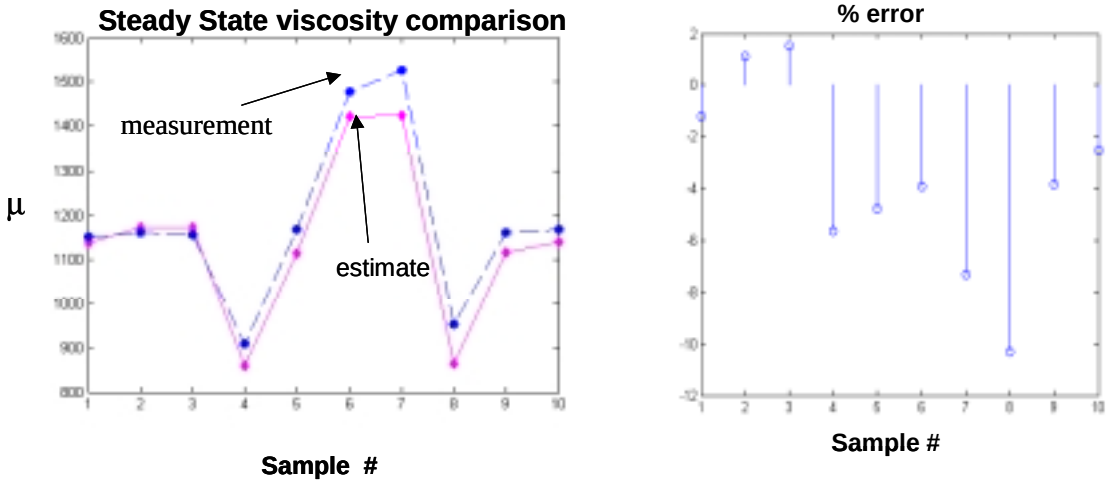

Figure 22: Comparison of on-line viscosity estimation and off-line lab viscosity measurements for run on 6/25/2001 with nominal (.46 IV) PPO blend

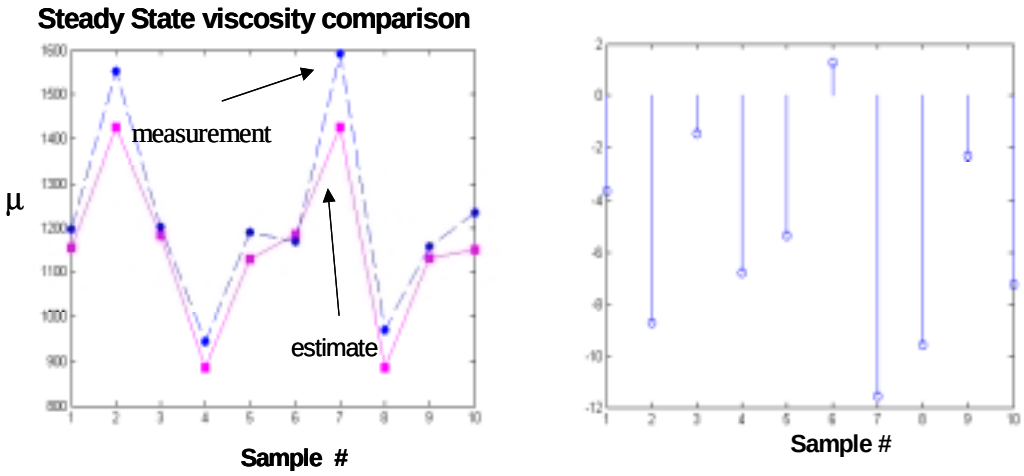

Figure 23: Comparison of on-line viscosity estimation and off-line lab viscosity measurements for run on 7/25/2001 with nominal (.46 IV) PPO blend

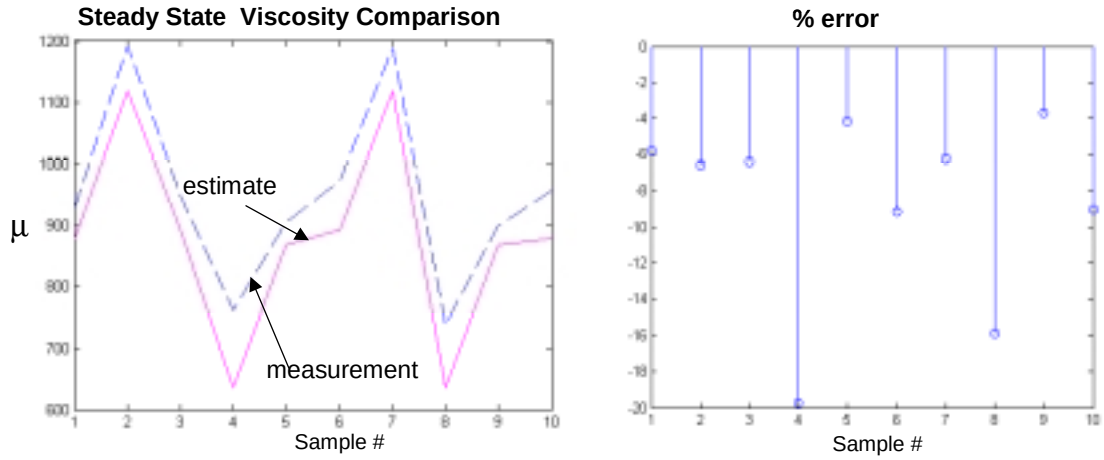

Figure 24: Comparison of on-line viscosity estimation and off-line lab viscosity measurements for run on 8/27/2001 with low IV (.33 IV) PPO blend

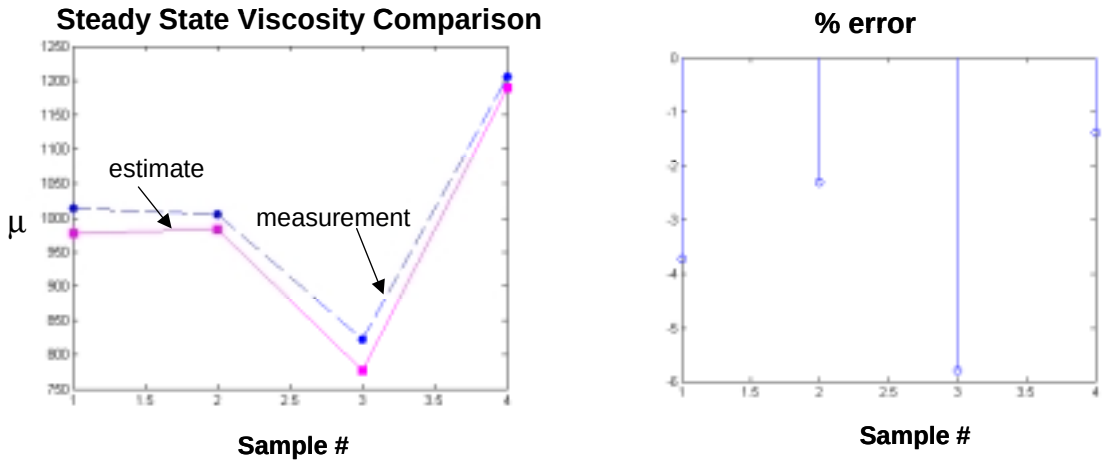

Figure 25: Comparison of on-line viscosity estimation and off-line lab viscosity measurements for run on 10/11/2001 medium IV (50/50 mixture of .46 IV and .33 IV) PPO blend

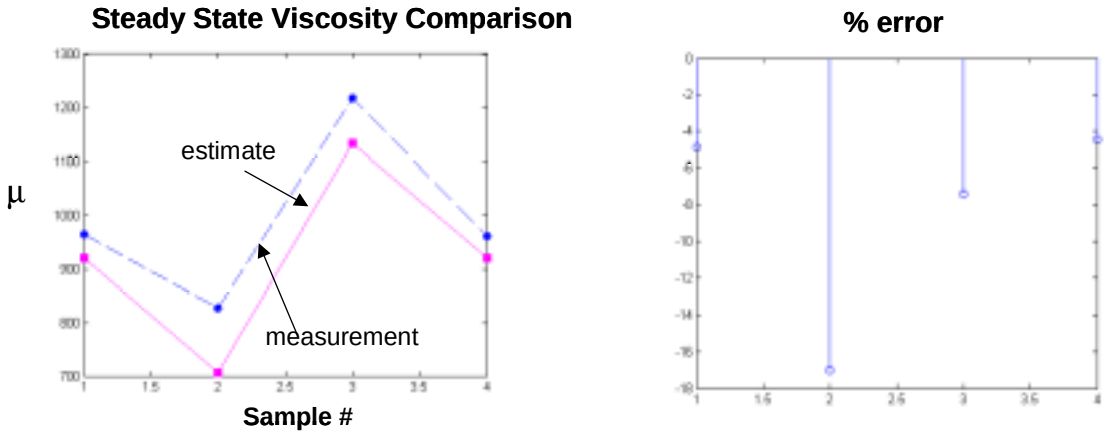

Figure 26: Comparison of on-line viscosity estimation and off-line lab viscosity measurements for run on 11/14/2001 with medium IV (50/50 mixture of 0.33IV and 0.46 IV) PPO blend

7.2 Viscosity Estimation Summary

Date of Experiment	No. of samples	Raw Materials used	Composition (PPO fraction)	Estimation error
5/8/2001	*10*	Nominal	0.42-0.61	-4 to +4%
6/25/2001	10	Nominal	0.43-0.62	-10 to +2%
7/25/2001	10	Nominal	0.43-0.62	-12 to +2%
8/27/2001	10	Low IV PPO	0.43-0.62	-6 to 0% (except 2 samples)
10/11/2001	4	Medium IV PPO	0.43-0.6	-6 to 0%
11/14/2001	4	Medium IV PPO	0.43-0.6	-8 to 0% (except 1 sample)

Table 3: Summary of viscosity estimation results

Table 3 above summarizes the results of model-based on-line viscosity estimation compared to off-line lab measurements. Altogether, we collected about 50 samples during steady state conditions in experiment runs conducted over several months with a wide range of variations in product composition and raw materials spanning multiple NORYL product grades. We compared the viscosity of these samples as measured in the lab, using a capillary rheometer with those estimated by the model-based estimation. The overall estimation results are very good with an error in the range of +/-10% of the measured values, which is within the range of error of the off-line viscosity measurement using capillary rheometer. The error is larger than 10% for specific samples (e.g. samples 4 & 8 on 8/27/2001 -Figure 24, and sample 2 on 11/14/2001 - Figure 26) that correspond to very low PPO content and thus low viscosity. These samples correspond to the maximum deviation from the nominal composition (PPO fraction 0.52) and the linear approximation for viscosity as a function of composition used in the die pressure model (see Eq 9 and Eq 10) becomes inaccurate under these extreme deviations, thus leading to larger error. One way to alleviate these inaccuracies under these extreme composition limits is to include higher order nonlinear terms in the dependence of viscosity on composition, albeit at the expense of additional model parameters and increased complexities in the recursive on-line parameter identification. A simpler approach would be to linearize the viscosity model close to the extreme composition limits to minimize the errors due to linearization.

8 Extruder Diagnostics

In this section, we address the problem of fault diagnostics for the extruder using the developed modeling and adaptation framework described in the previous sections. Figure 27 shows a schematic diagram of a typical extrusion process and various sources of variability that cause product variability. The sources of variability include a wide array of raw material, equipment and operator variations. Among these possible sources of faults, the major ones that occur most frequently and are not readily detected by simple practical means, and affect product quality are associated with variations in raw material quality and feeder variations. Motivated by this, we will focus on the detection of raw material and feeder variation as the main process faults, using available on-line measurements.

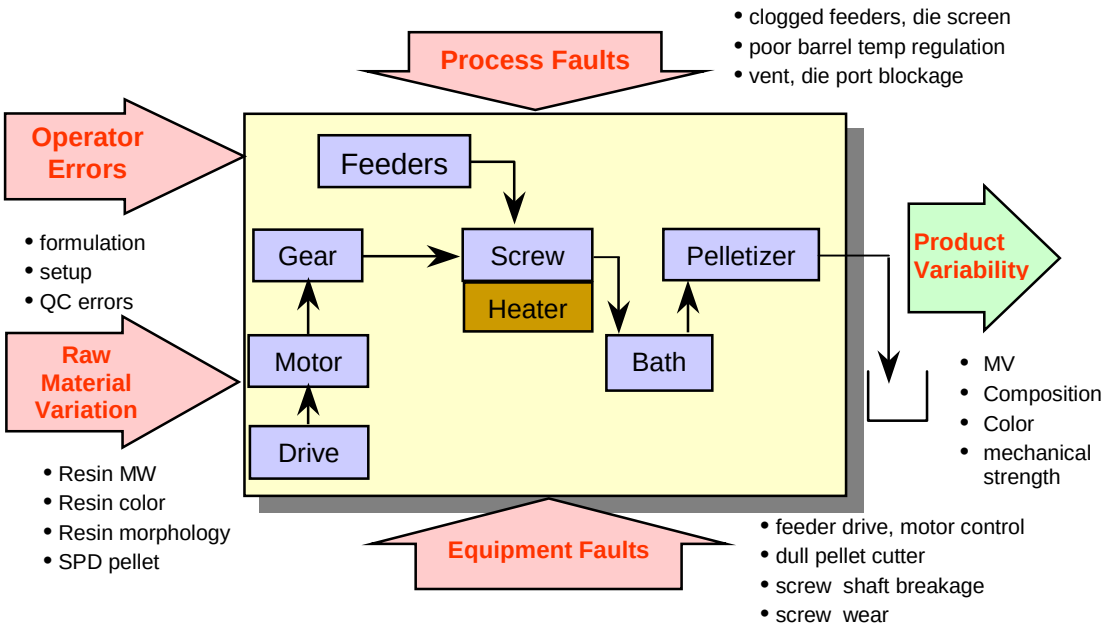

Figure 27: Schematic diagram of extrusion process and sources of product variability

8.1 Problem and Approach

The problem of fault diagnostics entails the *detection* that a fault has occurred, and the *classification* of the cause of the faults among multiple potential candidates. A standard issues that arises in the detection and identification of faults is the trade-off between false alarms, i.e. false declaration of faults in nominal conditions, and missed detects, i.e. missing the occurrence of an actual fault. A tradeoff between is required between acceptable limits of nuisance from false alarms and acceptable losses from missed fault detection. Another important issue for fault detection is the latency or time elapsed from

the occurrence of a fault to its detection, identification and correction to minimize the waste production in this time interval.

Figure 28 shows a schematic representation of the various phases during a typical fault occurrence, detection, identification and correction. In phase 1, the process is initially operating at nominal conditions and the model prediction using nominal model parameters matches well with the on-line measurements (e.g. for die pressure). An unknown fault then occurs (either abruptly or gradually over time) at the end of phase 1, which leads to the on-line measurements deviating from the model prediction (using nominal parameters). Depending on the type of fault, the difference between the measurement and the model prediction (or the integral square of the difference—see e.g. [17] for alternate approaches to detection and classification using comparison of model to measurements) would exceed a threshold, indicating the occurrence of a fault (at the end of phase 2). The source of fault is however not known at this stage. After the fault detection, the process can be excited with changes in the inputs (feed-rates and screw speed) and the model parameters adapted to match its prediction with the on-line measurement, thereby obtaining a new set of model parameters reflecting the "faulted" process conditions. At the end of this adaptation stage 3, the source of the fault is uniquely classified and enables appropriate corrective control action in phase 4, which may be either a physical action, e.g. recalibration of drifted feed-rate measurements, or an automatic on-line closed-loop control correction using inferred viscosity based on the adapted model parameters. Finally, the corrective control action brings the process back within specification limits to achieve on-spec production in phase 5. The time duration of the fault detection, fault identification and corrective control in phases 2, 3 and 4 determine the amount of off-spec waste produced during a fault. Note however, that the detection of a fault at the end of phase 2 enables the possibility of physically diverting the off-spec product during phases 3 and 4 to minimize the contamination of the finished product.

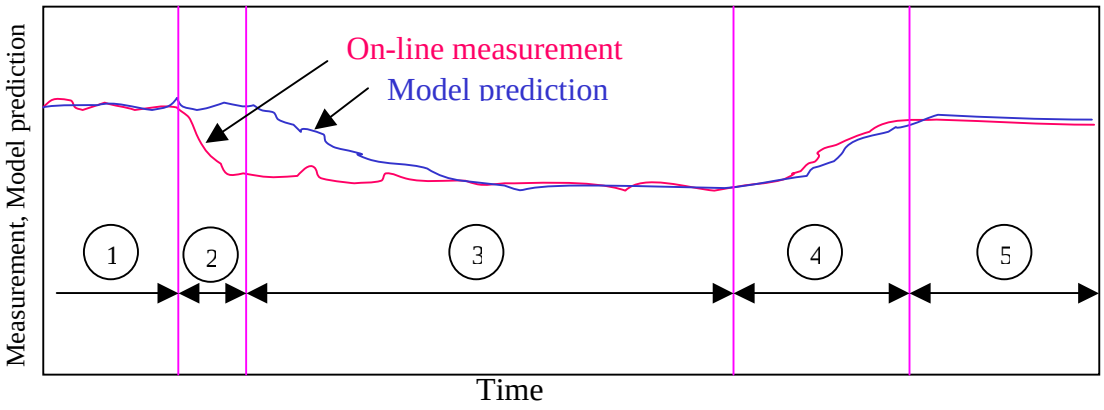

Figure 28: Schematic description of fault detection and correction with distinct phases – (1) initial nominal operation, (2) fault occurrence and detection – mismatch between model and measurement, (3) model update – on-line model adaptation and fault identification, (4) corrective control action for fault, (5) on-spec operation after fault correction.

The fault diagnostics clearly consists of two phases in the above description, the initial detection phase where a fault (unknown) is declared to have occurred, and the second classification phase, where a specific fault is identified, e.g. raw material change or feeder bias.

For our purposes the two key on-line extruder output measurements are die pressure and torque. During our experiments with NORYL, while both torque and die pressure were sensitive to composition changes, only die pressure was sensitive to raw material changes. Moreover, the changes in torque and die pressure were often correlated. Motivated by these, we focused on die pressure for the diagnostics algorithm. Using die pressure as the output signal, the detection of occurrence of a fault is addressed simply by monitoring the difference between the measured die pressure and the value predicted by the dynamic model as a function of measured inputs, i.e. feed-rates and screw speed. Under nominal conditions this difference will be below a threshold – chosen based on the noise characteristics of the signals ([17]). However, in the presence of a fault, i.e. feeder bias or raw material change, the product viscosity will change, thereby changing the die pressure. Thus, the measured die pressure will deviate from the model prediction using the nominal parameters, and for a sufficiently large enough fault, the discrepancy between the measured die pressure and the model prediction will exceed the threshold – thereby declaring a fault occurrence. Clearly, the choice of such a threshold for the mismatch between the model prediction and measured value depends on the signal to noise ratio and affects the occurrence of false alarms and missed detects. Based on the actual signal to noise characteristics and the normal operation spec-limits, an optimal threshold can be chosen to optimize the trade-off between false alarms and missed detects. Once a fault has been declared based on the discrepancy between the model prediction and the measured die pressure, the second stage of fault classification, i.e. the identification of the fault source will initiate.

There are several techniques available for fault identification, e.g. multi-model hypothesis testing, data classification and correlation with fault/nominal signatures, as summarized in Gertler for example [17].Multiple-model hypothesis testing approaches the problem of fault detection by comparing the measured output with predictions from a bank of models, one each for the nominal and all the fault conditions. With assumptions of linear dynamic models and Gaussian noise, one can compute the a posteriori likelihood that the data came from each model, and classification is as simple as picking the maximum likelihood model. It relies critically in properly modeling all individual faults and is computationally expensive. On the other hand, data-based classification and correlation techniques rely on identification of distinct signatures in the measured data for faults and nominal operation, which are often very problem-specific and difficult to generalize.

The approach selected for fault classification derives from a variation on the classic model based approach: to use the signature of the adaptively tracked process parameters as they change over time.. A side benefit of continuous parameter adaptation, is the ability to estimate the new viscosity after the occurrence of a fault, and enabling automatic corrective action using closed-loop control where feasible (see Section 9).

To facilitate the identification of the modified model parameters, the process is excited through small test signals added to feed-rates and/or screw speeds. Recursive estimates of the model parameters β_i for die pressure are obtained using the methods in the previous section. The adapted parameters β_i, will in turn, enable the identification of the fault source. Figure 29 depicts this approach to fault identification in more detail. The fault identification depends on comparing the obtained set of parameters β_i against a pre-calculated set of distinct signatures for nominal/fault conditions. Clearly, the generation of generic fault signatures that are not problem specific is important for successful application of this approach to a wide range of products/processes. We develop such generic fault signatures that are not related to a specific process or product. While we demonstrate the results of this approach as applied to the NORYL product, we emphasize that the approach should extend easily to other products due to the generic physics-based nature of the underlying model and fault signatures.

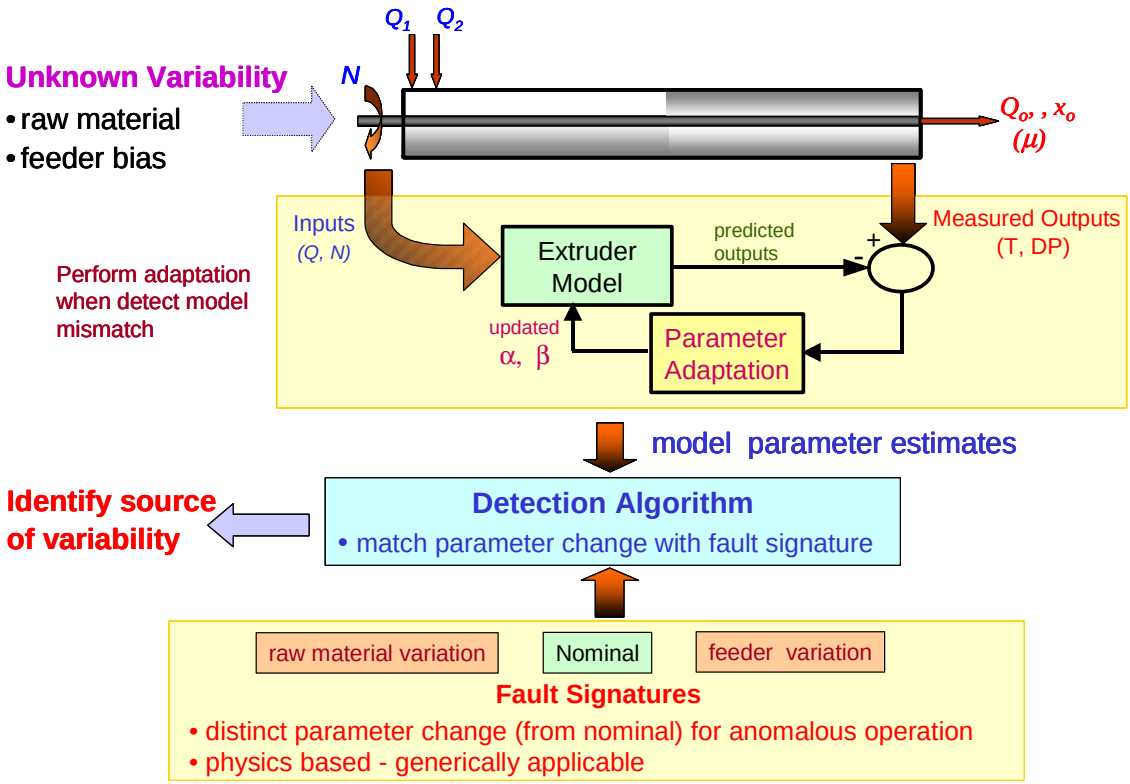

Figure 29: Schematic of fault detection approach

8.2 Fault Diagnostics – Noryl Case Study

8.2.1 Fault Signatures

The underlying principle behind the developed approach for fault detection is that any change observed in on-line identified parameters, β's, would be due to changes in operating conditions or in the raw material, assuming the screw geometry remains fixed during the operation (see Eq-A 15). In particular, faults like raw material and feeder variation affect the nominal viscosity μ_o and the slope μ_1 of the viscosity with respect to composition x_o in distinct manner. We will exploit the relation of the identified β's to the physical parameters μ's, in particular the relation of β_o and β_1 to μ_o and μ_1, respectively (see Eq 12) to identify and isolate these faults.

Note that from Eq 9, for a nominal shear rate or equivalently throughput $Q_o = \overline{Q}_o$, and nominal melt temperature $T_o = \overline{T}_o$, the viscosity varies with the product composition x_o according to the linear relation in Eq 15 around the nominal composition $\overline{x}_o$. Any changes in the raw materials PPO or PS or variations in PPO or PS feed-rates will affect the viscosity of the product and consequently, the die pressure, which will be manifested as distinct changes in the parameters μ_o and μ_1. Figure 30 shows the plots for viscosity as a function of composition under various raw material (PPO or PS for NORYL) changes and the corresponding distinct combinations of increase/decrease in μ_o and μ_1. These variations in μ_o and μ_1 form the basis for the distinct fault signatures.

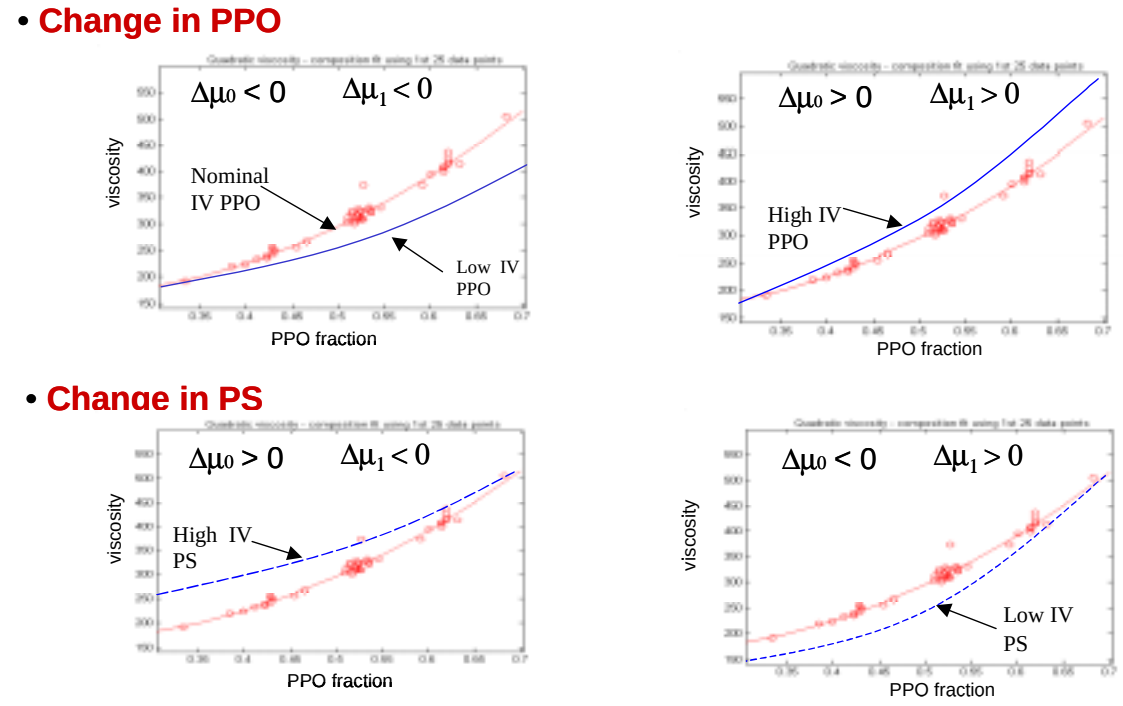

Figure 30: Fault signatures for changes in raw material

As seen in Figure 30 top left corner, if the raw material PPO changes from nominal IV to lower IV, while the other raw material PS is nominal, the resulting curve for variation in viscosity with respect to composition will be as shown in blue. In particular, in comparison to the nominal case (shown in red) the viscosity will remain unchanged at x_o=0 (pure PS, which is nominal) while it will have the maximum reduction at x_o=*1* (pure PPO). Thus, around the nominal composition $\bar{x}_o$, the new curve for viscosity (blue) will have a reduced value μ_o as well as a reduced slope μ_1, compared to the values for original nominal curve (red). Similar logic applies to other cases of raw material variations; for example, higher IV PPO, or lower IV PS, or higher IV PS as seen in Figure 30, will yield a distinct set of signatures for changes in μ_o & μ_1 corresponding to raw material changes. On the other hand, for nominal raw materials, an unknown bias in the PPO or PS feeders resulting in an increase/decrease of PPO fraction x_o will also affect the product viscosity and thus, die pressure.

Figure 31 shows the variation in μ_o & μ_1 for "small" variations in PPO/PS feeders. For instance as shown in the top left figure, a positive bias in the PPO feeder would imply that the observed throughput *Q* will be greater than the actual throughput. Similarly, the observed composition x_o will also be greater than the actual. However, the observed die pressure *DP* corresponds to the actual *Q* and x_o. Thus, since both the actual throughput and viscosity (as function of composition x_o) are lower, the observed die pressure *DP* will be lower than expected with respect to the observed *Q* and x_o. This will be estimated as a lower viscosity at nominal conditions and thus lead to the signature: $\Delta\mu_o < 0$. Note that for a "small" bias, the local slope will be unaffected i.e. $\Delta\mu_1 = 0$. Similarly, the signature for negative bias in PPO feeder would correspond to the signature: $\Delta\mu_o > 0$, $\Delta\mu_1 = 0$. In contrast to PPO feeder bias, a positive bias in the PS feeder would imply that the observed composition $x_{o,}$ will be less than the actual while the observed throughput *Q* will be greater than the actual. These changes in the feed-rate and feed composition have opposite effects on the expected change in die pressure (see Eq 10) and effectively reduce the net effect on die pressure, thereby making the detection of PS feeder bias more difficult. In our experiments, we observed that the effect of composition change (which affects viscosity and hence die pressure) is more dominant than the effect of throughput change, i.e. the net effect of positive PS feeder bias is an increase in the die pressure *DP*. This leads to the signature $\Delta\mu_o > 0$, $\Delta\mu_1 = 0$, which is similar to negative bias in PPO feeder.

In short, a "small" bias in PPO or PS feeder will correspond to a change in the nominal viscosity μ_o but no appreciable change in μ_1, which is distinct from signatures for raw material change. On the other hand if the feeder bias is large, then the slope μ_1 will also change from the nominal value and the resulting fault signatures will be similar to raw material changes. We assume that such large feeder biases will be identified through other independent means. For instance, in industrial applications the feeder hoppers are typically refilled automatically if the weight of the raw material in the hopper falls below a critical limit. For large gross errors in the feeders, the refill frequency will change significantly from nominal rates, thus indicating a large positive or negative bias in the

feeder. We will focus on the detection of "small" feeder biases, which cannot be readily detected through other simple practical means.

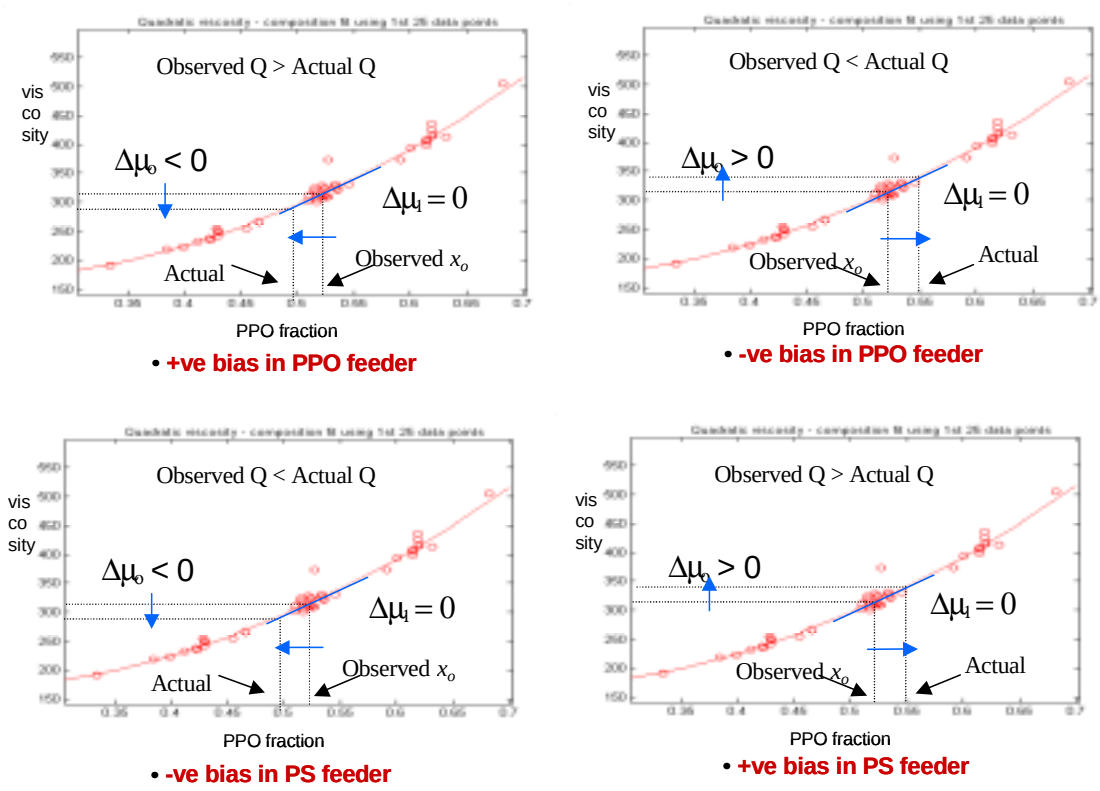

Figure 31: Fault signatures for PPO/PS feeder bias

Condition/Fault	$\Delta\mu_o$	$\Delta\mu_1$
Nominal raw material, no feeder bias	0	0
High IV PPO	> 0	> 0
Low IV PPO	< 0	< 0
High IV PS	> 0	< 0
Low IV PS	< 0	> 0
Positive bias in PPO feeder	< 0	= 0
Negative bias in PPO feeder	> 0	= 0
Positive bias in PS feeder	> 0	= 0
Negative bias in PS feeder	< 0	= 0

Table 4: Fault Signatures for raw material variation and feeder bias

Table 4 summarizes the fault signatures for raw material and feed-rate changes in terms of combinations of changes in μ_o and μ_1 from nominal values. Note that the signatures for positive/negative bias in the PPO feed-rate are the same as signatures for negative/positive bias in PS feed-rate, respectively. This is due to the fact the signatures are governed mainly by the PPO fraction in the product, which may arise from a change

in either feed-rate. Thus, the fault detection can identify a feed-rate bias distinctly from raw material changes but not distinguish between the PPO and PS feed-rates.

8.2.2 Fault Diagnostics with Noryl on 25mm Research Extruder

The fault occurrence, detection, identification and correction will occur in successive stages as shown in Figure 28. We ran multiple experiments with nominal and non-nominal raw materials over multiple days to test the performance of the fault diagnostics. In particular, we used either nominal PPO (high IV = 0.46) or non-nominal PPO (medium (0.4) / low (0.33) IV) while using nominal PS in all experiments. Furthermore, each experiment run started with the nominal raw materials or the faulty (lower IV) PPO from the beginning, focusing in particular on the fault identification stage, since the fault detection is achieved simply by monitoring the residual error between measured die pressure and the model prediction using nominal parameters against a threshold. Figure 32 shows the sequence of fault occurrence, detection and identification in a representative run using data from the experiment on Nov 14, 2001 with raw material variation. In this figure, we consider the scenario of starting with nominal operation in phase 1, and then a fault – PPO changed from nominal (0.46IV) to medium IV – occurring at t = 2 min.

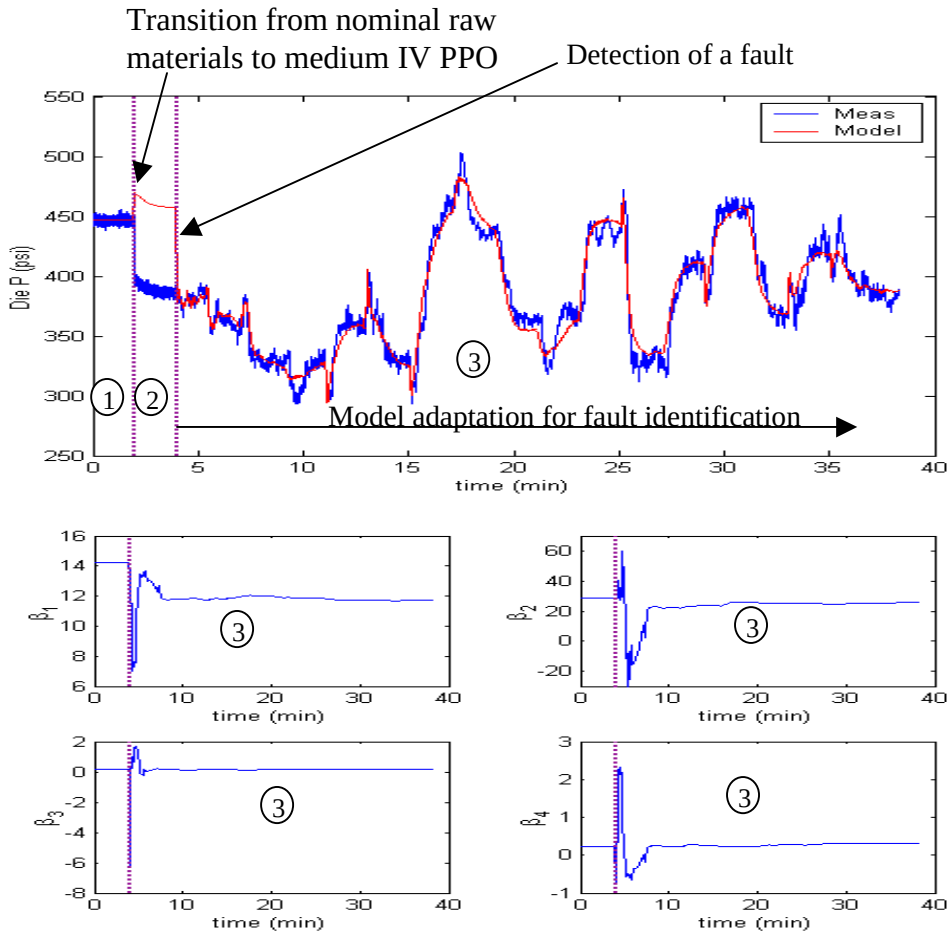

Figure 32: Fault occurrence, detection and identification using model parameter identification for a representative run with raw material change.

Clearly, in phase 1 under nominal conditions, the measured value for die pressure matches well with the model prediction using nominal parameters. However, after the fault, i.e. the transition from nominal raw materials to a medium IV PPO, the product viscosity, and thus, the die pressure drops significantly leading to a mismatch between the measured die pressure and the model prediction. A fault is detected when this residual error between the measured die pressure and the nominal model prediction crosses a threshold. The choice of the threshold affects the trade-off between false alarms and missed detects, and it depends on the signal to noise ratio. For the above change in raw material, clearly the change in die pressure is significantly larger than the measurement noise. Such a large signal to noise ratio allows an easy selection of a threshold. For instance, even a conservative choice for threshold of +/- 30 psi, would trigger a fault alarm in phase 2 within less than 2 minutes of the fault occurrence. The detection of a fault in phase 2 will then initiate the fault identification in stage 3. In this identification stage, the process is excited by a pre-defined PRBS input variation in the feed-rates and screw speed and the model parameters are updated using the on-line recursive adaptation. Finally, the new adapted parameters, specifically β_1 and β_2 (or equivalently μ_0 and μ_1 from Eq 12), are compared with the nominal values and the fault signatures in Table 4 to

identify the specific fault. The lower four plots in Figure 32 show the plots of the 4 parameters β_1-β_4 during this adaptation phase 3. The parameters β_1 and β_2, or equivalently μ_0 and μ_1, converge to a value lower than for nominal conditions by about $t=20$ min., correctly matching the fault signature for lower IV PPO. Thus, the model adaptation in phase 3 allows the identification of the correct fault.

Once a fault is correctly identified, then an appropriate corrective action can be taken to bring the process back on-spec, e.g. fixing the raw material change, or using closed-loop automatic control to correct for the raw material variation (see Section 9 for more details).

8.2.3 Fault Identification Results with Noryl for Raw Material Changes

We summarize the results of the fault identification algorithm based on the modeling and adaptation framework for the multiple runs with NORYL using nominal/non-nominal raw materials in . The actual nominal/fault conditions imposed in the individual experiments are listed in the second column and the nominal viscosity (at nominal PPO fraction) measured in the lab using samples collected during steady state conditions are listed in column 3. The estimated nominal viscosity μ_o and the slope μ_1 of viscosity with respect to PPO fraction obtained after the model adaptations in each run are listed in columns 4 and 5, respectively. As mentioned before, the fault identification relies on matching the deviations in μ_o and μ_1 from the nominal values against the fault signatures in Table 4. Due to the noise in the process measurements, the model parameters for nominal conditions will lie in a normally distributed region. Thus, a threshold has to be chosen to declare +ve or –ve changes in μ_o and/or μ_1 before comparing with the fault signatures. Again, these thresholds can be chosen statistically to optimize the trade-off between false alarms and missed detects and their choice depends on the signal to noise ratio. For instance, comparing the first three runs with nominal conditions, it is clear that the parameters μ_o and μ_1 are tightly clustered together and distinctly different from the other runs with non-nominal raw materials. This distinct separation between the parameter values for nominal and fault conditions facilitates a clear selection of the thresholds. For instance, a choice of the thresholds for $\Delta\mu_o$ = +/-50 and for $\Delta\mu_1$ = +/-150 would suffice to correctly identify the nominal conditions in the first three runs and declare the lower IV PPO in the last three runs (both $\Delta\mu_o$ and $\Delta\mu_1$ are –ve, matching the signature for lower IV PPO). The fault identification results are summarized in the last column of the table, which can be compared with the actual fault condition introduced during each experiment, given in column 2. Clearly, the proposed fault identification algorithm works very well to correctly identify the nominal runs and the specific faults with raw material changes in each run.

	Date of Expt.	Fault condition (raw material) introduced	Viscosity measured in lab at nominal composition	Estimated values of nominal Viscosity, μ_0 ($\Delta\mu_o$)	Estimate of Slope, μ_1 ($\Delta\mu_1$)	Fault Identification Result
Nominal raw materials	6/25/2001	Nominal (calibration run)	1152	1139 (-)	2944 (-)	Calibration run
	5/22/2001	Nominal	-	1167 (+28)	3083 (+139)	Nominal
	5/08/2001	Nominal	1129	1174 (+35)	2891 (-53)	Nominal
	7/25/2001	Nominal	1196	1155 (+16)	2844 (-100)	Nominal
Faulty raw materials	8/27/2001	Low IV PPO	920	877 (-262)	2537 (-407)	lowerIV PPO
	10/11/2001	Med IV PPO	1010	1002 (-137)	2550 (-394)	lowerIV PPO
	11/14/2001	Med IV PPO	964	940 (-199)	2647 (-297)	lowerIV PPO

Table 5: Diagnostics results for experiment runs with nominal/non-nominal raw materials

In addition to the above six runs, we also analyzed later experiment runs conducted for closed-loop control. Table 6 shows the results for the control runs and yields the correct fault detection for the run on 12/06/2001. For the run on 12/04/2001 with medium IV PPO, the calculated slope μ_1 is close to the nominal value while the nominal viscosity μ_o is lower than nominal – matching the signature for a small feeder bias. However, since we deliberately changed the raw material, it would mean that two faults (raw material change and feeder bias) occurred simultaneously, which cannot be isolated unambiguously based on our fault detection method. The last run on 12/14/2001 during closed-loop control yields μ_0 close to values for nominal raw materials and a slope μ_1 that is distinctly lower than nominal runs. This change in μ_0 and μ_1 does not match any of the raw material or feeder bias fault indicating possible multiple faults. Indeed, after thee xperiment, we found that the feeders had a large bias, which together with the choice of medium IV PPO led to a combination of faults in raw material and feed-rate. As mentioned earlier, the fault diagnostics, in general, cannot correctly identify simultaneous multiple faults since their effects are confounded. Note however that in all these three runs, including the ones with multiple faults, the viscosity estimation in column 4 was very good (within 10%) of the lab measurements given in column 3 – this will enable the corrective closed-loop control based on the updated viscosity estimate.

Date of Expt.	Fault condition (raw material) introduced	Viscosity measured in lab at nominal composition	Estimate of nominal Viscosity, μ_0 ($\Delta\mu_o$)	Estimate of lope, μ_1 ($\Delta\mu_1$)	Fault Identification Result
12/04/2001	Med IV PPO	995	930 (-209)	2920 (-24)	Feeder bias
12/06/2001	Med IV PPO	980	968 (-171)	2594 (-350)	Lower IV PPO
12/14/2001	Med IV PPO	1095	1096 (-43) 1135* (-4)	2554 (-390) 2516* (-428)	Multiple faults?

Table 6: Diagnostics results for control runs (*estimated after feeder bias correction)

8.2.4 Fault Identification of Feeder Bias

We also tested the fault detection for PPO/ PS feeder bias through specifically designed off-line simulations using actual recorded input/output data from the nominal run on 06/25/2001. In particular, we added a specific positive/negative bias in the PPO or PS feed-rates and performed the recursive parameter identification to test the performance of the fault detection based on the fault signatures in Table 4. A positive bias in, for example, the PPO feed-rate means that the observed feed-rate is higher than the actual feed-rate. Figure 33 shows the comparison of measured die pressure with the die pressure predicted using the observed feed-rates (with the bias introduced in PPO/PS feeder) and nominal parameters. For instance, in the case of positive PPO feeder bias (upper left plot), the observed throughput and PPO fraction are higher than the actual values and thus the die pressure prediction is higher than actual. The fault detection results obtained for the four cases using the parameter identification are summarized in Table 7. Clearly, the calculated changes in μ_o, μ_1 match with the expected fault signatures. However, while the parameter μ_o changes quite significantly from the nominal value for a bias in the PPO feeder and is easily detected, the change in this parameter for PS feeder bias is quite small, i.e. detection of PS feeder bias is difficult as mentioned before due to the competing effects of changes in feed-rate and composition in this case as mentioned earlier.

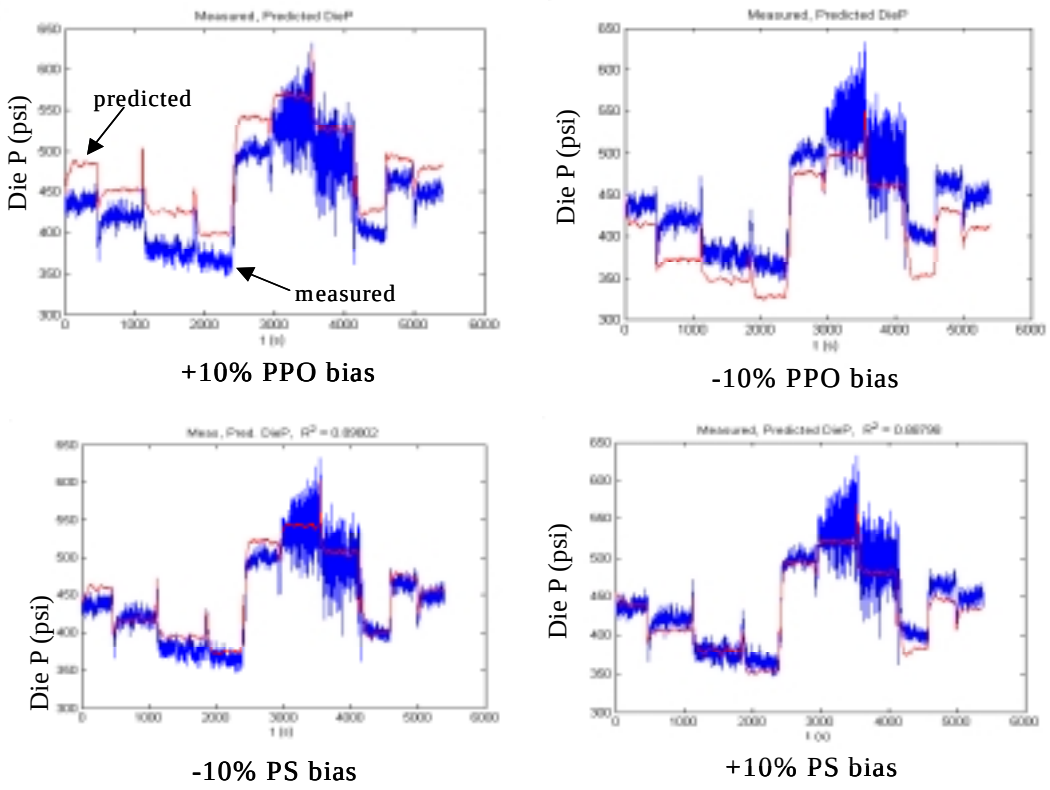

Figure 33: Comparison of measured and predicted die pressure for bias in PPO/PS feeder using nominal parameters.

Condition/Fault	μ_o ($\Delta\mu_o$)	μ_1 ($\Delta\mu_1$)	Detection result
Nominal	1139 (-)	2944 (-)	Calibration
+10% bias in PPO feeder	1042 (-97)	2922 (-22)	$\Delta\mu_o < 0$, $\Delta\mu_1 = 0$
-10% bias in PPO feeder	1228 (+89)	2926 (-18)	$\Delta\mu_o > 0$, $\Delta\mu_1 = 0$
+10% bias in PS feeder	1160 (+21)	2914 (-30)	$\Delta\mu_o > 0$? , $\Delta\mu_1 = 0$
-10% bias in PS feeder	1109 (-30)	2945 (+1)	$\Delta\mu_o < 0$? , $\Delta\mu_1 = 0$

Table 7: Parameter identification and fault detection for feeder bias

8.3 Diagnostics Summary

In summary, the proposed modeling and adaptation provides a natural framework for fault detection and identification using on-line process measurements and can be used as the basis for taking corrective control action in the presence of faults. We have developed a novel model-based fault detection methodology that is not tied to any specific process or product grade and demonstrated its successful application on the 25mm research extruder with NORYL polymer product. The key features of the developed diagnostics algorithm are:

(i) The approach is generically applicable to wide range of extruder applications owing to the generic physics-based underlying model and physically motivated fault signatures that are not problem specific.
(ii) As demonstrated by the multiple runs over a span of several months, the proposed fault detection works very well to consistently identify raw material or feeder faults, which are the main process faults that affect product quality. The distinct fault signatures allow distinguishing between raw material changes and feed-rate variations. However, owing to similar effects of the two raw material feed-rate changes, it is not possible to distinguish between a bias in the PPO or the PS feed-rate.
(iii) While we demonstrated the application of the developed fault detection approach to a process with two main raw materials, it can be extended to the case of more than two key raw materials – at the expense of increased number of model parameters for viscosity and die pressure and thus, correspondingly increasing complexity in the adaptation and fault identification. In particular, for multi-component mixtures with N components, the relation for viscosity will involve N-1 slopes $\mu_{1,i}$ and the resulting fault signatures will involve unique combinations of changes in μ_o, $\mu_{1,i}$ making the fault detection for raw material changes more complex.

The fault diagnostics algorithm assumes however that the faults occur one at a time. The algorithm, in general, will not identify the correct fault in the case of multiple simultaneous faults since their effects are confounded. When multiple faults are occurring, the it is typical that severe upsets in machine operation have occurred and can be detected by more conventional limit checks are gross anomalies like dropped strands. The real power of the present technique is detecting small “drift” type faults that may take a while for the effects to be seen. With the proposed scheme, such faults can be detected, classified and dealt with before out of spec material is shipped.

9 Extruder Control

9.1 Approach to control in the presence of upsets

In this section, we present results on the closed-loop on-line control of viscosity. In the absence of an on-line measurement/estimate of product viscosity, a common industrial practice is to monitor on-line measurements like die pressure and torque to verify that they are within a desired tolerance of nominal values. However, such practice is often inadequate since the absolute magnitudes of these machine variables depend on both the process conditions that affect product quality, e.g. feed composition, raw material characteristics, and those that do not, e.g. throughput. In contrast, the online estimation of product viscosity using the measurement of machine variables (feed-rates, die pressure etc.) enables active closed-loop control of viscosity in the presence of disturbances like changes in raw material (see Figure 34). A change in raw material properties can be corrected by varying the incoming product composition to maintain the product viscosity

on target. Thus, the on-line closed-loop control of viscosity entails the following two key steps:

- On-line estimation (inferential sensing) of viscosity from measurement of machine variables (feed-rates, die pressure)
- Corrective action to change feed-rates, and thus product composition, to compensate for the effect of raw material changes and maintain product viscosity at its nominal set-point.

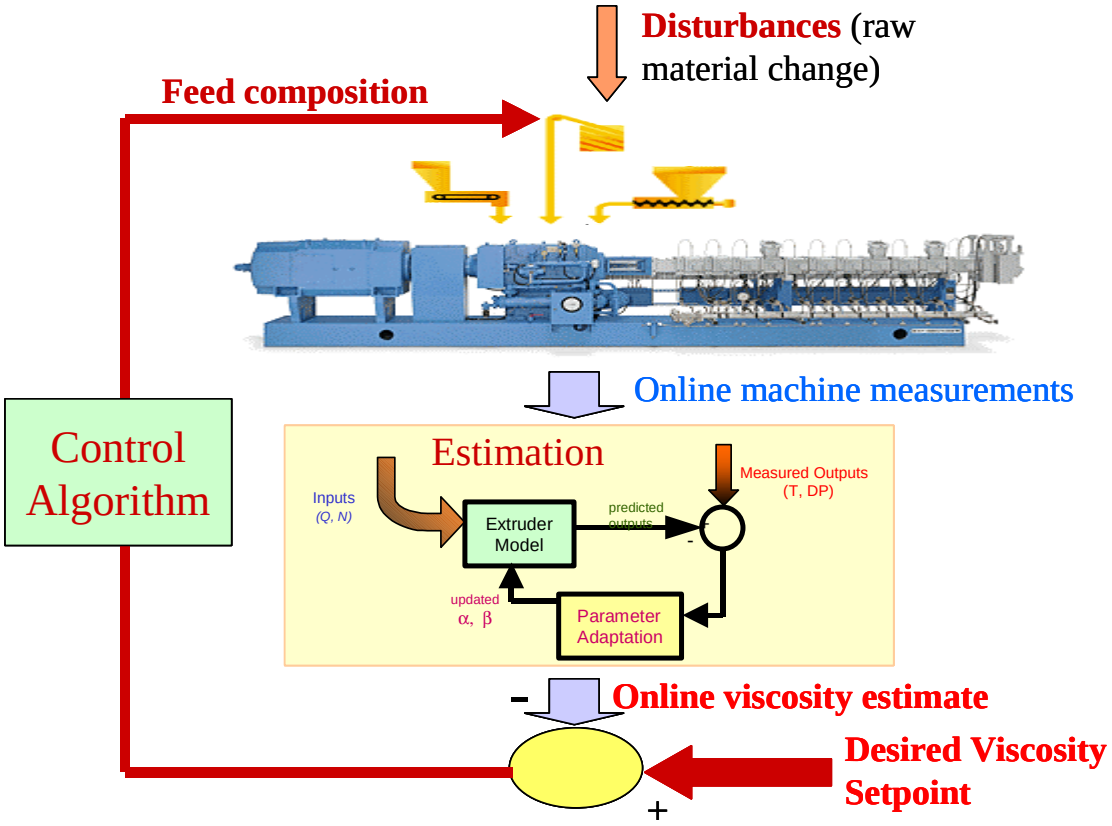

Figure 34: Schematic diagram for closed-loop control of product viscosity

9.2 Viscosity Adaptive Control

Figure 35 shows the schematic block diagram of the closed-loop control approach for maintaining viscosity close to the desired set-point (for any product grade). The product viscosity is affected by the main process disturbances like raw material and feeder variations. Under nominal conditions, the model predictions with nominal parameters β_i matches the on-line measurements of die pressure, and thus, the on-line estimate of product viscosity is obtained using the nominal parameters. In the presence of significant disturbances, the model predictions for die pressure will differ from on-line measurements leading to the model parameter adaptation. The newly adapted parameters will reflect the effect of the disturbances and provide a corresponding updated estimate of viscosity. The estimated viscosity is compared with the target set-point and the PI

controller is used to manipulate the feed composition to maintain the estimated viscosity at the set-point. The required feed composition is implemented by using ratio control logic to vary the individual PPO and PS feed-rates while maintaining desired throughput. These calculated PPO and PS feed-rates are finally provided as set-points for the lower level feeder controllers.

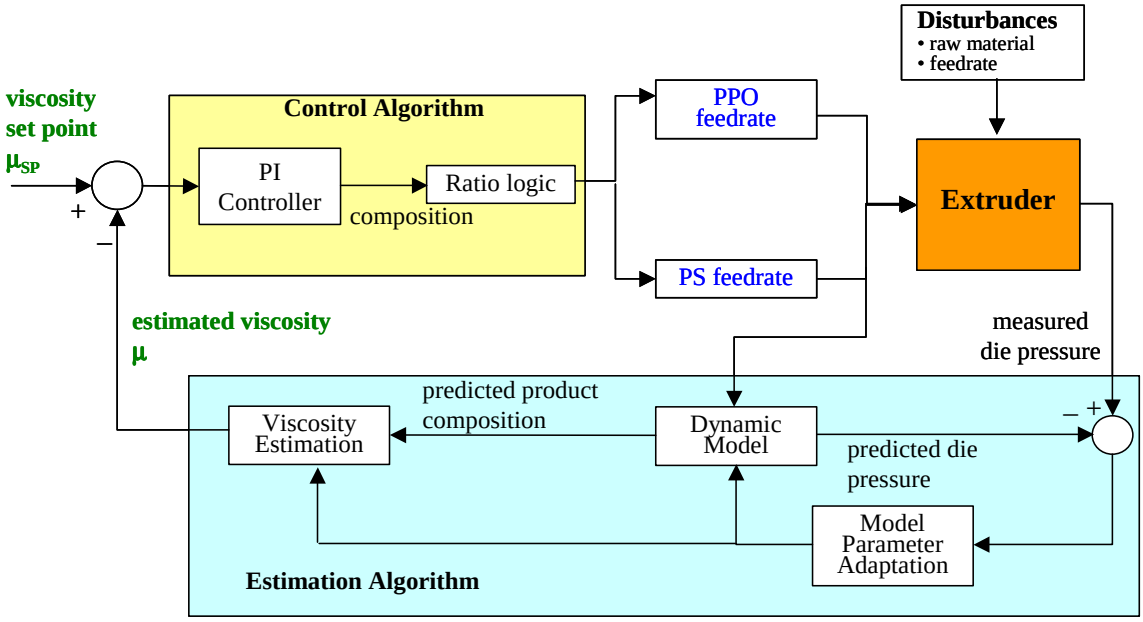

Figure 35: Shematic block-diagram of the closed-loop control algorithm based on on-line viscosity estimation

In order to tune the PI controller, the dynamics of the extruder are approximated by a first order model. In particular, the product viscosity μ is given as a function of the production composition x_o (see nomenclature in Section 5), where the product composition $x_o = x_2$ is given as a function of the feed composition x_i by the model in Eq 11. The overall response of the product composition, and thus viscosity μ, can be approximated by a first-order response:

Eq 16
$$\mu - \mu_o = \frac{\mu_1}{\tau_p s + 1}(x_i - \bar{x}_i)$$

with a time constant τ_p. For our experiments on the lab-scale extruder we calculated the time constant $\tau_p = 30$ seconds. The PI controller is then tuned for a closed-loop first order response:

Eq 17
$$\frac{\Delta\mu}{\Delta\mu_{SP}} = \frac{1}{\tau_f s + 1}$$

where $\Delta\mu$ and $\Delta\mu_{SP}$ denote the deviation in estimated viscosity and desired set-point from nominal values and τ_f is the desired closed-loop time constant for viscosity set-point

tracking – we tuned the PI controller to achieve the closed-loop time constant $\tau_f = 60sec$. For more details on the controller tuning, see Appendix A to Section 5.

9.3 Control implementation for research extruder

The developed algorithms for estimation and control using Matlab/Simulink were implemented on the extruder for closed-loop experiments using D-Space. Figure 36 shows the schematic representation of the various software/hardware elements of the final implementation on the lab-scale extruder. In particular, the KTron feeder controllers provided the internally calculated feed-rates as frequency signals, which were converted to voltage signal using frequency to voltage conversion. In addition, the measured torque, die pressure, melt temperature and screw speed were recorded as voltage signals. The conversion of the raw voltage signals to physical units was handled by the software algorithm in D-Space. The calculated feed-rate set-points from the control algorithm in D-Space were in volts, which were converted to frequency signals using voltage to frequency converters to interface with the KTron feeder controllers for automatic adjustment of the feed-rate set-points. The software in D-Space was provided with a GUI to allow monitoring the signals in real time, and provide the capability to enable/disable the parameter adaptation and closed-loop automatic control (see **Figure 6**). In our experiments, we manipulated the screw speed manually during the PRBS excitation for parameter adaptation – screw speed was kept constant at nominal value during closed-loop control. However, even the screw speed control on the extruder drive could be interfaced with the D-Space implementation to allow a completely automated pre-programmed PRBS feed-rate, screw speed sequence during the parameter adaptation.

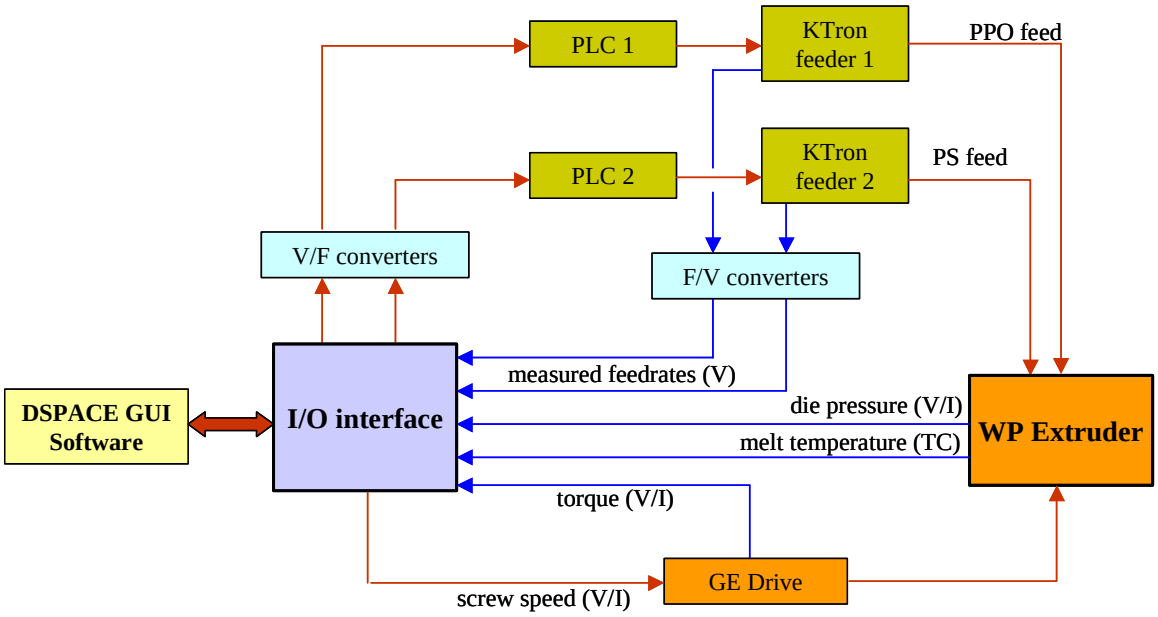

Figure 36: Schematic diagram of the final implementation using D-Space for closed-loop control experiments

Experimental Control results with Noryl Material

Figure 37 depicts the set-point tracking experiment on 12/14/2001 with nominal raw materials. As seen in the top figure, in the first part of the experiment, the system was subjected to a PRBS input variation to facilitate the parameter identification. The bottom plot shows the PRBS variation in the PPO and PS feed-rates during this adaptation phase. Note that the estimated viscosity also varies during this phase, partly due to the adaptation of the model parameters β, and partly because of the variation in the feed composition during the PRBS excitation of the feed-rates. After this parameter adaptation phase, in the second part of the experiment, the closed-loop controller was enabled and the set-point for viscosity was increased from the initial nominal value of 1116 Pa-s to 1250 Pa-s and then decreased back to 1116 Pa-s. Clearly, the controller steered the estimated viscosity of the system to the desired values by manipulating the PPO and PS feed rates. In particular, the controller increased the PPO:PS feed ratio as expected to achieve the higher viscosity when the set-point for viscosity was increased to 1250 Pa-s, and then reduced it back to nominal after the set-point was reduced back to 1116 Pa-s.

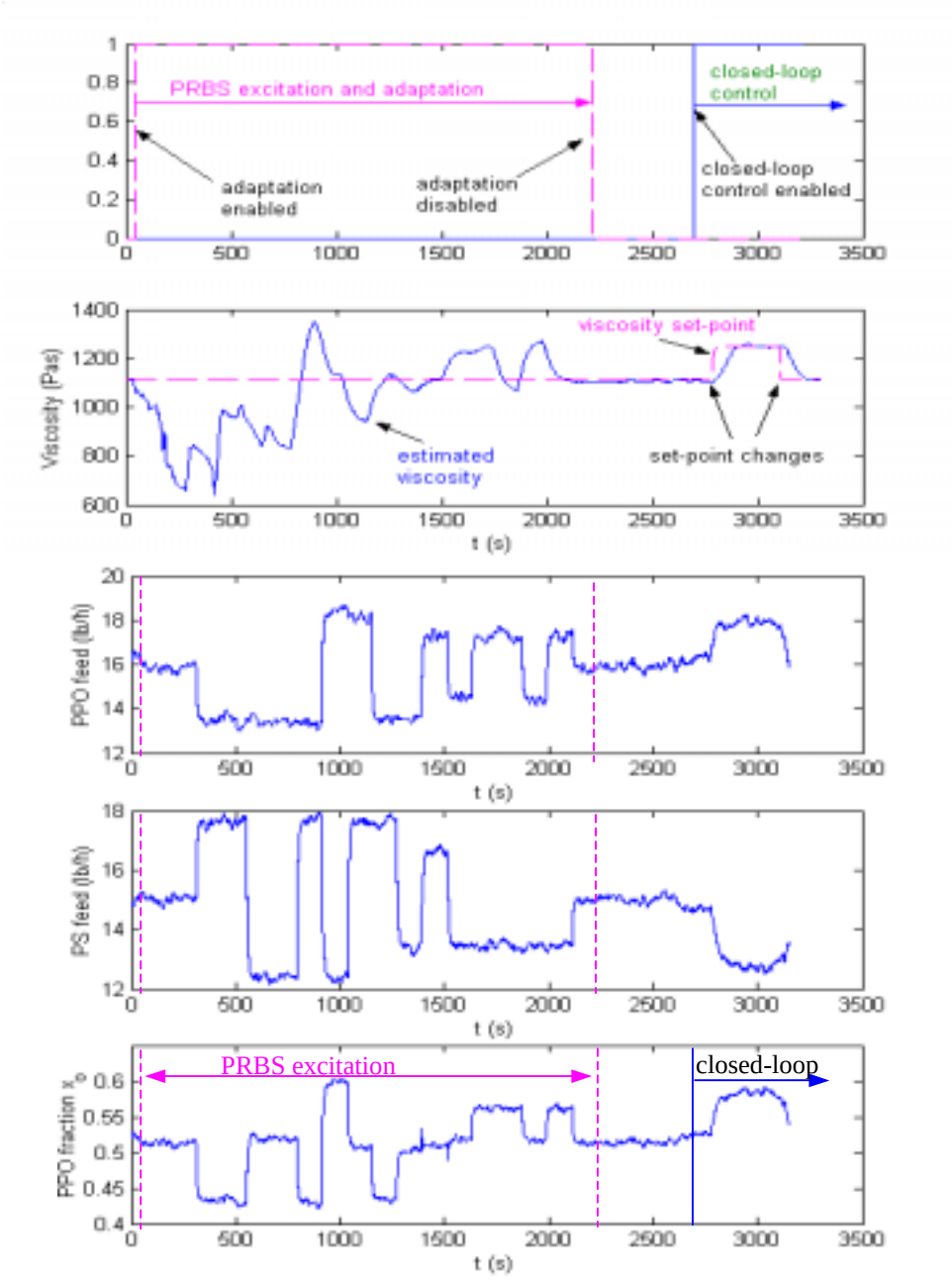

Figure 37: Closed-loop control of viscosity – set point tracking with nominal raw materials on 12/14/2001

The blue plot in the figure represents the on-line viscosity estimate, which is dependent on the composition determined by the measured feed-rates of the PPO blend and PS. If the feed-rates were with out any bias, (feed-rates were implemented by the low level K-Tron controller exactly the same as set-points of the feeders: 16 lbs/hour PPO blend, 15

lbs/hour PS rate for nominal composition fraction of 0.516) then the viscosity estimate seen in

Figure 37 would be within measurement error range of the off-line viscosity measurement. But the off-line lab measurements for two samples collected before and after the set-point change and denoted with red line in Figure 38 (same Figure 37 as with off-line measurement data) are higher than estimated values demonstrated in

Figure 37. This means that a large feeder bias caused a higher PPO fraction (this high viscosity was later found to correspond to PPO fraction of 0.571) in the mixture, thereby increasing the viscosity and the die-pressure measurement.

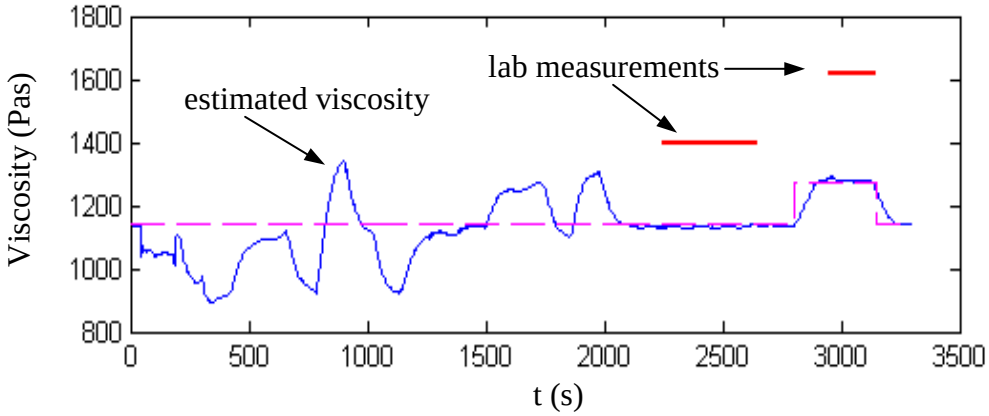

Figure 38: Comparison of closed-loop control of viscosity –set point tracking using nominal raw materials - with off-line viscosity measurement on 12/14/2001

On the day of the experiment (12/14/01), we observed that even with nominal raw materials and running at the nominal feed PPO composition of 0.571, the measured die pressure was higher by 15% than similar nominal experiments done until that date. Moreover, the identified parameters led to a higher μ_o and μ_1, i.e. $\Delta\mu_o > 0$, $\Delta\mu_1 > 0$, a fault signature corresponding to high IV PPO. However, this was not possible since the nominal PPO used in the experiments was already the highest IV (0.46IV) PPO available for our experiments. In fact, this fault signature was caused by the large feeder bias (possibly due to different set of feeders used on 12/14/01), which as mentioned in the diagnostics section can yield a fault signature similar to raw material change - in this case similar to a higher IV PPO. As mentioned in the diagnostics section, the detection of such large feeder biases can be addressed separately through simple practical means (e.g. feed hopper refill frequency). The developed diagnostics algorithm focuses only on "small" feeder biases that have a distinct signature compared to nominal runs or runs with bad raw materials.

Given the large feeder bias indicated by the off-line lab viscosity measurements for the samples collected during the nominal run, which were about 20% higher than that observed for similar nominal raw material and composition samples on prior days, we

analyzed the data from the run after correcting the feed-rates with estimated feeder bias. More specifically, the increased viscosity corresponded to an increased PPO fraction of 0.571 as opposed to the nominal composition of 0.516, indicating a bias in PPO and/or PS feeders. Moreover, the increased viscosity and online die pressure measurements were of the same order of magnitude indicating that the total throughput *Q* was close to nominal and only the PPO fraction had changed. To verify this hypothesis, we re-evaluated the online data from the run with an imposed positive bias correction in measured PPO feed-rate (+1.7 lb/h), a negative bias correction in PS feed-rate (-1.7 lb/h) and using the original calibrated value of *k* obtained from the nominal calibration run on 06/25/2001. The resulting viscosity estimation during the adaptation and closed-loop control is shown in Figure 39. It shows the estimated viscosity (shown in blue in the bottom plots) is close to the off-line measurements (shown in red), corroborating the feeder bias hypothesis.

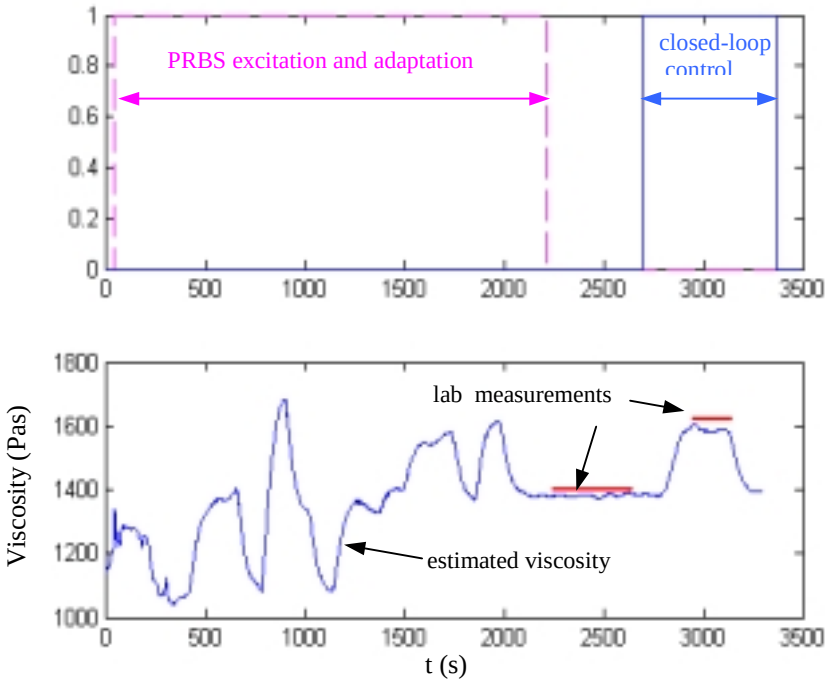

Figure 39: Experiment run on 12/14/2001 with nominal raw materials, accounting for PPO and PS feeder bias

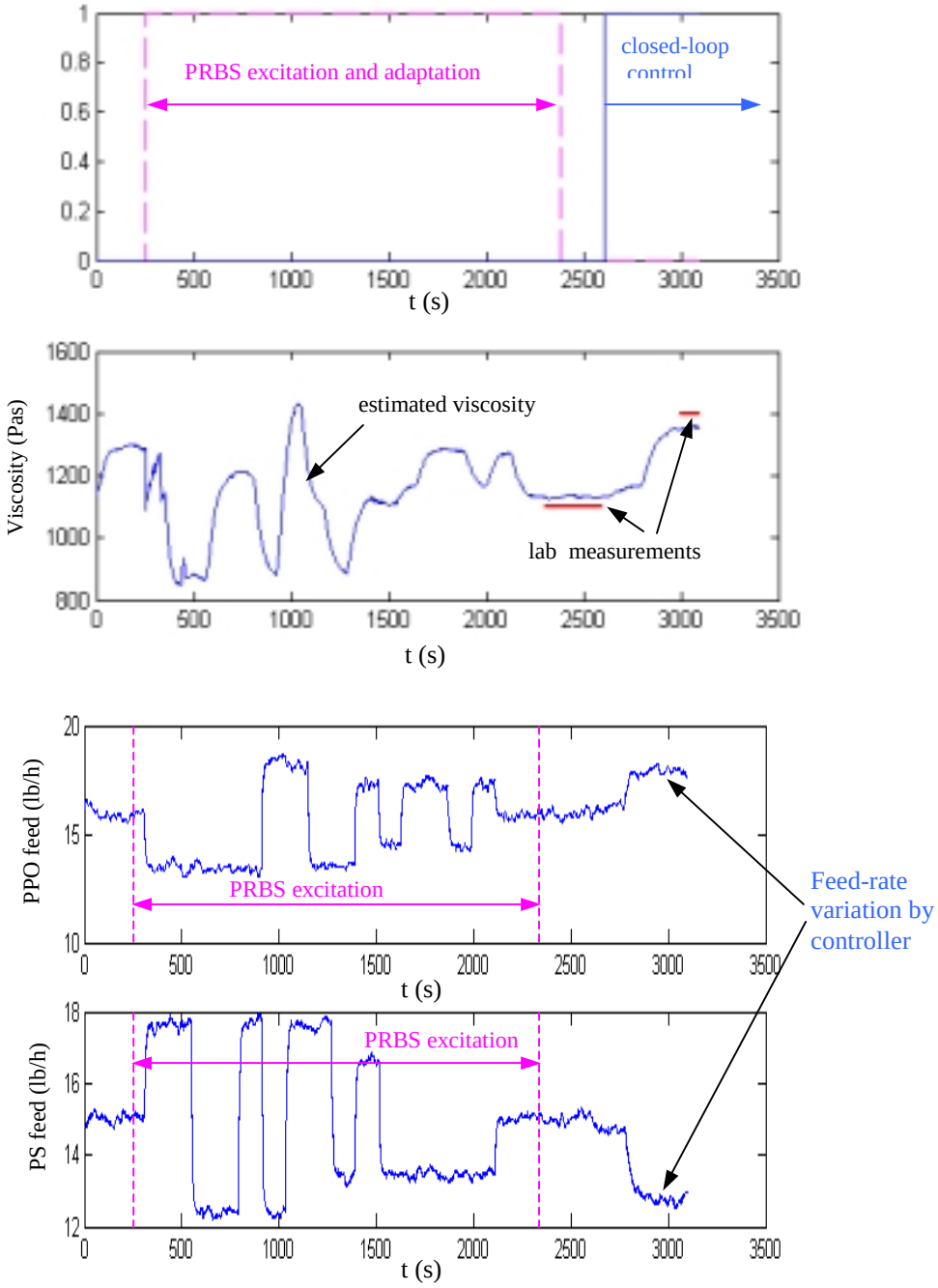

Figure 40: Experiment run on 12/14/2001 with medium IV PPO, accounting for PPO and PS feeder bias

On 12/14/2001 a further control test using medium IV PPO blend and nominal PS mixture was conducted. Since the same unknown feeder bias was present for the same day, we analyzed the data offline with the above-mentioned feeder bias corrections. The results are shown in Figure 40. Again, in the beginning a PRBS excitation on the feed-rates and screw speed was imposed to aid the adaptation. With the new adapted model

parameters a new viscosity estimate was obtained. Finally, the closed-loop control was enabled and the viscosity set-point was increased. Clearly, the controller yielded the increased viscosity by increasing the PPO feed concentration, specifically by increasing the PPO feed-rate and decreasing the PS feed-rate to maintain the nominal total feed-rate. The values of viscosity measured in the lab using two samples collected at steady state, one before the set-point increase and the other after the set-point change are compared with the on-line estimate. Again, the on-line estimate of viscosity matches well with the lab measurements and the closed-loop controller smoothly changed the product composition and thus viscosity during the set-point increase.

As demonstrated by the above figures the closed-loop control scheme works well to compensate for the effects of unknown raw material changes and track changes in desired viscosity set-point. The effectiveness of the control scheme is clearly dependent on the performance of the online viscosity estimation.

10 Scale-Up for Production-Scale Extruders

10.1 Scale of Dynamic Input-Output Model of Extruder

In this section, we address the scale-up of the developed approach and its application to industrial production scale extruders. In particular, we study the application of the approach developed above on the lab-scale 25mm extruder when scaled up to the production-scale 120mm extruders at GEP Selkirk. We obtained and analyzed data recorded at 0.2 Hz from the GEP Selkirk site on a specific extruder line that was instrumented to measure and record the signals like torque, die pressure, feed-rates and screw speed during DOE runs conducted on Nov 21, 2000 and Jan 18, 2001 while making Noryl PX5511 product. In these two DOE runs, the process inputs, i.e. the screw speed and the PPO, PS feed-rates were varied in a PRBS manner with small variations from the nominal operating values so as to excite the system dynamics enough for analysis while maintaining the product quality within desired specifications.

To test the scale-up of the model developed for the lab-scale extruder, we applied the model to the data from the DOE run on Jan 18, 2001 and obtained the best-fit model parameters using least squares off-line optimization. Thereafter, we used the model with these best-fit parameters and compared its predictions of torque and die pressure using the data from the DOE run on Nov 21, 2000, to test the validity of the model. Our initial comparison of the measured torque and die pressure data for the two DOE runs showed the nominal die pressure on Jan 18, 2001 to be significantly lower than on Nov 21, 2000 even though the operating conditions were exactly the same. This occurred due to the use of a different screen-pack – used to filter out particulates in the molten product just after the die pressure probe – which effectively changed the resistance to flow and thus the pressure drop. We corrected for this difference by adding a constant bias value from the die pressure measured on Jan 18, 2001 to make it consistent with the nominal value on Nov 21, 2000. Furthermore, the melt temperature measurement on the extruder was

faulty; it measured a constant temperature irrespective of any changes in throughput and/or screw speed. In the absence of a good melt temperature measurement, we used a simple first-order model to predict the changes in the melt temperature (we need only the changes from the nominal value for fitting our model) as a function of the screw speed and throughput (see Eq-A 21) and used it in the die pressure relation (see Eq-A 18).

Figure 41 shows the comparison of the measured torque and the model predictions for torque during the DOE run on Jan 18, 2001. The model can be seen to fit the measured torque variations during the DOE run very well. Figure 42 shows the comparison of the model predictions and measured values of die pressure during the same DOE run. Again, the model prediction for die pressure matches very well with the measured die pressure variations. We tested the validity of the model with the obtained best-fit parameters by comparing it against the data from the DOE run on Nov 21, 2000. Figure 43 and Figure 44 show the model predictions for torque and die pressure compared to measured values on Nov 21, 2000, respectively. Clearly the model predictions match very well with the measured values, i.e. the model validates very well with independent set of data. This validation demonstrates the scale-up of the developed modeling approach and its applicability to large industrial production-scale extruders.

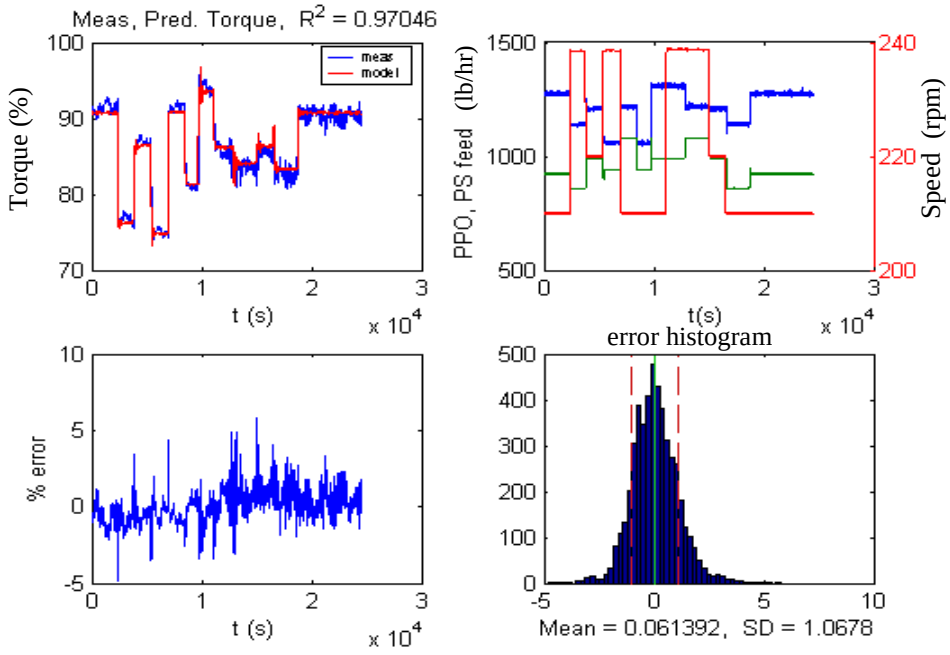

Figure 41: Comparison of model-predictions and measured value of torque on a 120mm extruder during a DOE run at GEP Selkirk on Jan 18, 2001.

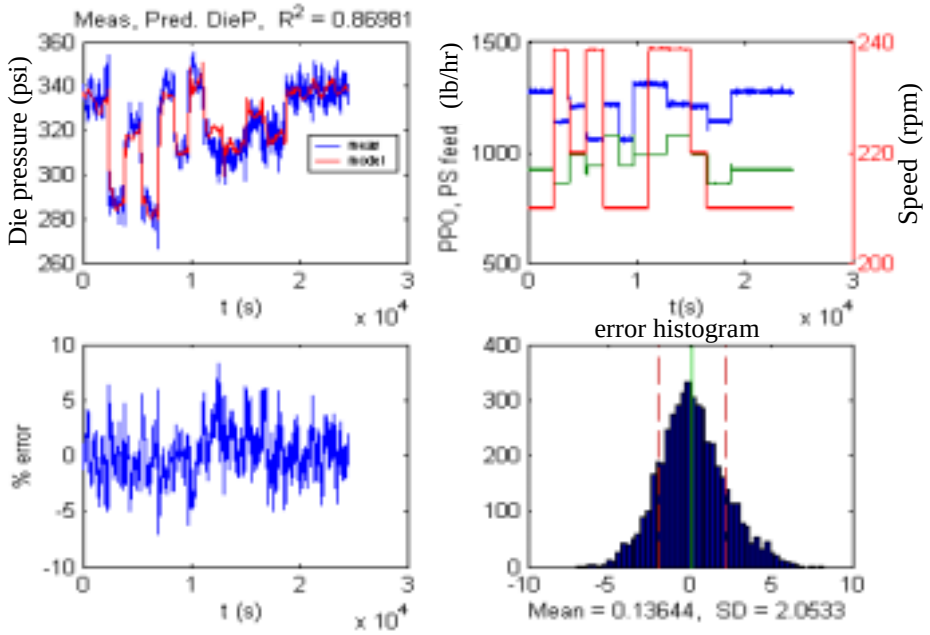

Figure 42: Comparison of model-predictions and measured value of die pressure on a 120mm extruder during a DOE run at GEP Selkirk on Jan 18, 2001.

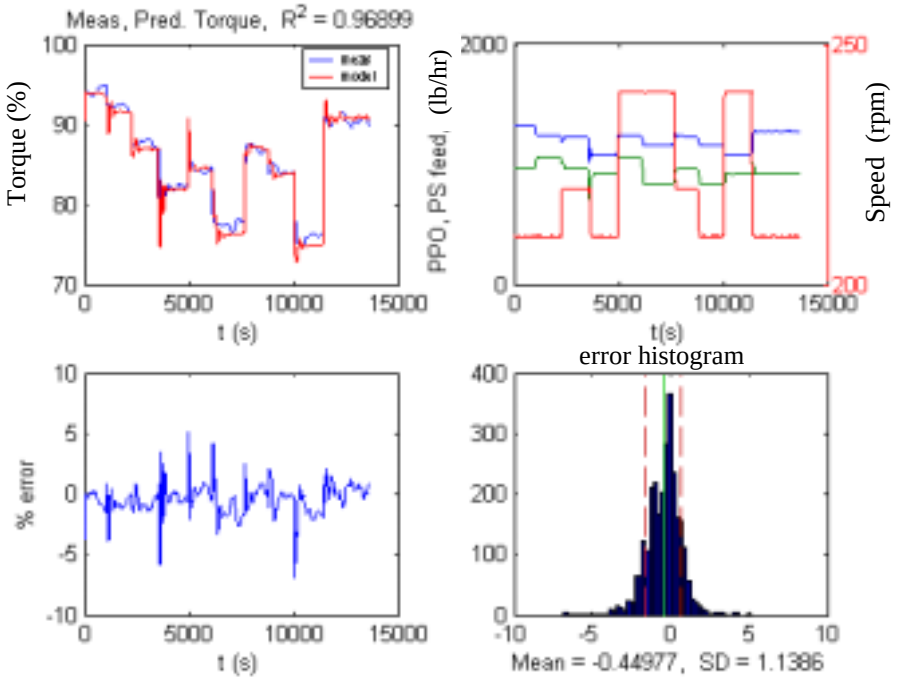

Figure 43: Validation of model for torque using DOE data on a 120mm extruder at GEP Selkirk on Nov 21, 2000.

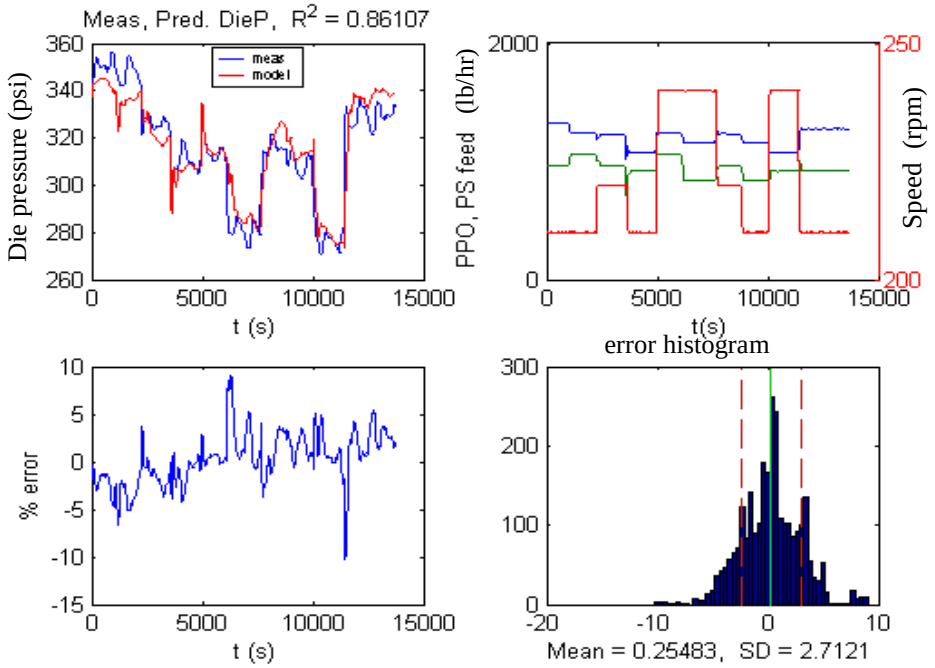

Figure 44: Validation of model for die pressure using DOE data on a 120mm extruder at GEP Selkirk on Nov 21, 2000.

10.2 Scale-Up of On-line Adaptation of Model Parameters

For the DOE run on Jan 18, 2002, we tested the performance of the recursive adaptation of the model parameters β, starting from slightly perturbed values to test the performance of the adaptation. Table 8 summarizes the results of the parameter adaptation starting from the initial perturbed values to yield the final adapted values, which are close to the best-fit values obtained by the off-line least squares optimization. Figure 45 shows the comparison of the measured die pressure and the model prediction during the adaptation starting from the initial perturbed values of β. It can be seen that the model adaptation works well to match the predicted values of die pressure with the measured values and yield the correct values of the parameters β.

	Adaptation		Off-line optimization
	Initial values	Final values	Optimal values
β1	17.38	15.365	15.38
β2	19.02	22.46	23.0
β3	1.077	0.87	0.87
β4	3.43	3.23	3.13

Table 8: Scale-Up of parameter adaptation for die pressure for 120mm extruder data from DOE run at GEP Selkirk on Jan 18, 2001.

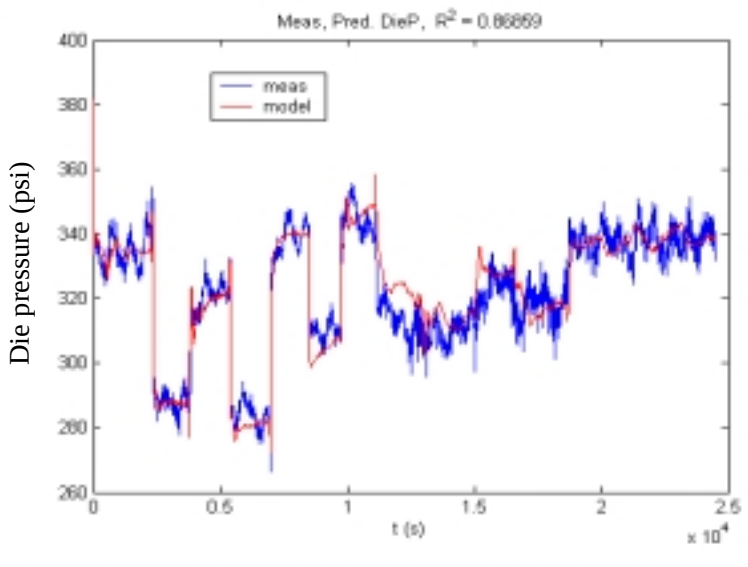

Figure 45: Comparison of measured and model predicted values of die pressure during parameter adaptation with DOE data from 120mm extruder at GEP Selkirk on Jan 18, 2001

10.3 Scale-Up of Viscosity Estimation

In order to perform the viscosity estimation using the estimated parameters β_1 and β_2, and the product composition x_o, the calibration parameter k needs to be calculated to perform the conversion between β_1 and β_2 and μ_o and μ_1 (see Eq 12). We had QA lab measurements of viscosity of 10 samples collected at various steady state operating conditions during the DOE run on Nov 21, 2000. Since, this was the only viscosity data we had for the DOE runs conducted at GEP Selkirk, we performed the calibration using a few samples and compared the estimation against others. More specifically, a linear fit between the measured viscosity and PPO weight fraction is performed to calculate the

parameters μ_o and μ_1 and thus, calculate the calibration parameter *k.* The linear fit yielded the linear relation for viscosity:

Eq 18
$$\mu = 25.49 + 272.6 * x_o$$
$$= 178.15 + 272.6 * (x_o - \bar{x}_o)$$

with μ_o*=178.15* and μ_1*=272.6* at the nominal mean PPO fraction $\bar{x}_o = 0.56$. Thereafter, the values of μ_o and μ_1 and β_1 and β_2 were used to calculate the calibration parameter *k* and estimate the product viscosity for other samples using the product composition x_o. The results are summarized in Table 9. Clearly, the estimated viscosity matches very well with the measured values in the QA lab, with maximum error less than 4% even for the samples not used in calculating the calibration parameter.

Sample no.	PPO fraction x_o	*Measured viscosity (Pas)*	Estimated viscosity (Pas)	% error
*1**	0.58	*186*	185.0	-0.5376
2	0.58	186.6	185.7	-0.48
3	0.58	182.7	184.9	1.20
4*	0.58	184.6	184.8	0.11
5	0.54	171.4	174.9	2.04
6*	0.56	175.4	180.3	2.79
7	0.54	168.6	175.0	3.80
8*	0.54	174.2	175.1	0.52
9	0.58	186.9	185.8	-0.59
10	0.56	178.8	180.6	1.01
*11**	0.58	183.7	185.7	1.09
12	0.54	171.9	175.1	1.86

Table 9: Comparison of measured and estimated values of viscosity for samples collected during DOE run on Nov 21, 2000 at GEP Selkirk (* samples used in calculating the calibration parameter)

10.4 Scale-Up Summary

The above-mentioned results clearly demonstrate the scale-up of the developed model-based framework for estimation, diagnostics and control. In particular, the excellent fit and validation of the model with data from a production-scale 120mm extruder demonstrates the validity of the physics-based model and its application to any extruder irrespective of size. Furthermore, the model-based adaptation also applies equally well to the large production-scale extruder. Finally, the viscosity estimation using the model and the model-based estimation works very well and the estimated viscosity was within 4% of the off-line measurements in the QA lab, well within the accuracy of the capillary rheometer. Due to limited resources, we addressed only the modeling, adaptation and viscosity estimation on the 120 mm extruder and did not have the opportunity to

investigate the fault diagnostics and closed-loop control through multiple experiments. However, the extension of the modeling, adaptation and viscosity estimation to the 120mm extruder gives ample confidence in the scale-up of the diagnostics and closed-loop control results as well.

We summarize the various steps in the developed model-based approach for estimation, diagnostics and control to any extruder application in Figure 46.

Diagnostics

- Generate fault signatures for main raw material and feeder variations for each product grade/family
- Tune thresholds for fault detection and identification based on signal-to-noise ratio and desired specifications on product quality – trade-off false alarms vs. missed detects

Modeling

- Collect experimental data from extruder with a PRBS excitation of the inputs – if normal daily operation has enough variability, may be possible to use that historical data instead
- Obtain an initial value of the model parameters using off-line least-squares optimization to get the best-fit between the model prediction and measured values of torque and die pressure
    - Identify these parameters under nominal conditions for product grades or families of similar product grades (similar key raw materials and composition)
    - Fix the machine-dependent parameters (one for each extruder for multiple extruder lines) and use on-line adaptation for process-dependent parameters

Estimation

- Initial calibration:
    - Obtain viscosity vs. composition (key raw materials) data for each product grade/family - use historical data if it covers wide enough composition range, else perform controlled experiments
    - Fit linear/nonlinear correlation between viscosity and composition for each grade/family – linearize around nominal compositions for each grade/family if required
    - Calibrate conversion parameter between model parameters β_1, β_2 and the parameters μ_o, μ_1 in linearized viscosity-composition relation
- Parameter adaptation and estimation:
    - Initiate model with nominal parameters β for each grade/family
    - Perform on-line recursive adaptation if there is mismatch between model predictions and measured values of torque and die pressure
    - Obtain on-line viscosity estimate with model parameters β and predicted product composition
- Occasional verification of viscosity estimation with lab measurements of samples collected during steady state operation

Control

- Specify target specifications and bounds for viscosity for each product grade
- Tune PI controller based on parameters for first-order approximation of process dynamics and desired closed-loop response

Figure 46 : Steps for implementing developed model-based estimation, diagnostics and control algorithm in an extruder application.

11 Benefits

11.1 Overview of benefits derivation

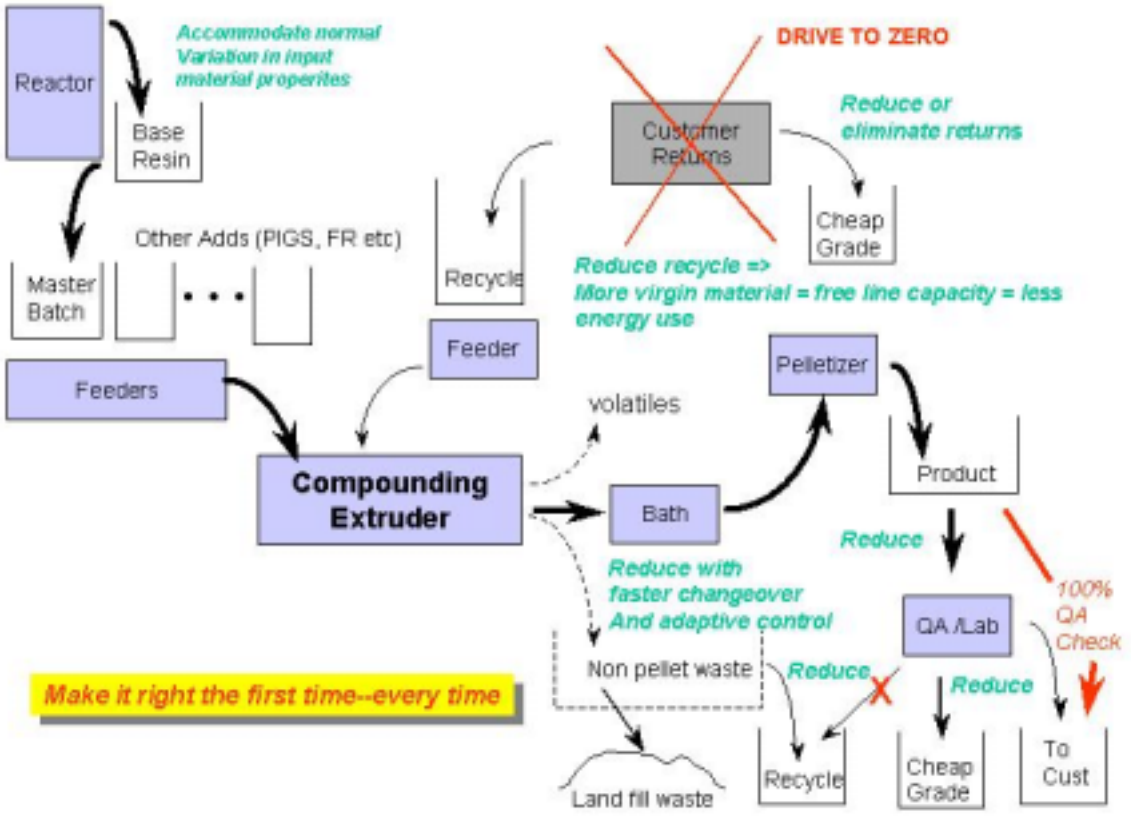

Figure 47 - How Intelligent Extruder Derives Benefits

As shown in Figure 47, the *Intelligent Extruder* System provides benefits that include reduced waste and energy use, improved quality, and by reducing recycled product, increases system capacity to process virgin product, potentially delaying the need to add costly compounding equipment.

The intelligent extruder monitor and diagnostic system provides benefits to a polymer producer by alerting process control room operators and production line personnel when out-of-spec material is being produced, and the closed loop adaptive control system (if used) provides a means to bring production back into compliance automatically when process corrections are feasible by changing the appropriate feed-stocks or other manipulated variables. Specific benefits can be grouped as follows:

- Improved first pass yield by reducing the quantity of out of spec material that must be recycled or sold as cheaper grade
- Reducing the quantity of material that must scrapped to landfill
- Reducing or eliminating material that escapes quality checks but is shipped to the customer and returned, incurring transportation expense and unhappy buyers
- Reducing the energy consumed in the net land-filled waste plus material recycled (recyclable waste plus customer returns)
- Reduced loading on the quality lab for process checks
- A continuous quality audit assures material shipped meets customer expectations, and reduces or eliminates the likelihood of returns: monitoring and controlling consistency of product is often as import to end users as conformance to absolute specifications

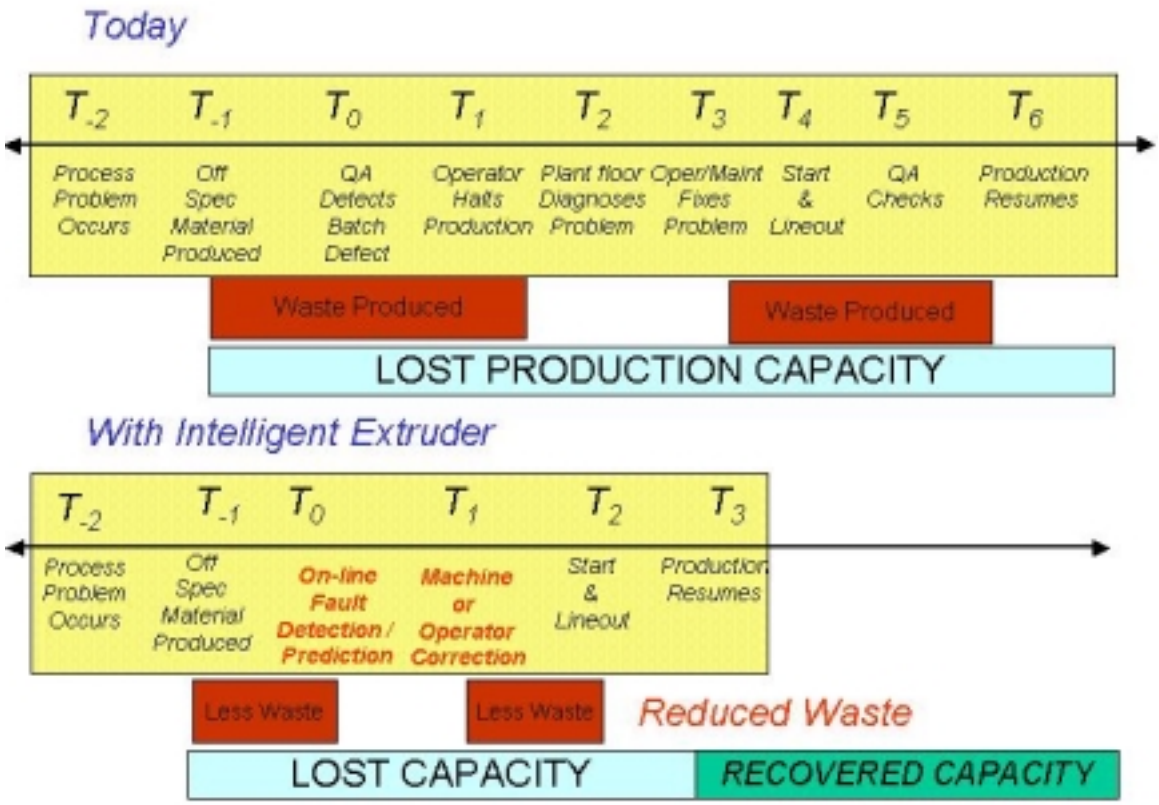

Figure 48 Process Timeline for Benefit Calculations

Figure 48 shows an event time line for a typical extruder based process contrasted with a timeline with *Intelligent Extruder* in place. As suggested in the figure, benefits in waste material reduction and recovered production capacity come simply from more rapid detection of process upsets and corrections which get the process back on line.

11.2 Approach to benefits quantification

To quantify the potential benefits, the following factors must be considered:

- ***Frequency of Process variation—***The temporal behavior of process upsets, must be quantified, either statistically from past QA data (including customer returns, base resin shifts, etc) or based on first principles understanding. Understanding this factor would be done as part of an initial process audit; for example, based on a pareto of multiple factors as defined in Section 3.1 would be considered. Often this data is hard to come by in our experience, either because the temporal sampling resolution is not frequent enough, or determinable (e.g. customer returns).
- ***Frequency of QC checks during a production run***—Because of cost and logistics, QA tests from a lab may only be done initially in the formulation for short runs, or at low frequencies (e.g. each shift) for long campaigns. The lag between when an upset occurs and QA (or the operator in extreme cases) detects it is waste or off spec material.
- ***Time and method to correct the problem***—Recovery time is dependent on the problem and specifics of the material; for the 80% of quickly correctable problems (base resin shifts, feeder blockages etc), it is vital to know whether operator intervention is required (e.g. feeder blockage or strand drops) or can be handled through automation (adjustment to feed constituent rate set points).
- ***Time to restart and QC check the process***

There is no easy way to get numbers for a given process. GE sales teams or the customer would use a variety of calculation tools and information about the process capability to assess the potential benefits of the Intelligent Extruder services offering. For example, Figure 49 shows a typical spread sheet that was prototyped to aid in quantifying the benefits in applying Intelligent Extruder at GE Plastics.

Compounding Extruder/Finishing Line Economics

Project:	**GEP Selkirk - Line No. 8**				Analysis Period:	24	hours
Product Type:	Noryl PX5515				Noryl PX5515 Sales Price	$ 1.90	/pound
Order size:	20,000	pounds			***Revenues:***	***$ 91,854***	
	Feeder A:	**Feeder B:**	**Feeder C:**	**Feeder D:**	Feedstock Costs:	24,450	27%
Type:	Screw	Vibratory	Belt	Belt	Energy Costs:	1,619	2%
Feeder Composition:	PPO	Chalk	PS	The rest	Recycle Costs:	44	0%
Feed Ratio:	21%	29%	15%	35%	Total Operating Costs:	*$ 26,113*	28%
Feedstock Cost:	$ 0.75	$ 0.75	$ 0.25	$ 0.25	***Contribution Margin:***	***$ 65,741***	71.6%
Sp. Energy (kw-hr/kg):	0.25						

Production Rate:	**2037.5**	lbs/hr
Finished Production Rate:	2014.3	lbs/hr (includes losses)
Order Transition Time:	101.568	seconds

Motor RPM's

210.0

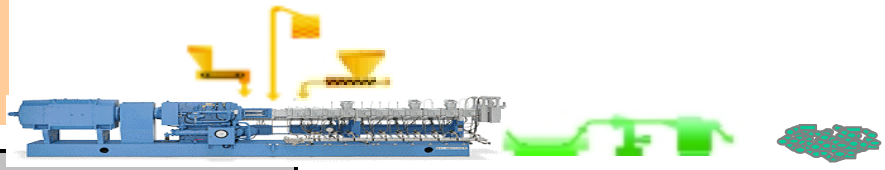

Machine Info		
Machine Type:	ZSK-120	
Screw Size:	4.72	inches
Screw Pitch:	2.36	inches
Gear Ratio:	0.13503	speed out/in
Screw Length (L/D):	24	inches/inches

Yield loss at transition (1st pass):	0.3%	(perfect setup)
CTQ sampling time:	5	minutes
Yield loss at transition w/sampling:	**1.1%**	
% Recycle possible:	80%	
Recycle costs:	$ 0.10	/pound

Figure 49 Process Spread Sheet used for Benefits Analysis with Customer

Range of Expected Energy and Waste Reduction Benefits Results

The following data represents a composite over several engineering plastic polymers similar to those used during this study. A summary of findings for the industry:

1. The range of first pass yield, the quantity of material that meets customer requirements and can be shipped after one pass through the production line, was approximately 88% for a poorly performing line to 98% for a well performing line (98-99% is the perfect stoichiometric yield due to volatile removal of about 1-2%).
2. Taking 94% as an average (actual data is confidential), about 6% of material produced cannot be sold. Of this about 2% is non-pellet waste, including volatiles, drool piles from startup, or strand waste from startup.
3. The remaining 4% is pellet waste that is out of specification due to viscosity, mechanical properties, color or other defects.
4. The cost of land-fill is about the same as virgin polymer, and recycle in high grade materials can degrade properties, so minimal recycle can be assumed
5. Based on industry data and data from GE, about half or 2% is candidate for improvement with our *Intelligent Extruder* system technology. Where first pass yields are lower, the percentage will generally be even >2%, so we will use this as a conservative bound. That is, if it can be assumed that our technology can yield a 2% improvement in FPY from 94% to 96% (or 88 to 90% etc), the savings are significant.

To put a 2% FPY improvement in context, GE produces approximately 7 billion pounds of material per year. Table 10 shows a comparison of the potential benefits to GE to go from 94% to 96% FPY. The benefit is a savings of $91MM, 140MM lb less solids to the land fill, and about 146 MM Mwhr less energy use, and discharged 7MM lbs fewer volatiles into the atmosphere. For simplicity we have combined the distillation and drying energy to make the resin with specific energy per lb to process the resin in the extruder. The reader can readily put his or her own numbers to run the calculation for their own situation. To be fair, this projection assumes all extruders for all materials would get the full 2% benefit, but the spread of benefits would also be offset by a spread in FPY in which the upside could be greater for lines/materials with low FPY.

Assumptions

Pounds Produced	7.00E+09

	First Pass Yield	Loss	Material (lb)	Material ($)	Energy (kwhr)	Energy ($)	Finishing ($)	Profile of Waste Produced: Cost ($-MM)	Solids (MM-lb)	Energy (Mwhr)
Base	94.00%	6.00%	4.20E+08	2.10E+08	4.37E+08	2.18E+07	4.20E+07	**$274**	**420**	**436,800**
2% FPY Delta										
Comparison	96.00%	4.00%	2.80E+08	1.40E+08	2.91E+08	1.46E+07	2.80E+07	**$183**	**280**	**291,200**

Data

kwh cost ($)	$0.05	Average industrial contract price
resin mat'l cost ($)	$0.50	Base resin +pigments+fillers+other additives
spec energy (kwh/lb)	1.04	Includes energy (steam/elect) to produce resin + extruder energy
finishing cost ($/lb)	$0.10	Average non-energy compounding cost per pound
volatiles (lb-vol/lb-resin)	8.000E-05	Average for various engineering polymers

Savings

$-MM	$91
Land fill (MM-lb)	140
Energy (Mwhr)	145,600
Energy (Quad)	4.968E-04
Volatiles (MM-lb)	7.0

Table 10 Impact of 2% FPY Improvement on GE Production

If this table is extrapolated to the whole engineering polymer industry which is about 30MM pounds per year, the results are shown in Table 11. Again this assumes 100% penetration and that all production could benefit, but the interested application engineer can readily work the numbers to their situation

Assumptions

Pounds Produced	3.00E+10

	First Pass Yield	Loss	Material (lb)	Material ($)	Energy (kwhr)	Energy ($)	Finishing ($)	Profile of Waste Produced: Cost ($-MM)	Solids (MM-lb)	Energy (Mwhr)
Base	94.00%	6.00%	1.80E+09	9.00E+08	1.87E+09	9.36E+07	1.80E+08	**$1,174**	**1800**	**1,872,000**
2% FPY Delta										
Comparison	96.00%	4.00%	1.20E+09	6.00E+08	1.25E+09	6.24E+07	1.20E+08	**$782**	**1200**	**1,248,000**

Data

kwh cost ($)	$0.05	Average industrial contract price
resin mat'l cost ($)	$0.50	Base resin +pigments+fillers+other additives
spec energy (kwh/lb)	1.04	Includes energy (steam/elect) to produce resin + extruder energy
finishing cost ($/lb)	$0.10	Average non-energy compounding cost per pound
volatiles (lb-vol/lb-resin)	8.000E-05	Average for various engineering polymers

Savings

$-MM	$391
Land fill (MM-lb)	600
Energy (Mwhr)	624,000
Energy (Quad)	2.129E-03
Volatiles (MM-lb)	30.0

Table 11 Extrapolation of 2% FPY Improvement to Engineering Polymer Industry

To more carefully quantify the benefits in a particular manufacturing context, it is necessary to work up the details specific the process as outlined above and to establish whether composition/viscosity properties and the root causes of variability can have the same impact as suggested here. Potential users wishing to carry out a careful audit to quantify potential benefits of the *Intelligent Extrude*r system on their process should contact GE Industrial Systems for assistance.

12 Commercialization Plan

12.1 Market Opportunity

The technology developed as part of this program presents sizable market opportunities in the application of process control equipment and services primarily, but not limited to, the plastics industry in which compounding screw extruders are used. To the end user, as discussed in the Benefits discussion above, this technology presents a significant opportunity to eliminate waste and increase yield, increase throughput, product quality, and as a result, competitiveness. Because of the attractiveness of this market, GE Industrial Systems (GEIS) has maintained ongoing discussion for an alliance with Coperion Werner & Pfleiderer Inc (USA) (CWP) in order to expedite the introduction of this technology to the market.

GEIS is a supplier of large AC and DC motors, adjustable speed drives, process control equipment and related services. CWP is a supplier of state of the art compounding twin-screw extruders, related controls and services. Both parties have supplied equipment to the plastics industry for over 15 years. Sales opportunities are anticipated from, in order of priority, new CWP extruders, modernization of existing CWP extruders, modernization of other existing extruders, and new and existing extruders in other industries, as tabulated in Table 12 Market Segmentation .

In all of the markets in Table 12, it is the team's opinion that service is the cornerstone of the product offering as it provides the opportunity to optimize the process and to recognize further opportunities for savings and reduction of wastes. Based upon historical data, service revenues could exceed 20% of the overall project revenues (precise numbers are proprietary to GEIS and CWP) and are attractive due to generation of an ongoing revenue stream and an installed based for future upgrades as software innovations are developed.

Market Opportunity	Anticipated Market (based on CWP data)	Technical, cost and competitive factors
New CWP Extruders	**40 units/year***	"Value" price will far exceed cost, so economic justification will be inherent to the selling process. Customer alternative is to buy traditional manual control
Existing CWP Extruders	5000 units worldwide at 1% annual replacement = **50 units/year***	These customers would normally purchase new control equipment only for reliability reasons. Will need to overcome customer reluctance to new technology ("selling up") through strong economic justification. Customer alternative is to do nothing unless reliability is an issue.
Other Existing Extruders	10,000 units worldwide, 0.25% annual replacement =**25 units/year***	Selling up to advanced technology may be difficult w/smaller users who have differing requirements and limited capital resources.
Extruders in other Industries	Food – market 10 times plastics market Metal casting– few customers, but huge savings opportunity	Technology or CTQ's may not be applicable to these processes

Table 12 Market Segmentation linked to extruder sales

To examine the market opportunity more broadly, a cross-functional team from GE, CWP and potential customers (GE Plastics and a small independent supplier) developed data that identified other segments where Intelligent Extruder technologies might be relevant. The results of these discussions are summarized in Figure 50: Potential Extruder Market Segments. In addition to the polymer industry segment that is our focus, coatings (insulation, toners, etc), fiber and film manufacture and injection molding all looked attractive as follow on segments to pursue. These markets combined could exceed by 2-3X the value of the polymer manufacturing industry; though these are gross market estimates only, it reinforces the potential synergy of the underlying polymer finishing *Intelligent Extruder* technologies with related segments.

This team also drilled down into the polymer market opportunity to better understand the factors driving the market. Findings are summarized in Figure 51: Detailed Opportunity Fishbone for Intelligent Extruder. Overall, this sub-segment was believed to offer approximately a $260MM market for the kinds of advanced automation and monitoring products and services being developed in this program, initially targeted and achieving resin quality and consistency for the target customers.

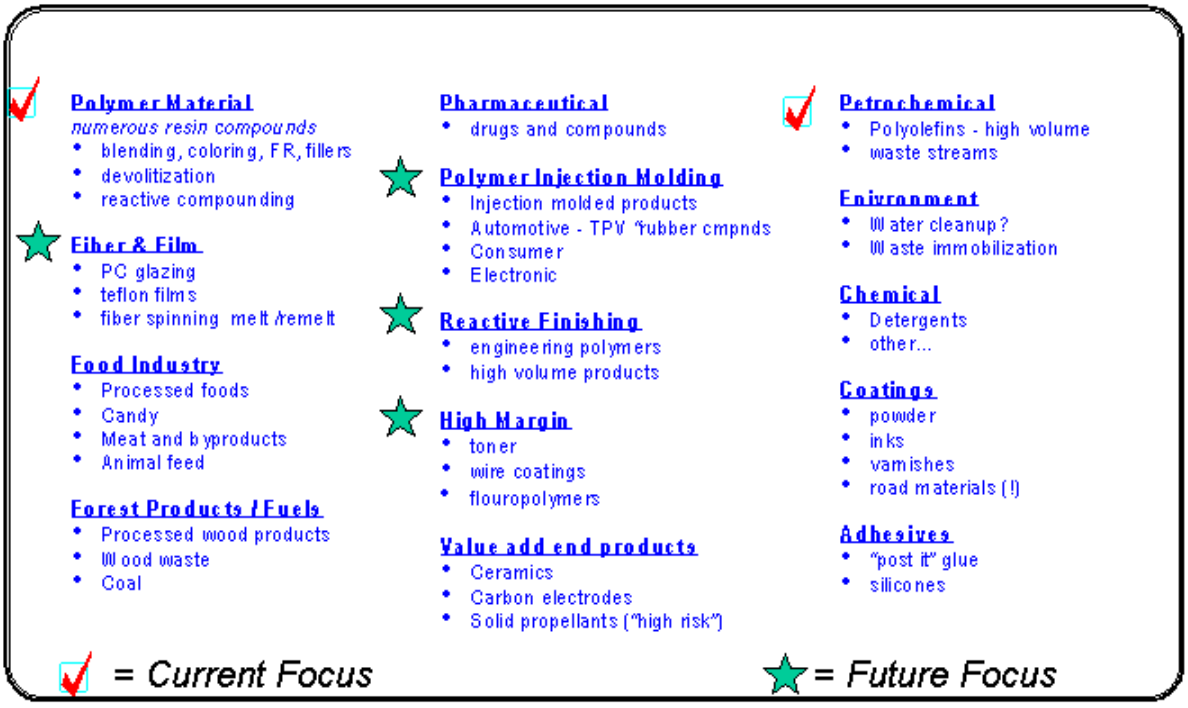

Figure 50: Potential Extruder Market Segments

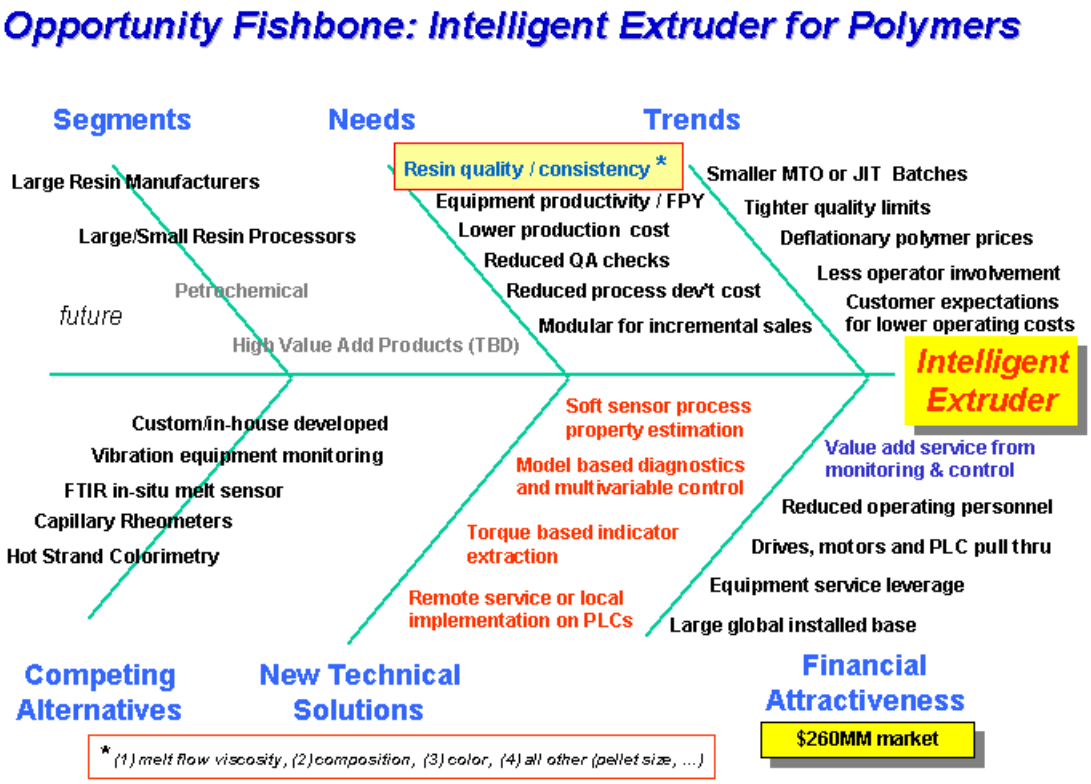

Figure 51: Detailed Opportunity Fishbone for Intelligent Extruder

12.2 Commercialization Strategy

The commercialization of new process control technologies is not new to GE Industrial Systems. GE has successfully supplied such breakthrough technologies to customers in a number of industries since the early 1960's when the on-line computer became commercially viable. As stated above, to expedite the introduction of this technology to the marketplace, GEIS and CWP have proposed forming a technology and market development alliance. Throughout the definition of this alliance, joint marketing discussions have included "what is the product and who will produce it?", "how will customers obtain this product?", and "how will the product be sold?".

12.2.1 Product – Advanced Process Control and Service

A typical extruder control system is expected to consist of an adjustable speed drive with coordinated control, an operator interface with process displays and reporting, a general purpose controller for miscellaneous control and sequencing functions, and a controller for the monitoring, diagnostic and adaptive control functions described above.

The goal remains to have a standard platform that is simple, easy-to-use, and inexpensive so that it may be sold on its own. Furthermore, the platform will be constructed so as to

facilitate service opportunities including data collection to help field engineers to conduct initial plant surveys locate additional opportunities for finishing operations improvements, and remote diagnostics. To enhance market opportunities and accommodate customer needs, modular software will be written so as to facilitate implementation on alternate control platforms from other vendors.

12.2.2 Remote Service Offering

From the outset, it was the vision that service offerings could be provided remotely, after initial setup and equipment validation, utilizing GEIS' Onsite Center in Salem, Virginia. Using telephone or secure web-enabled links, data would be downloaded through the factory floor process control equipment, where data conditioning and processing algorithms would be maintained. This facility already exists for remote monitoring of drive equipment in the steel and paper industry, providing a scalable infrastructure to support the needs of this program.

12.2.3 Distribution – Utilizing CWP's Distribution Channels

The new control and services platform developed will be sold as an integral part of each new mid and high end extruder sold by CWP wherever possible. Therefore, CWP's direct sales and distribution channels will be utilized. In the CWP extruder retrofit market, where there are also opportunities for mechanical equipment upgrades, CWP sales and distribution channels will be used, just as for new extruders. For other extruder retrofit opportunities, sales and distribution will be directly by GE.

12.2.4 Commercialization Sales Tools

Through the alliance with CWP, it is planned, outside the scope of this program, that the marketing objectives would be achieved by developing several sales tools. These are expected to include the following:

- Plant-wide Benefits/payback awareness presentation – a customer presentation that will outline the benefits of the technology developed as it is implemented at the time of the presentation and the project costs. An "experience list" will be developed as the technology is installed in various facilities.
- Standard technical specifications which describe the capabilities of the technology and its associated control functionality.
- Utilize full-scale technology pilot plant for future customer sales references.
- Jointly-developed Advertising and Sales Promotion (A&SP) tools which will include brochures, catalog pages, and Internet Web Pages.
- Additional promotional events are anticipated, such as technical papers presented in trade associations as well as KWP's own Polymer Processing Conference held annually in Ramsey, NJ.

Each of these sales tools would have been distributed to the GE and CWP sales forces, as appropriate, and each tool updated as the technology matured in actual target implementations.

12.3 Commercialization Status

In spite of a promising market, and the potential for 2% increases in first pass yield, the team has not yet succeeded in commercializing the *Intelligent Extruder* as system as of the writing of this report. A key barrier may be the complexity of the system coupled with the requirement to maintain a data-base for the models used based on material grades. Although efforts have shown various means to streamline this data-base through adaptive control, more work needs to be done to stream-line the effort required. In simple terms, the team needs to invest more into developing the value story in the context of specific market opportunities. Readers interested in using, adapting or extending any part of this work should contact GE Industrial Systems or Coperian Werner & Pfleiderer to initiate further discussion, including assessment of the applicability to their process.

13 Conclusions and Follow on Recommendations

Concepts developed in this program allow waste and energy reduction in polymer compounding operations for high value engineering materials. With advanced diagnostic and control software applied to existing extruder drive systems, benefits are obtained from a continuous quality audit synthesized by inferring material properties from readily measured machine variables. This allows rapid detection of out of spec material and corrective action in contrast to the infrequent quality checks that are performed today. We estimate that about 2% of first pass yield losses can conservatively be attributed to out of spec material produced this way, and caught after manufacture or when received at the customer. By increasing first pass yield by 2%, the 30 Billion pound per year engineering plastics producers in North America would save some $391MM dollars in material and energy costs, avoid land fill solids in excess of 600MM lbs, save 624,000 Mwhr of electrical and equivalent steam energy, and remove 30MM lbs of volatiles from the atmosphere. This also represents 600MM lbs of found capacity, equivalent to 51, 2000 lb/hr extruders operating two shifts, 5 days a week for a year.

All the algorithms developed can be run on readily available process control instrumentation available off the shelf from multiple suppliers, using PCs, PLCs with PC-class process cards, or plant level DCS systems. Maintenance and calibration of the algorithms is required, but means are proposed to efficiently develop and maintain this required data. Viscosity estimation within 10% was demonstrated on both 25-mm research extruders and a 120-mm production system at GE plastics. A means to detect and classify a number of common feeder and disturbance faults was developed, under the restriction only one fault at time occurs (though this can be relaxed), and the system was demonstrated on the research extruder under various operating conditions. Diagnosis is based on certain characteristic process models. Parameters specific to machine geometry are identified once, and parameters specific to a grade must be estimated. But means to efficiently adapt the material parameters around a nominal grade is demonstrated,

simplifying the required database that must be developed. While the methods developed do not eliminate the need for a QA lab, the load for QA testing should be greatly reduced

In this program, the power of exploiting greatly simplified but dynamic process models was demonstrated. It is believed that more information is contained in machine variable data, particularly torque at frequencies at and above the rotation speed of the machine. Though we did not have time or resource to conduct experiments with it, a new torque observer algorithm was developed and studied in simulation. Because no extruder testing was actually conducted, the results are relegated to Appendix B, which shows that "high" frequency reaction torque components can be synthesized from measurements of voltage and current (and/or power) in any AC drive. By eliminating troublesome strain gauges or complex torque sensors, this algorithmic technique we believe can form the basis of new diagnostics to complement those developed in this program, and should be implemented and tested in a future research program.

Two program goals that were not achieved were the successful commercialization of the system, and the feedback control system scale-up demonstration. The full scale production system used for validating scale-up did not have provision for closing the loop on extruders, and changes needed were not high enough priority to GE Plastics given their commercial production constraints. There is no fundamental barrier to demonstrating this capability in a follow up study when a willing partner can be identified. As to commercialization, the GE Industrial Systems sales team has curtailed further investment in marketing this technology until an appropriate customer /partner can be identified. Parties interested in some or all aspects of *Intelligent Extruder* should contact GE Industrial Systems through their regional office for further discussions.

14 References

1. Houpt, Paul K., Campo, Peter, U.S. Patent 5,559,173, *System for Controlling the Color of Compounded Polymers using In-Process Measurements*, Sept. 24 1996
2. Campo, Peter J., Schneiter, John L., and Dixon, Walter V., U.S. Patent 5,526,285, *Imaging Color Sensor*, Jun. 11, 1996
3. Gertler, Janos J., "Survey of Model Based Failure Detection and Isolation in Complex Plants, *IEEE Control Systems Magazine*, December 1988.
4. Isermann, Rolf, "On Fuzzy Logic Applications for Automatic Control, Supervision and Fault Diagnosis," IEEE Transactions of Systems, Man and Cybernetics, Vol. 28, No.2, March 1998
5. Pabedinskas, A., Cluett, W.R., "Controller Design and Performance Analysis for A Reactive Extrusion Process," Polymer Engineering and Science, Vol. 34, No. 7April 1994
6. Gottfert, A., "Real time viscosity control with capillary rheometer, Kunststoffe 76, Vol. 12, 1986,p.1200
7. Dealy, D.M., Broadhead, T.O, "Process Rheometers for Molten Plastics: A Survey of Existing Technology," Polymer Engineering and Sci., Vol. 33, No. 23, Dec.1993.

8. McKay, B. et al, "Extruder Modeling: A Comparison of Two Paradigms,", UKACC/IEE International Conference on Control, Conf. Publication No. 427, 1996
9. Eerikainen, T., Zhu Y-H, Linko, P., "Neural networks in extrusion process identification and control," Food Control Volume 5, No. 2, 1994, p. 111
10. Hansen, M.G., Vedula, S., "In-line Fiber-Optic Near-Infrared Spectroscopy: Monitoring of Rheological Properties in an Extrusion Process." Journal of Applied Polymer Science, Vol 68, 1998, p.859
11. Gao, J., Walsh, G. C., Bigio, D., Briber, R. M., Wetzel, M. D., "A Residence Time Distribution Model for Twin Screw Extruders," AIChE J., vol 45, no. 12, pp 2541-2549, 1999.
12. Gao, J., Walsh, G. C., Bigio, D., Briber, R. M., Wetzel, M. D., "Polymer Eng. & Sci.," vol 40, no. 1, pp 227-237, 2000.
13. Curry, J, Anderson, P., "Controlling the Crosslink Density of Co-Reactive Polymers in an Extruder Reactor," SPE ANTEC Papers (1990b) 36 p.1938
14. Curry, J., Jackson, S., Stoehrer, B, van der Veen A., "Control Strategy for Free Radical Degradation of Polypropylene via Reactive Extrusion", Chem. Eng. Prog. (1988) 84 p.43
15. Curry, J. , Kiani, A., "Experimental Identification of the Distribution of Fluid Stresses in Continuous Melt Compounders, Part. II," SPEC ANTEC Papers(1991) 114, p.37
16. Jones, R.W and McClelland, J.F, "On-line analysis of solids and viscous liquids by transient infrared spectroscopy," Process Control and Quality, 4 (1993), p. 253-260 (Elsevier, Amsterdam).
17. Gertler, Janos J, Fault Detection and Diagnosis in Engineering Systems, Marcel Dekker, NY 1998
18. Ljung, Lennart, System Identification: Theory for the User, Prentice-Hall, N.J. 1987

APPENDIX-A Extruder Dynamic Models

A.1 Dynamic model for Hold up

The transient variation in the holdup M_1 due to changes in total feed-rate Q and screw speed N is described simply by the total material balance:

$$\frac{dM_1}{dt} = Q - Q_{1o}$$

Eq-A 1

In the above equation, the total inlet feed-rate to this section (from the feeders) is Q while the total outlet mass flow rate, denoted by Q_{1o} , varies with the operating conditions, in particular the fill fraction ϕ (i.e. the fraction of the total void volume filled with the material holdup) and the screw speed N. More specifically, the maximum flow capacity of this section Q_{1fc} corresponding to the maximum filled capacity M_{1fc} (based on the void volume from screw geometry) is proportional to the screw speed N, i.e., $Q_{1fc} = k\,N$ with the proportionality constant k depending on the screw design/geometry. During regular operation, when this section is only partially filled and the fill fraction is $\phi = M_1 / M_{1fc}$, $(0 < \phi < 1)$, the total outlet mass flow rate is given by

$$\begin{aligned} Q_{1o} &= k\,\phi\,N \\ &= k\left(\frac{M_1}{M_{1fc}}\right)N \\ &= \frac{M_1 N}{B} \end{aligned}$$

Eq-A 2

where $B = M_{1fc} / k$ is a parameter that depends only on the screw design/geometry. Combining equations Eq-A 1 and Eq-A 2 gives the dynamic mass balance relation for the holdup M_1

$$\frac{dM_1}{dt} = Q - \frac{M_1 N}{B}$$

Eq-A 3

Note that at steady state, the inlet and outlet mass flow rates are equal, i.e. $Q = Q_{1o}$, and the dynamic material balance in Eq-A 3 reduces to the steady state version: $M_1 = BQ/N$. In contrast with the partially filled section, the total holdup M_2 in the filed section is constant (since the void volume is filled to maximum capacity). Furthermore, the outlet flow rate from this filled section is always the same as the inlet flow rate, which in turn is the same as the outlet flow rate from the partially filled section, i.e. Q_{1o}.

A.2 Dynamic model for composition

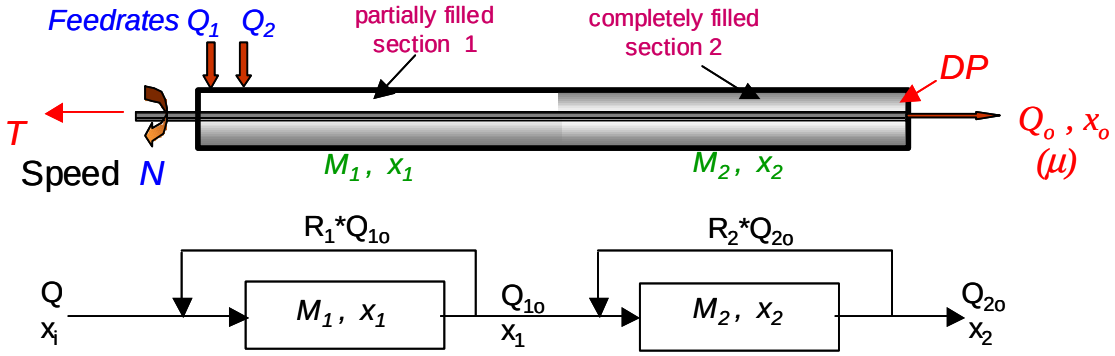

Figure 52: Schematic representation of mixing in partially and completely filled sections.

A way to obtain a simple parameterized model that can capture varying degrees of mixing, from no mixing at one extreme to perfect instantaneous mixing at the other, is to use a combination of plug flow with recycle. More specifically, consider the schematic representation in Figure 52, where raw material is fed to the partially filled section at total flow rate $Q = Q_1+Q_2$ and composition $x_i = Q_1/(Q_1+Q_2)$, and exits from this section to the completely filled section at a total flow rate Q_{1o} and composition x_1. The internal mixing inside this section can be modeled through a recycle with a flow rate R_1*Q_{1o} , where R_1 denotes the ratio of recycle to outlet flow rate. The combination of the recycle stream and the feed stream yields a net inlet stream with a total flow rate $Q_{1i} = Q+R_1*Q_{1o}$ and composition $x_{1i} = (Q*x_i+R_1*Q_{1o}*x_1)/(Q+R_1*Q_{1o})$.

If we model the material flow through the section as pure plug flow (i.e., first in first out) then its dynamics are described by a simple time delay, i.e.,

$$x_1(t) = x_{1i}(t-t_{d1})$$

with a time delay

$$t_{d1} = M_1 / (Q_{1o}*(1+R_1))$$

governed by the total material holdup and the total outlet flow rate. The above relations in time can be expressed equivalently in the Laplace domain:

Eq-A 4

$$x_{1i}(s) = \frac{(Q * x_i(s) + R_1 * Q_{1o} * x_1(s))}{(Q + R_1 * Q_{1o})}$$

$$x_1(s) = x_{1i}(s)e^{-t_{d1}s}$$

Solving for $x_{1i}(s)$ from the above relations yields the overall input-output relation between the inlet composition $x_i(s)$ and the outlet composition $x_1(s)$:

Eq-A 5

$$x_1(s) = \frac{Qe^{-t_{d1}s}}{Q + R_1 * Q_1(1 - e^{-t_{d1}s})} x_i(s)$$

The above relation provides a general mixing relation for the partially filled section, where the recycle ratio R_1 is the parameter that can be fit to capture the actual degree of mixing in a given screw design. In particular, the case $R_1=0$, i.e. no recycle, corresponds to no mixing and the input-output relation in Eq-A 5 reduces to a pure time delay

Eq-A 6 $$x_1(s) = x_i(s)e^{-t_{d1}s}, \quad \text{where } t_{d1} = \frac{M_1}{Q_{1o}}$$

On the other hand, the case with infinite recycle, i.e. $R_1=\infty$, corresponds to perfect instantaneous mixing and the input-output relation reduces to a simple first order response

Eq-A 7 $$x_1(s) = \frac{1}{\tau s + 1} x_i(s), \quad \text{where } \tau = \left(\frac{M_1}{Q} \right)$$

So, the parameter R_1 can be fit with measured input-output data to capture the actual degree of mixing in the section for a particular screw configuration. Similarly, the mixing in the completely filled section can be captured through a combination of plug flow and recycle to obtain the following input-output relation:

Eq-A 8 $$x_2(s) = \frac{e^{-t_{d2}s}}{1 + R_2 * (1 - e^{-t_{d2}s})} x_1(s), \quad \text{where } t_{d2} = \frac{M_2}{Q_{2o}} \quad \& \quad Q_{2o} = Q_{1o}$$

Section 1: Torque relation

We develop the following relationship for the total torque

Eq-A 9 $$T = \alpha_0 + \alpha_1 M_1 (\alpha_2 + N) x_1 + \alpha_3 M_2 N x_2$$

which has three main components corresponding to the offset and the contributions from the partially-filled and completely-filled sections. The above equation yields torque as an instantaneous function of the total holdups (M_1, M_2), the compositions (x_1, x_2), and the screw speed N – it is an algebraic output map relating the process inputs/states to the output in a standard state-space description. The validity of such a relation can be tested against steady state input-output data from the extruder. In particular, at steady state, the relations in Eq 1 and Eq 5 can be used for the holdups and compositions to arrive at the equivalent relation for steady state torque:

Eq-A 10 $$T = \alpha_0 + \alpha_1 \alpha_2 B \frac{Q}{N} x_i + \alpha_3 A N x_i + \alpha_1 B Q x_i$$

Section 2: Die pressure relation

Eq-A 11
$$DP = \left(\frac{128L}{\pi D^4 \rho}\right) Q_o \mu_T \quad = \quad k Q_o \mu$$

In the above relation, L, D denote the length and diameter of the pipe, ρ is the density of the material and they are lumped into an unknown parameter k. Furthermore, Q_o is the flow rate of the product through the die plate and μ denotes the viscosity of the product at the prevailing temperature and shear rate at the die. The viscosity of the product depends on the composition, i.e. the weight fraction x_o of PPO, temperature T_o in the melt zone and the shear rate on the molten product as it flows through the die plate holes. While the melt temperature T_o is measured using a thermocouple in the melt pool just before the die plate, the shear rate is considered to be proportional to the total material flow rate Q_o.

We will approximate the nonlinear dependence of the product viscosity on composition, temperature and shear rate with a linear approximation that is valid in a local neighborhood of the nominal point of operation. In particular, we will use the following linear approximation for the product viscosity:

Eq-A 12
$$\mu = \mu_o + \mu_1(x_o - \bar{x}_o) - \mu_2(Q_o - \bar{Q}_o) - \mu_3(T_o - \bar{T}_o)$$

where ($\bar{}$) denotes respective nominal steady state values at the nominal operating point. In the above linear approximation for viscosity, μ_o denotes the nominal viscosity at the nominal operating point, while μ_1, μ_2, μ_3 denote the slope of viscosity with respect to composition, shear rate and temperature, respectively at this operating point (see Figure 53)

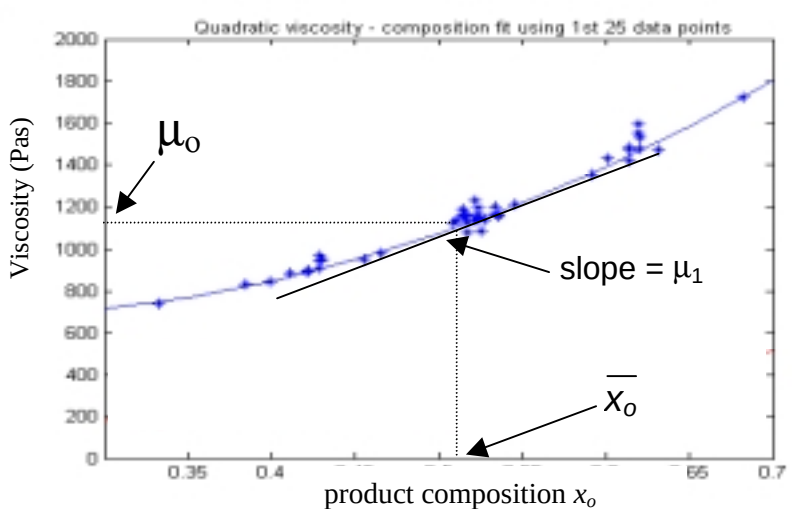

Figure 53: Viscosity vs composition of PPO

Inserting the linear relation for viscosity from Eq-A 12 in

Section 2: Die pressure relation
Eq-A 11,

we obtain the following model for die pressure:

Eq-A 13 $$DP = kQ_o[\mu_o + \mu_1(x_o - \bar{x}_o) - \mu_2(Q_o - \overline{Q}_o) - \mu_3(T_o - \overline{T}_o)]$$

The above equations together comprise a dynamic model for the extruder that relate the changes in the process inputs (feed-rates, screwspeed) to the measured output variables (torque, die pressure):

Eq-A 14

$$\frac{dM_1}{dt} = Q - Q_{1o} \qquad (Q = Q_1 + Q_2, \quad Q_{1o} = \frac{M_1 N}{B})$$

$$M_2 = A$$

$$x_1(s) = \frac{Qe^{-t_{d1}s}}{Q + R_1 * Q_{1o}(1 - e^{-t_{d1}s})}\ x_i(s)\ , \qquad (x_i = \frac{Q_1}{Q_1 + Q_2}, \quad t_{d1} = \frac{M_1}{Q_{1o}(1 + R_1)})$$

$$x_2(s) = \frac{e^{-t_{d2}s}}{1 + R_2 * (1 - e^{-t_{d2}s})}\ x_1(s), \qquad (t_{d2} = \frac{M_2}{Q_{1o}})$$

$$T = \alpha_0 + \alpha_1 M_1(\alpha_2 + N)x_1 + \alpha_3 M_2 N x_2$$

$$DP = kQ_{1o}[\mu_o + \mu_1(x_2 - \bar{x}_2) - \mu_2(Q_{1o} - \overline{Q}_{1o}) - \mu_3(T_o - \overline{T}_o)$$

Section 3: Linearized DP equation and Nonlinear DP equation

Linear form:

Eq-A 15

$$DP = [\bar{DP} - k\overline{Q}_o\mu_o + k\overline{Q}_o{}^2\mu_2] + [k(\mu_o - \mu_1\bar{x}_o) - k\overline{Q}_o\mu_2]Q_o + (k\mu_1)Q_o x_0 - k\mu_3 Q_o \Delta T$$

or written in a compact form

Eq-A 16 $$DP = \beta_o + \beta_1 Q_o + \beta_2 Q_o x_o - \beta_3 Q_o \Delta T$$

The above relations for die pressure DP yield a simple relationship between the model parametes β_i and the physical parameters μ_i.
On the other hand, if we adopted a model structure for die pressure without any linearization, i.e. retaining the same structure as equation, Eq-A 13:

Eq-A 17 $$DP = kQ_o[\mu_o + \mu_1(x_o - \bar{x}_o) - \mu_2(Q_o - \overline{Q}_o) - \mu_3(T_o - \overline{T}_o)],$$

then it can be written in the following compact form:

Eq-A 18 $$DP = \beta_1 Q_o + \beta_2 Q_o \Delta x_o - \beta_3 Q_o \Delta Q_o - \beta_4 Q_o \Delta T$$

In this new nonlinear structure, comparing Eq-A 17 and Eq-A 18, we obtain another simple relationship between μ_0, μ_1 and β_1, β_2 involving only the calibration parameter *k* and independent of any other terms. More specifically,

Eq-A

$$\beta_1 = k\mu_0$$
$$\beta_2 = k\mu_1$$

This simplification of calculation for μ_0, μ_1 from the identified parameters β's results in better estimates and improved diagnostics.

Section 4: Model for Melt Temperature variation

In the absence of good melt temperature measurement, we can use a simple first-order dynamic model to predict the variations in the melt temperature from its nominal value. In particular, assuming the heat input from the heating barrels to the extruder is constant while the heat generated in the extruder due to friction in the screws varies as a function of the operating conditions, we can obtain the model for melt temperature variation through a simple dynamic heat balance. It should be mentioned that the ratio of heat input from the barrels to the heat generated internally due to friction in the screws is smaller in larger industrial-scale extruders compared to the smaller lab-scale extruders due to the reduced surface area to extruder volume. The heat generated H by the screws is proportional to the shaft work, i.e. $H = k_1*T*N$, where T is the shaft torque, N is the screw speed and k1 is a proportionality constant. This heat generated is used to melt the solid raw materials and raise the temperature of the molten product to the outlet temperature T_o from the inlet temperature T_i, i.e. at steady state,

Eq-A 19

$$H = k_1 * (T * N) = Q_o(\Delta H_m + c_p(T_o - T_i)) \quad \text{or}$$
$$\frac{H}{Q_o} = k_1 * \frac{T * N}{Q_o} = \Delta H_m + c_p(T_o - T_i)$$

where Q_o is the throughput, ΔH_m is the heat of melting the raw materials, c_p is the specific heat capacity of the molten material, T_i is the inlet temperature (assumed constant) and T_o is the outlet melt temperature. Since, we need only changes in the melt temperature from the nominal steady state value T_{os} corresponding to the nominal values of T_s, N_s, Q_{os}, we can obtain the following relation for the change in melt temperature by subtracting the above relation from a similar relation at the nominal steady state:

Eq-A 20

$$\Delta T = T_o - T_{os} = k_2\left(\frac{T * N}{Q_o} - \frac{T_s * N_s}{Q_{os}}\right) = k_2 * \Delta\frac{T * N}{Q_o}$$

where k_2 is another proportionality constant and $\Delta(T*N/Q_o)$ denotes the deviation in the specific energy generation, $SE= (T*N/Q_o)$, from the nominal steady state value. Finally, since we are interested in the dynamic transient responses of the changes in melt temperature, we get it by using a first-order transient response in conjunction with the above steady state value (the first-order response can be obtained by performing a simple lumped dynamic energy balance):

Eq-A 21
$$\Delta T = \frac{k_2}{\tau s + 1} * \Delta \frac{T * N}{Q_o}$$

where τ is the time constant for the transient response in the melt temperature. In the absence of a good measurement of melt temperature, the above relation for ΔT can be used in the die pressure relation (Eq-A 16 or Eq-A 18).

Section 5: Closed-loop Control

The process response between the product viscosity μ and the feed composition x_i has the following (linearized) first-order dynamics:

Eq-A 22
$$\mu - \mu_o = \frac{\mu_1}{\tau_p s + 1}(x_i - \bar{x}_i)$$

Since IMC tuning (see, e.g. Morari and Zafiriou, 1989 [3]) of a first order process such as the one given above, for a corresponding first-order closed-loop response:

Eq-A 23
$$\frac{\Delta \mu}{\Delta \mu_{SP}} = \frac{1}{\tau_f s + 1}$$

yields a Proportional and Integral (PI) action controller, a PI controller is tuned for robust control of this process with Internal Model Control (IMC) rulings. The resulting PI controller in Laplace domain is in the following form:

Eq-A 24
$$C(s) = \frac{\tau_p s + 1}{\mu_1(\tau_f s)} = \frac{\tau_p}{\mu_1 \tau_f}\left[1 + \frac{1}{\tau_p s}\right]$$

in which the proportional gain and the integral time constant are apparent in terms of the process parameters μ_1 and τ_p, and the IMC tuning factors, i.e. the closed-loop time constant τ_f.

A.3 References for Appendix A

1. Gao, J., Walsh, G. C., Bigio, D., Briber, R. M., Wetzel, M. D., "A Residence Time Distribution Model for Twin Screw Extruders," AIChE J., vol 45, no. 12, pp 2541-2549, 1999.
2. Gao, J., Walsh, G. C., Bigio, D., Briber, R. M., Wetzel, M. D., "Polymer Eng. & Sci.," vol 40, no. 1, pp 227-237, 2000.
3. Morari, M. and Zafiriou, E. Robust Process Control, Prentice-Hall, Inc., New Jersey, 1989.

APPENDIX B - Extruder Drive Torque Estimation using Electrical Variables

B.1 Summary

Reaction torque from a loaded extruder is one potential indicator for process health. In prior unpublished studies by Coperian Werner-Pfleiderer, strain gauges in line with the drive shaft on special research extruders showed that there was potential information contained in the shaft torque at frequencies at or above the shaft rotation rate which could be correlated to proper filling, mixing performance and screw condition, for example. Unfortunately, strain gauges are not easy to install, maintain and calibrate in a production environment, so definitive work on interpreting relationships between dynamic torque behavior and quality has not received much attention. Here we propose some alternative methods for extracting high frequency torque dynamics which do not rely on strain gauges or any other mechanical sensor in the drive line. The proposed methods instead exploit readily available electrical sensors, which are commonly found in modern drives used in extruders and which can often be retrofit to older machines. Software algorithms are derived which use these electrical measurements to extract torque data that is usually removed by filtering since it is not required for the functioning of the motor control. Scope of this development is limited to preliminary simulations, since we did not have time or resources to evaluate what quality attributes and/or diagnostics can be rigorously linked to the torque data; we have included these results as a foundation for future "Intelligent Extruder" developments.

B.2 Requirements and Objectives

An "observer" is a software algorithm which takes as inputs certain measured variables and produces as outputs unmeasured variables of interest, such as torque. For this project the requirements for the observer are as follows:

1) Obtain a method to determine the fundamental component and harmonic components of the electrical torque produced by a synchronous or asynchronous machine driving an extruder. Machine is assumed to operate at speed > 0 rpm.
2) Provide means that the observer can be implemented:
   - *As part of the drive controller.*
   - *As a separate unit (e.g. PC or process equipment) able to interface with any inverter.*
3) The observer should have a frequency response reaching up to a couple of kHz to be able to observe the extruder dynamics of interest
4) Motor constants are assumed available when used stand alone.

5) The observer will be simulated using SABER with the best possible approximation to the GE-Innovation drive control.

Requirement (1) assures that the methods will be applicable to the majority of production scale extruders installed today, and normal operation is always at non-zero speed allows simplification. Frequency response in (2) is a conjecture based on suggestions by Coperian W-P, but the actual frequency range of requirement must be established by experiment. Since we were not able to implement the torque observer, the SABER simulation provided a well validated drive simulation we could could use to at least provide a proof of concept.

B.3 Approaches to observer based torque estimation

Instantaneous electromagnetic torque computation can be derived by implementation of the following expression:

Eq B- 1 $$t_e = \tfrac{3}{2} P \bar{\lambda}_{sg} \times \bar{i}_{sg}$$

Where P is the number of pole-pairs, $\bar{\lambda}_{sg}$ is the space phasor of the stator flux linkages expressed in a general reference frame and $\bar{i}_{sg}$ is the space phasor of the stator currents in the same general reference frame. Eq 1 can be further represented using two-axis components for stator flux and stator currents as:

Eq B-2 $$t_e = \tfrac{3}{2} P(\lambda_{sd} i_{sq} - \lambda_{sq} i_{sd})$$

In general, there are two ways to obtain the flux value generated by a machine:

Eq B- 3 $$\lambda(t) = \int_0^t v(t)dt$$

Or

EqB-4 $$\lambda(t) = kL \cdot i(t)$$

Use of Eq 3 leads to a method known as the Voltage model [1]. On the other hand, using Eq 4 leads to a method known as Current model [2]. Both models are depicted in Figure 1.

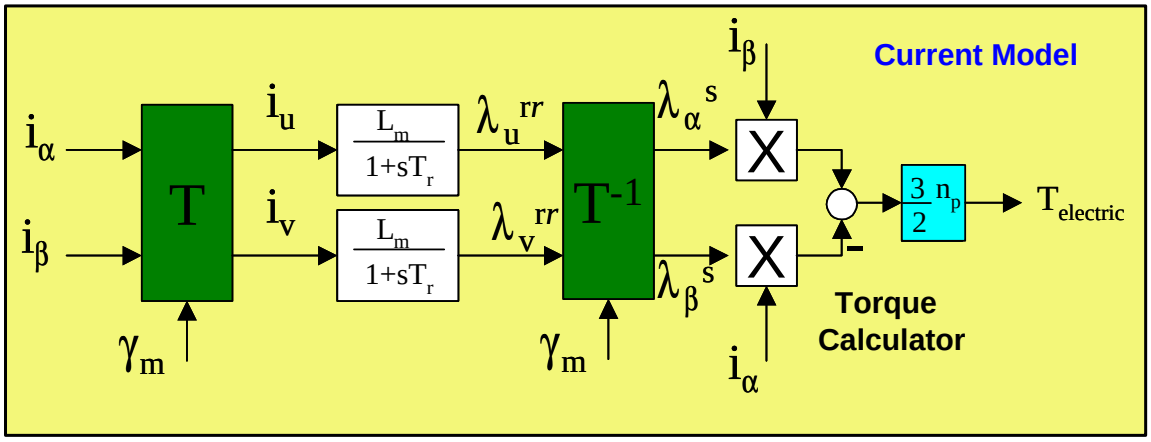

(a)

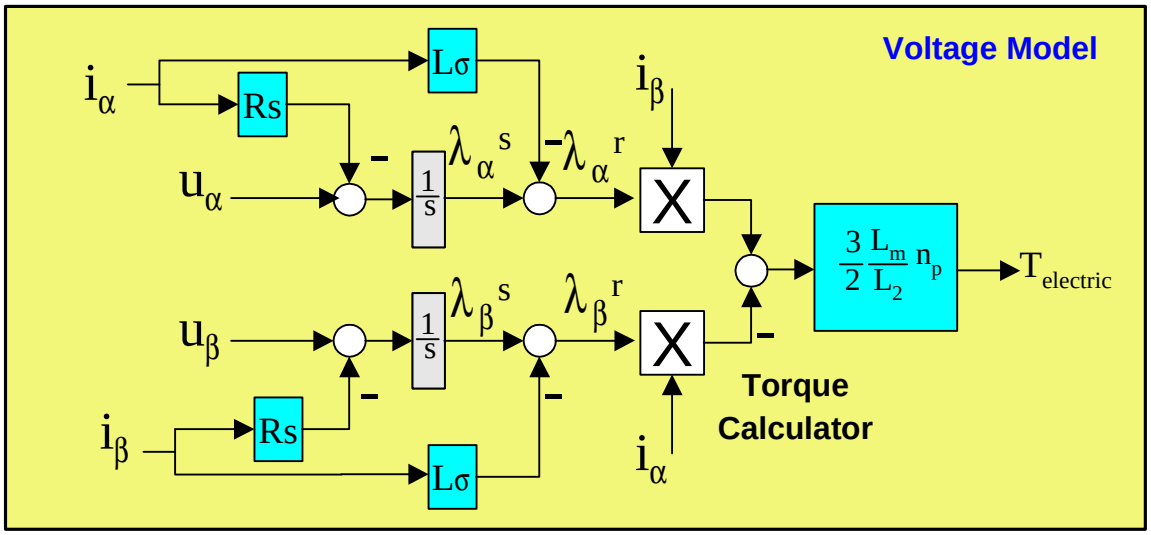

(b)

Figure 1: Block diagram: (a) Current model. (b) Voltage model

The Current model requires sensing of motor currents as well as motor parameters such as mutual inductance and electric time constant and coupling inductances. Computation of angle γ_m requires the actual rotor mechanical speed. But no motor voltages are required at all. On the other hand, the Voltage model requires motor voltages and currents plus some motor parameters such as stator resistance and inductances. Voltage model requires an integrator as shown in Eq 3; the use of integrators at low speeds may lead to saturation yielding in inaccurate torque calculation. Since both methods employ electric motor parameters it is important to note that those parameters change under different environmental and electrical conditions, e.g. stator resistance is affected by temperature and inductance may saturate.

Current model	Voltage model
• Parameter Sensitive (temperature, inductance saturation) • It works well at low frequencies. • Requires the motor mechanical speed • Not suitable for analog implementation • Resulting torque has the full frequency spectrum • DSP implementation: *Resulting torque have limited frequency spectrum due to sensors and sampling*	• Works well at high frequency. • Integrator has problems with sensors offset • Does not work at zero freq. • Parameter sensitive (Temperature) • Analog implementation possible: *Complicated to implement in analog circuitry* *Integrators have to be replaced by 1st order transfer function* *Resulting torque have the full frequency spectrum* • DSP implementation: *Requires complicated voltage sensor (VCO's, ASIC)* *Resulting torque have limited frequency spectrum due to sensors*

Table B-1: Salient characteristics for voltage model and current model for torque estimation

A combination of methods mentioned above can be achieved as shown in Figure 2 [3].

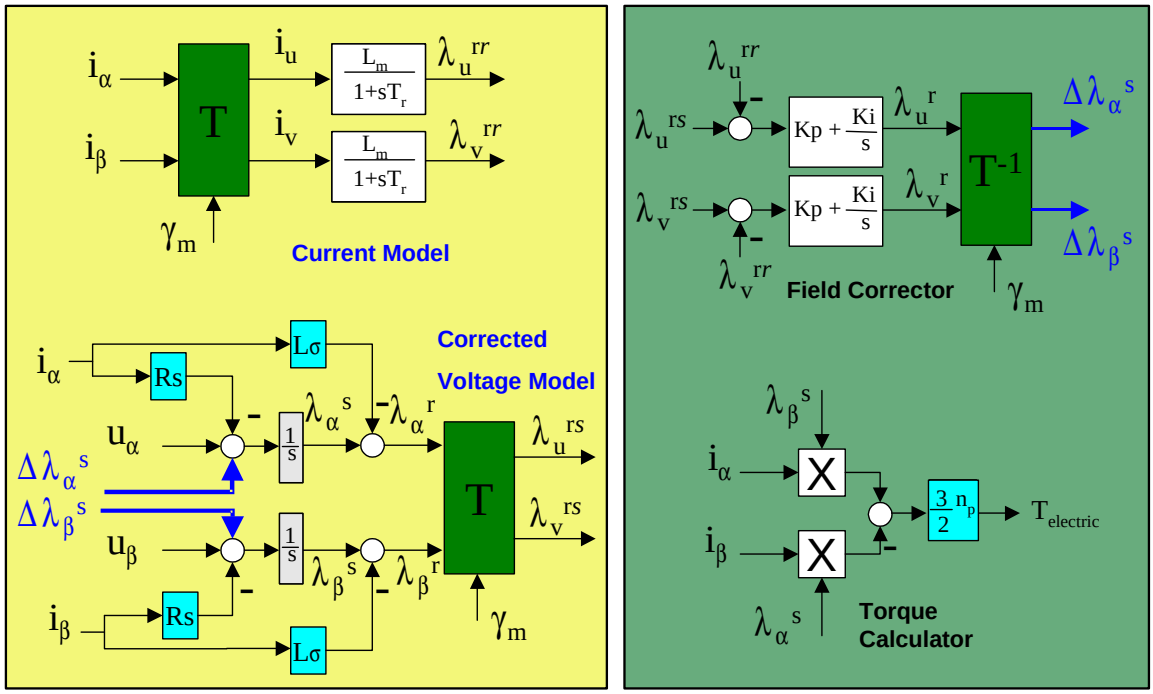

Figure B-2: Current/voltage model

Salient features of this method are presented in Table B-2

Current/Voltage model
• The use of both models allows the extension of the operating region down to zero frequency. • Requires knowledge of motor parameters. • Digital signal processing CPU required for implementation due to its complexity. • Requires complicated voltage and current sensors.

Table B-2: Salient characteristics of Current/Voltage model

Another method, based on machine's electric power, is derived from the following expression:

Eq B-5 $$P = t_e \cdot \omega_e$$

Where P is the electric power and ω_e is the machine angular speed. Figure 3 and Table 3 show the main features of this method.

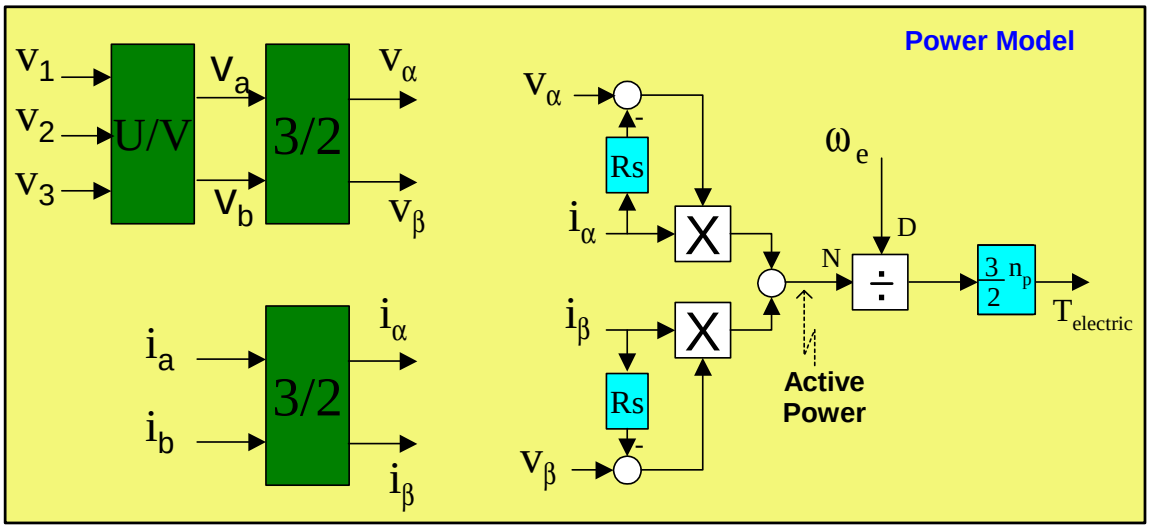

Figure B- 3: Power model

Power model
• Less sensitive to parameters variation. • It works only for frequencies not equal zero due to division. • Easily implemented with analog circuits. • Requires the applied frequency from the inverter or a two phase PLL for its generation • Can provide the full torque spectrum if implemented in analog fashion. • The model is valid for synchronous and asynchronous motors.

• Two line-to-line voltages could also be used as long as they are isolated (LEM voltage sensors). • A small DSP could be used to set up gains and parameters from a PC serial interface. • DSP could also include thermal models to correct for resistance variations.

Table B-3: Salient characteristics of Power model

B.4 Saber Simulation

Results regarding the Power model are presented in this section. Figure 4 shows the schematic diagram for SABER used to simulate the motor drive and the torque observer. Some basic assumptions for the simulation are:

- Detailed induction motor model considering only copper losses and saturation.
- Detailed model of a PWM inverter considering: dead-time, device losses and DC voltage ripple.
- Sampling delays and quantization are included in the speed-current control for the motor model.

The following parameters correspond to the values normally found in GE Innovation Series controller. These are readily modified for other motors or controllers.

DC link voltage=900V	r_s=0.319Ω
PWM frequency=2.5KHz	r_r=0.220Ω
Sampling Time=250μs	l_s=0.00269H
Power=15KW	l_r=0.004139H
Pole pairs=2	l_{mo}=0.077H

Table B-4: Parameters used in simulation

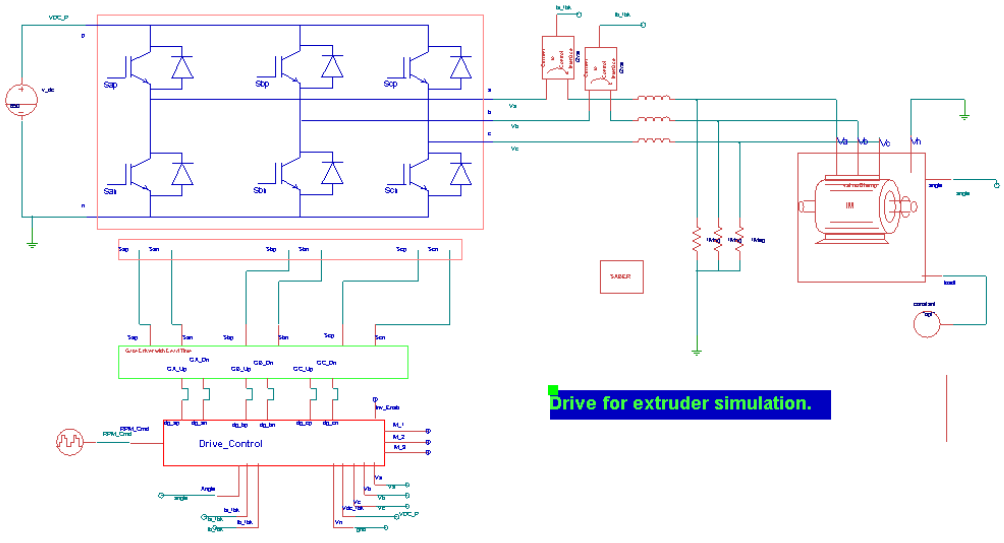

Figure B-4: Schematic diagram used for SABER simulation

A virtual torque sensor (ideal) in the simulation is attached to the motor to obtain the "actual" torque. Information from this torque sensor is compared with results from the torque observer for validation. Figure 5 shows the behavior of the motor during the

starting process. Waveforms for motor speed in rad/s, motor current in Amps, observed torque in Nm and motor torque in Nm are presented. Observed torque represents the torque estimated using the Power model.

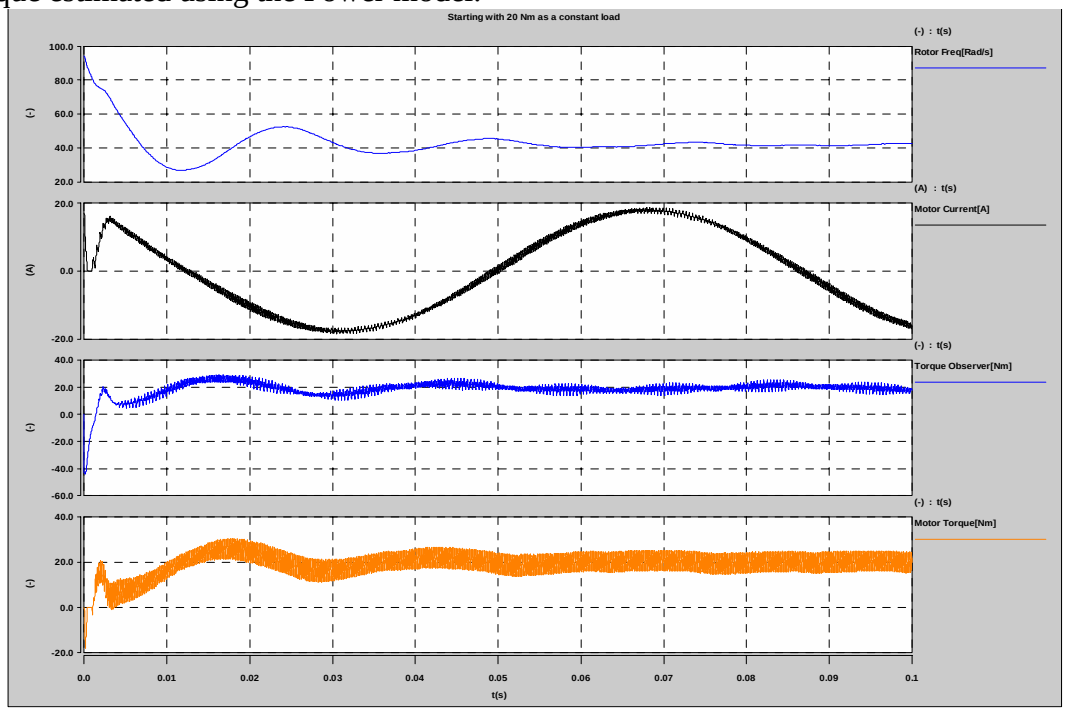

Figure B-5: Behavior of motor at starting. From top to bottom: Rotor speed, Motor current, Observed torque, Motor torque.

It can be noticed that the observed torque is following the actual torque very closely and settles down at steady state.

Figure B-6 is a continuation in time of Figure B-5. It shows the motor running at 40 rad/s under no-load conditions (T≈0Nm) when a step load of 20Nm is applied at t=75ms. In consequence the torque developed by the motor jumps from 0Nm to 20Nm. This test shows the ability of the observed torque to follow sudden load changes.

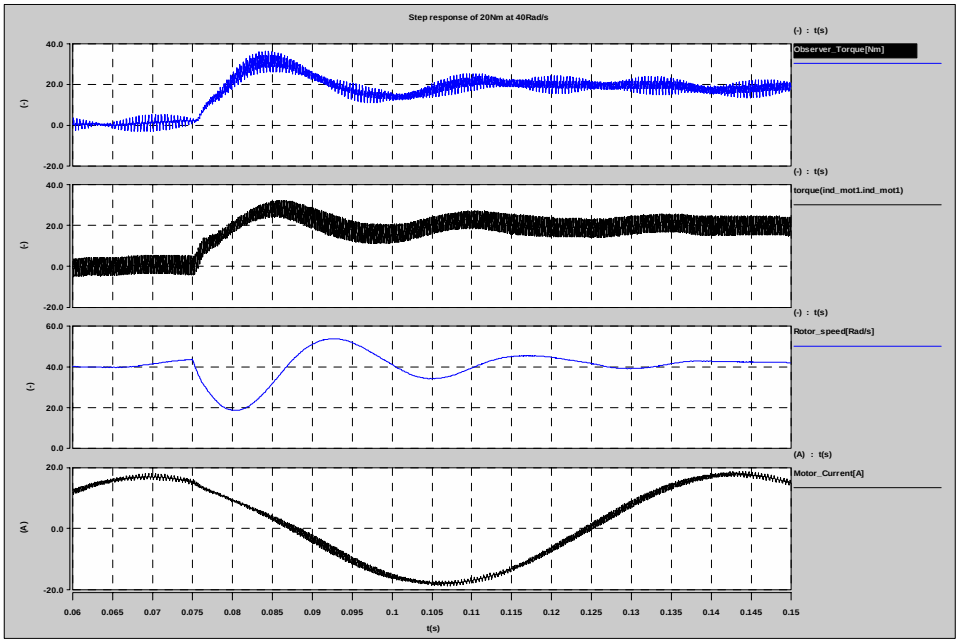

Figure B-6: Behavior of motor during a step load. From top to bottom: Observed torque, Motor torque, Rotor speed and Motor current.

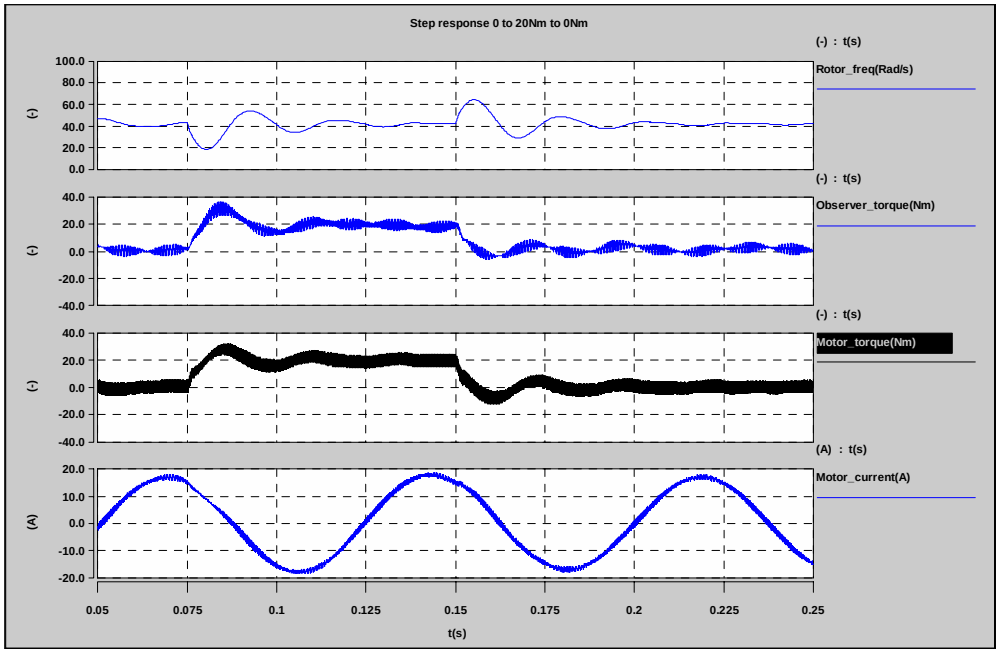

Figure B-7: Behavior of motor during sudden application and demotion of load. From top to bottom: Rotor speed, Observed torque, Motor torque and Motor current.

Figure B-7 shows the motor running at approx. 40 rad/s under driving a load of 20Nm applied at t=75ms. Later, the load is removed at 0.15s. This figure shows the ability of the observer to follow step loads when the motor is loaded or unloaded.

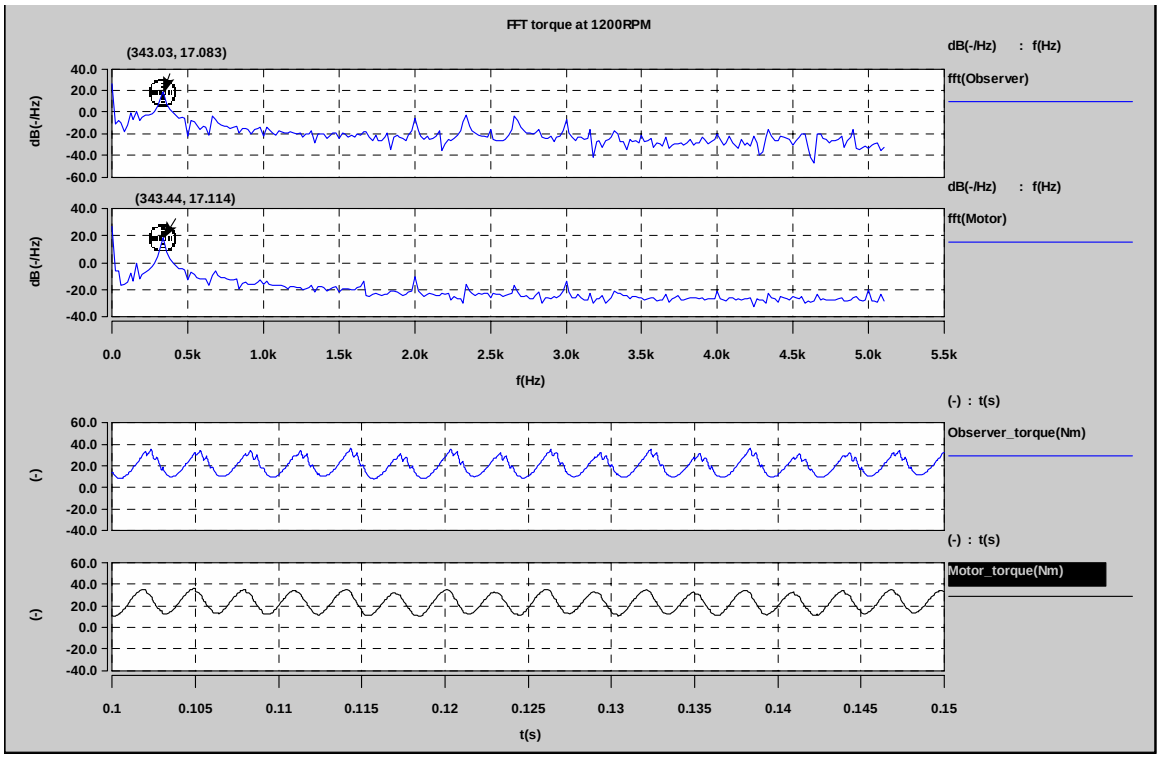

Figure B- 8: Torque during steady state. Top traces: FFT of Observed torque, FFT of Motor torque. Bottom traces: expanded view of Observed torque and Motor torque respectively.

Bottom traces of Figure 8 shows the response of the torque with oscillation due to non-compensated dead-time at inverter side. The frequency of this oscillation is six times the fundamental frequency. It can be noticed that even under irregular conditions the observed torque is able to follow the actual motor torque. Top traces in same figure shows the frequency spectrum for the aforementioned torque traces. The magnitude of fundamental torque component is shown to illustrate the accuracy of the observed torque.

B.5 Conclusions from simulation results

- The observer using the Power model is able to detect the torque with a wide bandwidth if implemented using analog components, allowing reaction torques at per-revolution resolution to be seen for use in advanced diagnostics

- The observer based on the Power model could be combined with a small microprocessor or DSP and multiplying D/As to input the motor parameters and correct them on line for temperature variations.

Since no attempt was made in the scope of this program to implement these concepts on a functioning extruder, it remains to validate the value of high frequency information in the estimated torque to diagnose process and equipment problems in extruders and drives.

B.6 References for Appendix B

[1] P.L. Jansen, R.D. Lorenz and D.W. Novotny. **Observer-based direct field orientation: analysis and comparison of alternative methods**. IEEE Transactions on Industry Applications, vol. 30, no. 4, July/August 1994.

[2] C. Lascu and A.M. Trzynadlowski. **A TMC320C243-based toque estimator for induction motor drives**. IEEE International Electric Machines and Drives Conference, pp.733-735, 2001.

[3] S. Kühne and U. Riefenstahl. **A new torque calculator for AC induction motor drives that improves accuracy and dynamic behavior**. In Proceedings of the IEEE International Symposium on Industrial Electronics, pp. 498-503, 1999.

[4] ***"Sensorless vector control and direct torque control***": Peter Vas; Oxford University Press, 1998.

[5] ***"Dynamic simulation of electric machinery":*** Chee-Ming Ong; Prentice Hall PTR 1997.